NATURAL FRACTIONATION OF URANIUM ISOTOPES

Dissertation
zur Erlangung des Doktorgrades
der Naturwissenschaften

vorgelegt beim Fachbereich Geowissenschaften / Geographie
der Johann Wolfgang Goethe – Universität
in Frankfurt am Main

von
Janine Noordmann
aus Neustadt

Frankfurt 2013
D30
Fassung aktualisiert am 24.01.2015

vom Fachbereich Geowissenschaften / Geographie der Johann Wolfgang Goethe – Universität als Dissertation angenommen.

Dekan:	Prof. Dr. A. Junge
Gutachter:	Prof. Dr. S. Weyer
	Prof. Dr. M. E. Böttcher
Datum der Disputation:	24.01.2014

Table of Contents

LIST OF FIGURES

c(U) = 14 nmol/kg; Ku et al., 1977; Collier, 1985; Siebert et al., 2003; Weyer et al., 2008), and the orange bars represent the measured isotope composition of the uppermost sediments analysed for the Landsort Deep. The dotted and dashed blue lines are modelled seawater-freshwater mixing lines (dotted = concentration; dashed = isotope composition), as described in detail in the discussion section.

Fig. 4.6 Sediment depth profiles of core MUC 342390-2-7 from the Landsort Deep (Baltic Sea). The profiles shown are for selected major and trace elements (e.g., mass fractions, *w*, of Re, Mn, Fe, Mo and U), and isotope compositions of U ($\delta^{238}U$) and Mo ($\delta^{98}Mo$). The mass fractions of Mn and Fe are normalised to the Al mass fraction, and the Re mass fraction is normalised to the Mo mass fraction. Green dashed line: *w*(Fe)/*w*(Al) of average shale of 0.54 g/g according to Wedepohl (2004). The vertical black dashed lines represent the average shale for *w*(Re)/*w*(Mo) = 0.15 ng/µg (Turekian and Wedepohl, 1961; Esser, 1991) and *w*(Mn)/*w*(Al) = 0.0097 g/g (Turekian and Wedepohl, 1961; Bowen, 1979). The blue dashed line: mean ocean water $\delta^{238}U$ (Weyer et al., 2008). The mean ocean Mo isotopic composition for $\delta^{98}Mo$ = 2.3 ‰ according to Siebert al., 2003. The black dashed line at a depth of 6 cm separates the upper segment from the lower segment (see explanation in the text).

Fig. 4.7 Plot of *w*(U) / *w*(Al) (a) and the fraction of detrital U (b) vs. U isotopic composition, $\delta^{238}U$, of a sediment; green squares represent data for sediment core KY09-1 and green diamonds for KY09-3. The position of the sediment data in Fig. 4.7b assumes that the detrital sediment component has $c(U)_{det}$ = 2.5 µg/g (= average crust: Taylor and McLennan, 1985). The modelled curves and lines assume that authigenic U has $\delta^{238}U_{auth}$ = 0.0 ‰ and is mixed with detrital U of various compositions. In Fig. 4.7a, the blue curve is modelled for mixing with an average crust, i.e., $c(U)_{det}$ = 2.5 µg/g and $\delta^{238}U$ = -0.30 ‰ (Taylor and McLennan, 1985; Weyer et al., 2008; Noordmann et al., 2011). The red dashed lines are modelled for mixing with extremely crustal endmembers of $c(U)_{det}$ = 1 µg/g, $\delta^{238}U_{det}$ = -0.20 ‰, $c(U)_{det}$ = 10 µg/g, and $\delta^{238}U_{det}$ = -0.46 ‰, respectively. The purple line is modelled for mixing with $c(U)_{det}$ = 5 µg/g and $\delta^{238}U_{det}$ = -0.35 ‰, and those values have been chosen to match the composition of the uppermost fjord sediments. In Fig. 4.7b, the blue line is modelled for mixing of $\delta^{238}U_{auth}$ with $\delta^{238}U_{det}$ = -0.30 ‰ (= average crust: Weyer et al., 2008; Noordmann et al., 2011),

LIST OF TABLES

ZUSAMMENFASSUNG

Das Thema dieser Arbeit war die Untersuchung der natürlichen Variationen von den zwei primordialen Uranisotopen (^{238}U und ^{235}U) mit einem Schwerpunkt auf Proben, die (1) die kontinentale Kruste und ihre Verwitterungsprodukte (d.h. Granite, Shales und Flusswasser) repräsentieren (2) Produkte der hydrothermalen Alteration vom mittelozeanischen Rücken widerspiegeln (d.h. alterierte Basalte, Karbonatgänge und hydrothermales Wasser) und (3) aus abgegrenzten euxinischen Becken (d.h. Proben aus der Wassersäule und den dazugehörigen Sedimenten) stammen. Das allgemeine Ziel war das Verständnis, unter welchen Bedingungen und Mechanismen eine Fraktionierung der zwei häufigsten Uranisotope (^{238}U und ^{235}U) in der Natur erfolgt, zu verbessern.

Uran ist ein redox-sensitives Spurenelement, genauso wie Molybdän, das natürlicherweise in zwei Valenzzuständen auftritt (U^{IV} bildet unlösliche Komplexe und U^{VI} bildet lösliche Komplexe). Unter oxischen Bedingungen verhält sich Uran konservativ, da es aufgrund seiner langen Verweilzeit im Ozean von 0.5 Ma eine zeitlich stabile Konzentration im Ozean aufweist (Colodner et al., 1995). Dagegen ist es unter anoxischen/euxinischen Bedingungen partikelreaktiv und wird in organikreichen Sedimenten angereichert. Jüngste Studien beobachteten natürliche Variationen im $n(^{238}U) / n(^{235}U)$ in terrestrischen geologischen Proben (Stirling et al., 2007; Weyer et al., 2008; Brennecka et al., 2011a,b) und kurz darauf auch in Meteoriten (Brennecka et al., 2010a). Terrestrische Uranisotopenvariationen werden durch Isotopenfraktionierungen ausgelöst, die besonders zwischen oxischen und anoxischen Bedingungen auftreten, aber auch durch die Adsorption an Oxide (Stirling et al., 2007; Weyer et al., 2008; Bopp et al., 2009; Montoya-Pino et al., 2010; Brennecka et al., 2011a,b). Molybdänisotope wurden schon häufig verwendet, um paläo-redox

Bedingungen zu rekonstruieren, insbesondere vom Ozean aus dem Proterozoikum (2.5 Ga bis 0.5 Ga, Arnold et al., 2004; Kendall et al., 2009). Die eigentliche Idee von dieser Studie war, dass Uranisotope für einen ähnlichen Zweck verwendet werden können, d.h. um die paläo-redox Bedingungen im Ozean oder die Bedingungen der Anreicherung und Mobilisierung von Uran in der Umwelt zu rekonstruieren. Um Uran als solch ein Werkzeug nutzen zu können, ist es essentiell die Massenbilanz der Uranisotope im Ozean zu verstehen und die geochemischen Prozesse, die eine Uranisotopenfraktionierung auslösen können. Deshalb untersuchten wir (1) eine mögliche Uranisotopenfraktionierung während der Verwitterung der kontinentalen Kruste und dem anschließenden Transport in Flüssen auf dem Weg zum Ozean, um die Uranisotopenzusammensetzung des Uraneintrages für den Ozean genauer zu definieren; (2) das Ausmaß des Uranaustrags aus einer euxinischen Wassersäule (Kyllaren Fjord aus Norwegen und zwei Becken aus der Ostsee) und die damit einhergehende Uranisotopenfraktionierung und zusätzlich die Urananreicherung und Isotopenfraktionierung in organikreichen Sedimenten aus den gleichen euxinischen/anoxischen Becken (Kyllaren Fjord aus Norwegen und zwei Becken aus der Ostsee). Bei dieser Fragestellung wurde auch die Molybdänisotopenzusammensetzung bestimmt, um den Fragen nach zu gehen, inwiefern sich die Urananreicherung und Uranisotopenfraktionierung verglichen mit Mo unterscheidet und ob wir zusätzliche Informationen gewinnen, wenn man Uran- mit Molybdänisotopen kombiniert; (3) die Urananreicherung und Isotopenfraktionierung unter hydrothermalen Bedingungen am mittelozeanischen Rücken – eine andere wichtige Uransenke im Ozean; (4) ein Tiefenprofil aus einem Tailing von einer alten Bergbauhalde aus Schneckenstein (Deutschland), um die Eignung von Uranisotopen zu untersuchen, die Bedingungen der Uranmobilisierung in Tailings aus Bergbauhalden zu bestimmen.

Die Uranisotopenzusammensetzung von Flüssen und der kontinentalen Kruste

In Kapitel 3 ging es um die Frage, ob eine Uranisotopenfraktionierung während der Verwitterung der kontinentalen Kruste und dem anschließenden Transport des oxidierten und gelösten Urans durch die Flüsse zum Ozean stattfindet. Als repräsentative Proben für die kontinentale Kruste (die Hauptquelle für den Ozean) haben wir die Uranisotopenzusammensetzung, $\delta^{238}U$, von folgenden Proben bestimmt: Granite mit unterschiedlichen Altern aus Grönland, Japan, Deutschland und Swasiland, und drei post-archaische Tonschiefer aus Australien. Zusätzlich wurde die Uranisotopenzusammensetzung in der gelösten Fracht von Haupt- und Nebenflüssen bestimmt, d.h. von Flüssen aus Venezuela (Rio Portuguesa), Indien (Alaknanda, Bhagirathi, Ganges, Brahmaputra), Pakistan (Indus), Deutschland (Main, Nidda) und der Schweiz (Ticino, Birs, Saane).

Die untersuchten Gesteinsproben fallen alle in einen recht schmalen Bereich von $\delta^{238}U$, zwischen -0.45 ‰ und -0.21 ‰ (relativ zum Uranstandard NBL CRM 112-A), mit einem Durchschnittswert von -0.30 ‰ ± 0.04 ‰ (doppelte Standardabweichung). Deren Uranisotopenvariationen sind unabhängig von der Urankonzentration (11.8 µg/g bis 1.3 µg/g), dem Alter (3.80 Ga bis 328 Ma), der Probenlokalität und Grad der Differenzierung, welches anhand des gemessenen La/Yb Verhältnisses bestimmt wurde. Die Uranisotopenzusammensetzung, $\delta^{238}U$, der Flüsse liegt zwischen -0.32 ‰ und +0.01 ‰. Obwohl es Unterschiede in der jeweiligen Lithologie der Einzugsgebiete gibt, liegen alle Hauptflüsse in einem engen isotopischen Bereich von -0.31 ‰ bis -0.13 ‰ und können demzufolge kaum von dem Durchschnittswert der kontinentalen Kruste (-0.30 ‰) unterschieden werden. Die Nebenflüsse aus den Schweizer Alpen weisen einen wesentlich größeren Bereich im $\delta^{238}U$ (-0.29 ‰ bis +0.01 ‰) auf und zeigen auch viel niedrigere Werte in ihren Urankonzentrationen (0.87 nmol/kg bis 3.08 nmol/kg) verglichen mit den untersuchten Hauptflüssen (5.19 nmol/kg bis 11.69 nmol/kg).

Insgesamt zeigen die Flüsse eine schwerere Uranisotopenzusammensetzung als die Proben, die kontinentale Kruste repräsentieren. Diese Beobachtung deutet daraufhin, dass eine Uranisotopenfraktionierung während der Verwitterung und/oder dem

Transport in den Flüssen erfolgt. Die Flüsse mit der schwersten Uranisotopenzusammensetzung weisen gleichzeitig sehr geringe Urankonzentrationen auf, was darauf schließen lässt, dass die beobachtete Isotopenfraktionierung zwischen dem gelösten und dem partikelgebundenem Uran in den Flüssen erfolgt. Flüsse mit einer hohen Urankonzentration beinhalten einen höheren Anteil an gelöstem Uran und werden dadurch weniger durch eine mögliche Uranisotopenfraktionierung beeinflusst. Ein weiterer Grund für die Uranisotopenvariationen könnte auch in der Zusammensetzung des Einzugsgebietes der Flüsse liegen, da dieses in den Schweizer Flüssen hauptsächlich durch Karbonate geprägt ist und diese bisher wenig untersucht wurden.

Da Hauptflüsse die Hauptquelle des Urans für den Ozean darstellen, leiten wir von unseren Ergebnissen ab, dass der Uraneintrag im Vergleich zu der Uranisotopenzusammensetzung der kontinentalen Kruste kaum (wenn überhaupt) fraktioniert wurde.

Demzufolge schlagen wir für zukünftige Berechnungen in der Massenbilanz des Urans vor, den in dieser Studie ermittelten Durchschnittswert der Hauptflüsse, $\delta^{238}U$ = -0.23 ‰, als beste Abschätzung für die Quelle des Urans im Ozean anzusehen.

Uran- und Molybdän-Isotopenfraktionierung in modernen anoxischen Becken: Fallbeispiele aus dem Kyllaren Fjord (Norwegen) und der zentralen Ostsee

In Kapitel 4 wollten wir 1.) die Parameter untersuchen, die die Uranisotopenfraktionierung unter anoxischen Bedingungen bestimmen und 2.) die Uranisotopenfraktionierung mit der vom Molybdän vergleichen, da Mo auch ein redox-sensitives Spurenelement ist, dessen Fraktionierungsverhalten bereits länger untersucht wird. Dementsprechend bestimmten wir die Konzentrationen und

Isotopenzusammensetzungen von U und Mo in den Wassersäulen und den organikreichen Sedimenten aus drei derzeitigen anoxischen Becken (Ostsee: Landsort und Gotland Tief und der Kyllaren Fjord aus Norwegen).

Die Proben aus der Wassersäule des Kyllaren Fjords zeigen eine starke Verarmung an Mo und eine moderate Verarmung an U mit der Tiefe. Diese Ergebnisse zeigen eine große Übereinstimmung zu Studien aus dem Schwarzen Meer (Romaniello et al., 2009; Nägler et al., 2011), obwohl der Kyllaren Fjord eine wesentliche geringere Ausdehnung (Tiefe: 29 m vs. 2500 m) und Abgrenzung aufweist. Diese Konzentrationsprofile sind mit einem Anstieg im δ^{98}Mo und einer Abnahme im δ^{238}U in der Tiefe gekoppelt, von 2.4 ‰ bis 2.6 ‰ beziehungsweise von -0.35 ‰ bis -0.70 ‰. Die Sedimentproben von der Oberfläche aus dem Kyllaren Fjord zeigen leichte Anreicherungen im Mo und U (6 µg/g bis 37 µg/g beziehungsweise ~ 4 µg/g) und haben ein durchschnittliches δ^{98}Mo und δ^{238}U von 2.17 ‰ ± 0.20 ‰ bzw. -0.26 ‰ ± 0.10 ‰.

Die Wasserproben aus der Wassersäule der Ostsee zeigen eine geringe Abnahme in der Mo- und U-Konzentration (normalisiert zum Salzgehalt) und nur eine vernachlässigbare Mo- und U-Isotopenfraktionierung im Vergleich zum Meerwasser. Die obersten Sedimente aus der Ostsee (Landsort Tief) wurden größtenteils unter anoxischen Bedingungen abgelagert und sind hoch angereichert im Mo (bis zu 222 µg/g) und moderat angereichert im U (bis zu 8 µg/g). Allerdings zeigen deren Mo- und U-Isotopenzusammensetzung wesentlich leichtere Werte an (mit δ^{98}Mo von 0.05 ‰ ± 0.40 ‰ und δ^{238}U von -0.27 ‰ ± 0.22 ‰) als die von typischen organikreichen Sedimenten aus anoxischen Becken (z.B. das Schwarze Meer und der Kyllaren Fjord).

In Übereinstimmung mit den jüngsten Erkenntnissen aus dem Schwarzen Meer (Romaniello et al., 2009; Nägler et al., 2011), zeigen unsere Ergebnisse aus dem Kyllaren Fjord eine schwache Mo- und starke U-Isotopenfraktionierung während der Reduktion und der Austragung von beiden Elementen aus einer hauptsächlich ungestörten euxinischen Wassersäule. Da der Mo Austrag aus der Wassersäule fast quantitativ erfolgt und die Sedimente hauptsächlich authigenes Mo enthalten, speichern die Sedimente die Mo Isotopenzusammensetzung vom Meerwasser. Uran wird nur

partiell aus der Wassersäule entfernt und die Uranisotope zeigen eine starke Fraktionierung zwischen Wasser und Sediment. Daraus folgt, dass das Tiefenwasser eine leichte und die Sedimente eine schwere Uranisotopenzusammensetzung aufweisen, verglichen mit dem Ausgangswert des Oberflächenwassers. Unsere Ergebnisse zeigen, dass die Uranisotopenzusammensetzung der Sedimente abhängt von (1) dem Ausmaß des Uranaustrags aus der Wassersäule (in einer ähnlichen Art und Weise wie bei den Molybdänisotopen) und (2) der Sedimentationsrate, d.h. der Fraktion von authigenem- relativ zum dendritischen Uran in den Sedimenten. Aufgrund der hohen Sedimentationsrate zeigen die Sedimente aus dem Kyllaren Fjord nur eine moderate authigene Urananreicherung und eine leichtere Uranisotopenzusammensetzung als Sedimente aus dem Schwarzen Meer.

Im Gegensatz zum Kyllaren Fjord (und dem Schwarzen Meer) erfolgt in den anoxischen Becken der Ostsee eine starke Mo- und schwache U-Isotopenfraktionierung zwischen Wasser und Sediment. Von diesen neuen Kenntnissen leiten wir ab, dass durch die regelmäßig auftretenden Spülereignisse mit sauerstoffreichem Wasser die ursprünglichen anoxischen Mo- und U-Isotopensignaturen der Sedimente verändert wurden. Dies geschah möglicherweise aufgrund von mehreren Remobilisierungen von Mo und U durch oxisches Porenwasser und einer anschließenden Wiederausfällung unter anoxischen Bedingungen. Diese Schlussfolgerungen zeigen, dass die Sedimente durchgehend anoxischen Bedingungen ausgesetzt sein müssen, um eine Mo- und U-Isotopensignatur von den Redoxbedingungen während der Ablagerungen zu speichern.

Uranisotopenfraktionierung während der hydrothermalen Alteration von der ozeanischen Kruste

In Kapitel 5 behandelten wir die Frage, ob eine Uranisotopenfraktionierung während des Austrages von Uran aus Meerwasser am mittelozeanischen Rücken durch

die Alteration der ozeanischen Kruste erfolgt. Deshalb untersuchten wir hydrothermale Fluide aus dem Juan de Fuca-Rücken (niedrig- und hoch-temperierte Fluide), alterierte Basalte und die dazu gehörigen Kalziumkarbonate aus dem Pigafetta Becken, Bermuda Rise und dem Reykjanesrücken (ODP-Proben). Die hydrothermalen Fluide zeigen niedrige Urankonzentrationen (0.3 nM bis 1 nM) und eine variable Uranisotopenzusammensetzung ($\delta^{238}U$ = -0.59 ‰ bis -0.28 ‰). Aufgrund der niedrigen Urankonzentrationen und dem geringen verfügbaren Probenmaterial, ist die Unsicherheit im $\delta^{238}U$ für die hydrothermalen Fluide wesentlich größer als für bisherige untersuchte Meerwasserproben (Weyer et al., 2008). Die alterierten Basalte und die Kalziumkarbonate zeigen eine größere Uranisotopenfraktionierung zu einer schweren und leichten Uranisotopenzusammensetzung ($\delta^{238}U$ zwischen -0.63 ‰ und 0.27 ‰) und sind außerdem teilweise in deren Urankonzentration angereichert, verglichen mit nicht-alterierten Basalten.

Durchschnittlich zeigen hydrothermale Fluide eine etwas leichtere Uranisotopenzusammensetzung als Meerwasser ((-0.43 ± 0.25) ‰ vs. (-0.37 ± 0.03) ‰). Die stärkste Isotopenfraktionierung für alterierte Basalte verglichen mit frischen Basalten und Kalziumkarbonaten in den Gängen verglichen mit Meerwasser erfolgt hin zu einer schwereren Uranisotopenzusammensetzung. Diese Ergebnisse sind in Übereinstimmung mit einem Modell, das annimmt, dass die beobachtete Isotopenfraktionierung hauptsächlich ein Ergebnis von Redoxprozessen ist, z.B. die partielle Reduktion von löslichem U^{VI} aus dem Meerwasser während der hydrothermalen Alteration, was zu einer Anreicherung der schweren Uranisotope in der reduzierten Uranspezies (U^{IV}) führt und 2) das bevorzugte Entfernen von U^{IV} aus dem hydrothermalen Fluid und der Einbau in die alterierte ozeanische Kruste. Durch diesen Prozess wird das hydrothermale Fluid an schweren Uranisotopen verarmt und somit würden auch die alterierten Basalte und Karbonate ein niedriges $\delta^{238}U$ aufweisen, wenn sie mit dem isotopisch leichten hydrothermalen Fluid in Kontakt gekommen sind. Unsere ersten Ergebnisse sind definitiv nicht ausreichend, um die Prozesse am mittelozeanischen Rücken im Detail zu verstehen, aber sie deuten darauf hin, dass während der Uranabnahme am mittelozeanischen Rücken nur eine geringe

Uranisotopenfraktionierung erfolgt, verglichen mit der, die in anoxischen Becken erfolgt.

Uranisotopenfraktionierung in einem Tiefenprofil aus einem Uran-Tailing

Als eine Fallstudie untersuchten wir in Kapitel 6, ob die Uranisotopenzusammensetzung eine Möglichkeit bietet, um die Uranmobilisierung in Tailings aus Erzabbaugebieten zu verfolgen. Wir analysierten einen uranreichen Sedimentkern aus einem Tailing von einem ehemaligen Uranabbaugebiet in Schneckenstein (Deutschland). Das Tiefenprofil zeigte Korrelationen zwischen der Urankonzentration und der Uranisotopenzusammensetzung im Sediment an. Die stärkste Urananreicherung von 4.73 mg/g erfolgte zusammen mit der schwersten $\delta^{238}U$, -0.16 ‰, bei einer Tiefe von 25 cm. Möglicherweise wurde Uran im oberen Bereich des Tiefenprofils mobilisiert, aber wurde bei einer bestimmten Tiefe wieder ausgefällt, als die Bedingungen anoxischer wurden. Eventuell erfolgt die Uranreduktion in dem Bereich der Fe-Reduktion (und Mobilisierung) oder der Sulfatreduktion. Allerdings können auch Mikroorganismen eine Rolle bei der Uranreduktion spielen. Weitere Untersuchungen sind notwendig, um diese Hypothesen genauer diskutieren zu können.

Uranisotopenzusammensetzung von terrestrischen Uranmineralen

Bei vorangegangen Studien war eine Korrelation zwischen dem $\delta^{238}U$ und dem Valenzzustand von Uransedimenten (U^{IV} und U^{VI}) beobachtet worden (Stirling et al., 2007; Weyer et al., 2008). U^{IV}-Sedimente, z.B. Black Shales aus dem Schwarzen Meer,

zeigten eine eindeutige Tendenz zu einer schwereren Uranisotopenzusammensetzung, im Vergleich zu U^{VI}-Sedimenten, z.B. Fe-Mn-oxide oder BIFs, die eine deutlich leichtere Uranisotopenzusammensetzung aufweisen. Dementsprechend ging es in diesem Kapitel um die Frage, ob es diese eindeutige Zuordnung des $\delta^{238}U$ auch bei Mineralen in unterschiedlichen Uranoxidationsstufen gibt. Es wurden U^{IV}- und U^{VI}-Minerale und uranvererzte Gesteine auf deren Uranisotopenzusammensetzung hin untersucht. Dabei zeigten U^{IV}-Minerale ein $\delta^{238}U$ zwischen 0.01 ‰ und -0.29 ‰ und U^{VI}-Minerale ein $\delta^{238}U$ zwischen -0.02 ‰ und -0.50 ‰. Auch wenn die U^{IV}-Minerale im Durchschnitt eine etwas schwerere Uranisotopenzusammensetzung im Vergleich zu den U^{VI}-Mineralen aufweisen, so zeigt die Überlappung im $\delta^{238}U$, dass das $\delta^{238}U$ nicht nur vom Valenzzustand des Urans abhängt. Vielmehr scheinen andere Prozesse, wie die Koordinierung des Urans in den Mineralen oder ein variables $\delta^{238}U$ in dem ursprünglichen Material, aus dem das Mineral hervorgegangen ist, stärkeren Einfluss auf das $\delta^{238}U$ zu haben. Die uranvererzten Gesteine zeigten die größten Variationen im $\delta^{238}U$ von -0.46 ‰ bis 0.43 ‰. Dementsprechend könnte das $\delta^{238}U$ von diesen Proben besonders wertvoll sein, um die Prozesse der Urananreicherung besser zu verstehen, wenn man von diesen Proben weitere physikalische und chemische Eigenschaften kennt.

Ausblick

Unser Verständnis im Hinblick auf die Parameter, die eine Uranisotopenfraktionierung in unterschiedlichen anoxischen und oxischen Bedingungen kontrollieren, konnte durch diese Arbeit bedeutend verbessert werden. Insbesondere in Kapitel 4, da es einen Vergleich zu dem bereits besser verstandenen Molybdän Isotopensystem enthält. Die Ergebnisse dieses Kapitels zeigen, dass sich Uran- und Molybdänisotope in stark euxinischen Wassersäulen ($c(H_2S)$ > 11 µmol/L)

entgegengesetzt verhalten. Dementsprechend ergänzen sich die beiden Isotopensysteme und können genutzt werden, um die Ablagerungsbedingungen in abgeschlossenen Becken und die Redoxentwicklung des Paläoozeans zu untersuchen.

Weitere Studien sollten sich beispielsweise mit der Uranisotopenzusammensetzung und Uranspeziation (U^{IV} oder U^{VI}) von Porenwasser und dem dazu gehörigen Sedimenteprofil beschäftigen, um den Mechanismus des Uranaustrages aus einer Wassersäule besser verstehen zu können. Weiterhin könnte die Uranreduktion und Uranmobilisierung durch Experimente besser verstanden werden. Solche Untersuchungen könnten einen größeren Einblick in den Mechanismus während der Uranremobilisierung oder des Uranaustrages liefern, beispielsweise ob der Uranaustrag oder die Uranremobilisierung durch eine bestimmte chemische Zusammensetzung des Porenwassers, die Gegenwart von bestimmten Partikeln oder organischen Komplexen ausgelöst wird oder durch Mikroorganismen stimuliert wird.

Außerdem wäre es interessant, die Uranisotopenzusammensetzung in Flüssen durch Vergleich des gelösten Urans mit dem des Flusswasserfilters und Untersuchung des dazugehörigen Gesteins weiter zu verfolgen. Ein weiterer Aspekt ist die hier schon kurz beschriebene Untersuchung der Uranmobilisierung in der Umwelt mithilfe von Uranisotopen in Bergbauregionen, die gezeigt hat, dass noch viel Potential für weitere Studien vorhanden ist.

CHAPTER 1

Introduction

1.1 Purpose of this study and structure of the thesis

Uranium is a redox sensitive trace element, which was recently shown to fractionate its main primordial isotopes, ^{238}U and ^{235}U, in near surface terrestrial environments. However, little is currently known on the isotopic behavior of dissolved U in the water column under redox changing conditions (anoxic restricted basins, e.g. Black Sea or Baltic Sea) or during weathering of the continental crust. The main purpose of this study is to explore the parameters and mechanisms that govern U isotope fractionation in near surface environments and constrain the oceanic U cycle. Therefore, samples from the continental crust, rivers, hydrothermal fluids, the oceanic crust (Ocean Drilling Program, ODP, samples), anoxic basins (Baltic Sea and an anoxic fjord from Norway) and a former U mine tailing has been analyzed and will be discussed.

This thesis is subdivided into five sample chapters, preceded by an introduction (Chapter 1) and an overview of the applied methodology (Chapter 2). The introduction will give an overview about the current state of U and U isotope research.

Chapter 3 will present the results (trace element concentrations and the U isotope composition) from the analyses of rivers and the continental crust and will discuss possible sources for the isotopic variations in rivers and the continental crust, and the consequences for the oceanic U cycle.

Chapter 4 will present the results from water column and sediment samples from two modern anoxic basins: the Kyllaren fjord from Norway and the Gotland and Landsort Deeps from the Baltic Sea. As molybdenum shows strikingly similar behavior under these conditions, we also determined the Mo isotope composition for these samples for comparison. The combination of Mo and U isotope composition may give further insight into the parameters that control the U isotope composition in those settings. This chapter contains isotopic data, $\delta^{238}U$ for U and $\delta^{98}Mo$ for Mo, and trace element concentrations for iron, aluminum, manganese, rhenium, molybdenum and uranium for organic-rich sediments (core 342390-2-7) from Landsort Deep, which were obtained by Carolina Monotya-Pino and already presented in her thesis (Frankfurt, Germany, November 2011). These data are suitable as a comparison to our water samples from the Baltic Sea. In addition, we are planning on submitting the results from Chapter 4 to a peer-reviewed journal.

Chapter 5 will present the results (trace element concentrations and the U isotope composition) of hydrothermal fluids, hydrothermally altered oceanic crust (ODP samples) and their leached calcium carbonate veins to discuss the possibility of U isotopes being fractionated during hydrothermal alteration (second most important sink for U from the ocean). For comparison with fresh basalts, we determined the U isotope composition of ocean island basalts (OIB) from the Canary Islands (Tenerife and La Palma) and a volcanic region in Germany (Vogelsberg).

Chapter 6 will present the results (U concentrations and $\delta^{238}U$) of soil samples from different depths and water samples from a former U mine tailing in Schneckenstein (Germany). This chapter will discuss the usefulness of U isotopes to trace back U mobilization in the environment.

Chapter 7 will present the results of U minerals (U^{IV}, U^{VI} and mineralized bedrock) in order to investigate U isotope variations that are related to the valence state and bonding environment of U.

This chapter is followed by an overall conclusion, together with an outlook for possible further studies.

1.2 Characteristics of uranium and its isotope ratios

Uranium is the heaviest naturally occurring element on Earth (Stirling et al., 2007) and three U isotopes occur in nature, ^{238}U, ^{235}U and ^{234}U, which are all radioactive (α-emitter), though ^{238}U and ^{235}U are primordial: ^{238}U has the highest abundance and the longest half-life with 99.27 % and $4.5 \cdot 10^9$ a, respectively. ^{235}U has only an abundance of 0.72 % and a half-life of $0.7 \cdot 10^9$ a. The third naturally occurring U isotope is ^{234}U, which only occurs as a decay product of ^{238}U, has an abundance of 0.0054 % and a half-life of $2.46 \cdot 10^5$ a.

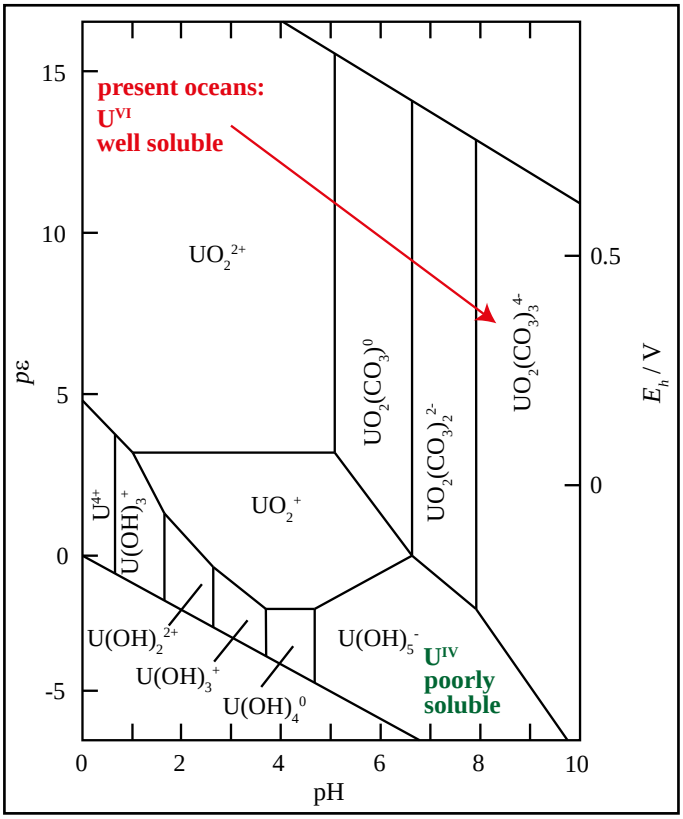

Fig. 1.1 Thermodynamic stability of U species at typical ground water CO_2 pressure of 10^{-2} bar in a pourbaix diagram (reduction potential, $p\varepsilon$ or E_h, vs. pH; modified after Langmuir, 1978).

Uranium is a redox-sensitive trace metal, which commonly occurs in two redox-states (U^{IV} and U^{VI}). Under oxygenated conditions (e.g. in the modern ocean), it forms soluble and non-reactive complexes with carbonate (e.g. $[UO_2(CO_3)_3]^{4-}$) and under more reducing conditions, it forms insoluble U^{IV} complexes (e.g. $U(OH)_5^-$), which can further precipitate as uraninite (UO_2). However, the speciation in aqueous solution depends on the redox potential (e.g. E_h or pε), pH and the available amount of dissolving complexing agents (Fig. 1.1, modified after Langmuir, 1978).

Due to the high incompatibility of U in mantle minerals, the continental crust is highly enriched in U to mass fractions in the lower µg/g range. Rivers transport the weathered and eroded continental crust to the ocean. As a result of the long ocean residence time ($5 \cdot 10^5$ a, Colodner et al., 1995) compared to the ocean mixing time ($1.6 \cdot 10^3$ a), U is homogeneously distributed in the ocean. Also, the ocean contains a U concentration that is a factor of 14 higher than in rivers (3.3 ng/g vs. 0.24 ng/g), which is mainly a result of the solubility of U complexes depending on the pH. Uranium is removed from the ocean into four sinks: the two major sinks are organic-rich suboxic sediments at continental margins (a large fraction of the U is likely buffered in carbonates) and altered oceanic crust through hydrothermal circulation at mid-ocean ridges (Fig. 1.2). The two minor sinks are oxic sediments, e.g. ferromanganese crust, and euxinic sediments, e.g. organic-rich sediments that will become black shales during diagenesis (Fig. 1.2). The removal of U under reducing conditions is usually triggered by microorganisms (Klinkhammer and Palmer, 1991), whereby it can form different complexes with oxygen and fluoride (Algeo and Maynard, 2004).

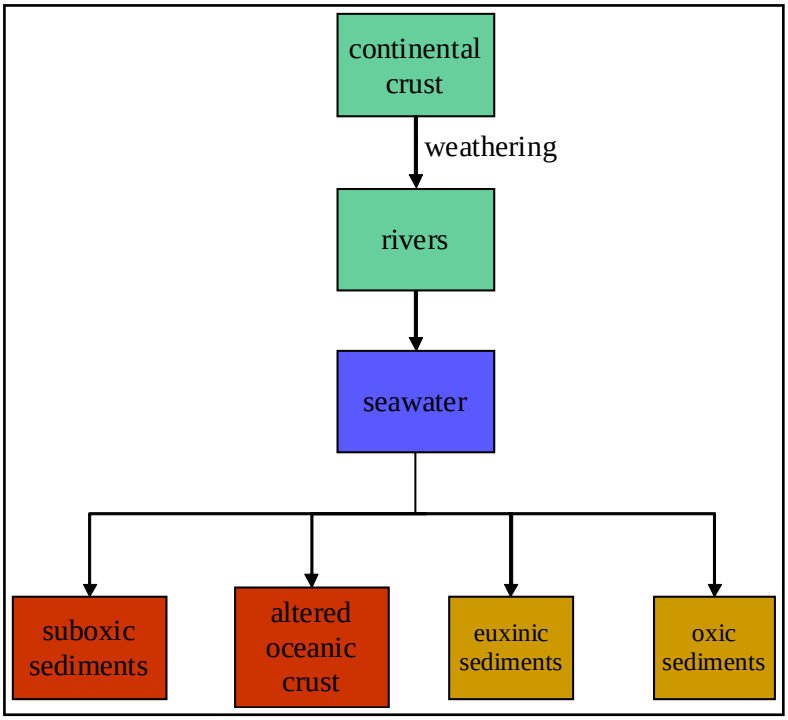

Fig. 1.2 Sources and sinks for the global oceanic uranium cycle (Chen et al., 1986; Morford and Emerson, 1999). The size of the errors and rectangles of the sinks represents the importance of the respective sinks.

Until recent studies from Stirling et al. (2007) and Weyer et al. (2008), it was assumed that ^{238}U and ^{235}U do not fractionate during chemical reactions, resulting in a canonical value for $n(^{238}U) / n(^{235}U)$, which was assumed to be 137.88. This value is (still) commonly used for U-Pb dating of zircons and other U enriched minerals. The assumption that no U isotope fractionation should occur, was based on the small $\Delta m/m^2$ between $M(^{238}U)$ and $M(^{235}U)$ that results in negligible mass-dependent isotope fractionation. However, the studies from Stirling et al. (2007) and Weyer et al. (2008) revealed surprisingly large $n(^{238}U) / n(^{235}U)$ isotope fractionation of ≈ 1.3 ‰ within terrestrial samples, mainly from the marine environment. Theoretical calculations by Bigeleisen (1996) and Schauble (2007) strongly suggested that an isotope fractionation for U can be caused by the nuclear volume dependent fractionation, also called the nuclear field shift. This mechanism only appears to be dominant for the heavier elements (e.g. Hg, Tl, U), where the mass dependent fractionation is negligible.

However, it results in an opposite isotope effect as the mass dependent isotope fractionation, since the heavier isotope will be located in the species where the electron density is the smallest, U^{IV}, as shown for a couple of terrestrial samples by Weyer et al. (2008).

The measured isotope ratios are usually reported in the delta notation, i.e. the relative difference between the samples and a standard (NIST SRM 950-A or NBL CRM 112-A) given in ‰ (Eq. 1.1).

$$\delta^{238/235}\mathrm{U} \,/\, ‰ = \left[\frac{\left(n(^{238}\mathrm{U}) \,/\, n(^{235}\mathrm{U}) \right)_{\mathrm{sample}}}{\left(n(^{238}\mathrm{U}) \,/\, n(^{235}\mathrm{U}) \right)_{\mathrm{standard}}} - 1 \right] \times 1000 \qquad \text{Eq. 1.1}$$

Weyer et al. (2008) showed that seawater has a homogeneous and light U isotope composition, with $\delta^{238}U$ = -0.41 ‰ ± 0.03 ‰ (relative to NIST SRM 950-A at 95 % confidence level). Additionally, they determined the range for the continental crust, by measuring granites and basalts (however only a small number of samples), which resulted in an average value of -0.31 ‰ ± 0.16 ‰ (Weyer et al., 2008). The suboxic sediments displayed the same range as the granites and basalts, with $\delta^{238}U$ between -0.16 ‰ and -0.41 ‰, which results in an average of -0.29 ‰ ± 0.19 ‰ (Weyer et al., 2008). The largest isotopic spread has been observed between samples that formed under euxinic conditions (represented by black shales from the Black Sea) and those deposited under oxic conditions (i.e. ferromanganese crust and banded iron formations: BIFs). Under reducing conditions, the forming sediments can be distinguished into suboxic (e.g. 10^{-5} to 10^{-4} mol O_2 L^{-1}), anoxic (< 10^{-6} mol H_2S L^{-1}, < 10^{-5} mol O_2 L^{-1}) and euxinic (e.g. ≥ 10^{-6} mol H_2S L^{-1}, 0 mol O_2 L^{-1}) sediments, according to the composition of the depositional environment. The investigated black shales contain, with essentially all U occurring in the valence state of IV, the heaviest U isotope composition, with $\delta^{238}U$ ranging between -0.06 ‰ and 0.43 ‰ (Weyer et al., 2008). In contrast, the oxic sediments (containing U^{VI}) are in average 0.2 ‰ isotopically lighter than seawater, with $\delta^{238}U$ ranging between -0.52 ‰ and -0.89 ‰ and one exceptional BIF sample at -0.29 ‰ (Weyer et al., 2008).

The underlying idea for the here presented in-depth investigation of U isotope fractionation was that U isotopes may be used as a paleo-redox proxy, i.e. for the determination of redox changes in the paleo-ocean. The prerequisites to use U isotopes as a paleo-redox proxy are (1) that U is homogeneously distributed in the ocean (i.e. that the ocean residence time was much larger than the ocean mixing time), (2) a strong fractionation of U isotopes between oxic and reducing conditions (oxic compared to euxinic sediments) and (3) the current modern oceanic U cycle has to be completely known and understood.

Therefore, this thesis aims to improve the modern oceanic U isotopic mass balance by the determination of $\delta^{238}U$ in the following reservoirs: 1) Rivers are investigated to verify the assumption that there is no U isotope fractionation during the weathering and transport of the continental crust to the ocean. 2) The hydrothermal alteration of the oceanic crust is investigated by the analyses of hydrothermal water and altered oceanic crust to verify that this sink from the ocean does not result in an U isotope fractionation. 3) Additionally, the conditions that result in the strong U isotope fractionation in sediments of restricted basins needs to be better understood, to be able to compare the isotope signatures of ancient sediments with those of modern environments. For this purpose, modern stratified water columns (e.g. basins within the Baltic Sea and the Kyllaren fjord from Norway) and respective sediments have been investigated. As the Mo isotope system is already better understood in such environments, the molybdenum isotope composition was also determined and reported as $\delta^{98}Mo$ (after Eq. 1.2).

$$\delta^{98/95}\mathrm{Mo} \,/\, ‰ = \left[\frac{\left(n(^{98}\mathrm{Mo}) \,/\, n(^{95}\mathrm{Mo})\right)_{\mathrm{sample}}}{\left(n(^{98}\mathrm{Mo}) \,/\, n(^{95}\mathrm{Mo})\right)_{\mathrm{standard}}} - 1\right] \times 1000 \qquad \text{Eq. 1.2}$$

Molybdenum is also a redox-sensitive trace element, which behaves very similar to U, e.g. occurs in two redox-states (Mo^{IV} and Mo^{VI}). Under oxic conditions it also behaves conservative with a long ocean residence time of 0.8 Ma (vs. 0.5 Ma for U, Morford and Emerson, 1999). Molybdenum is the most abundant transition metal in modern seawater (105 nmol · kg^{-1} H_2O, Morris, 1975; Bruland, 1983; Collier, 1985). However, under strongly euxinic conditions ($c(H_2S)$ > 11 µmol/kg, “geochemical

switch", Helz et al., 1996; Erickson and Helz, 2000) Mo becomes particle-reactive and gets quantitatively removed from the water column via multiple thio-molybdate-species (MoO_3S^{2-}, $MoO_2S_2^{2-}$, $MoOS_3^{2-}$, MoS_4^{2-}). Molybdenum isotopes have already been widely used to model paleo-redox conditions (e.g. Arnold et al., 2004; Kendall et al., 2009). Therefore, the measurement of Mo isotopes reveals if the conditions were constantly euxinic during deposition of the sediments. Thereby, combining U with Mo isotopes results in a deeper knowledge of the conditions that triggers U isotope fractionation.

1.3 The fractionation mechanisms of uranium isotopes

The isotope fractionation of elements is caused by two kinds of shifts: (1) the mass shift that depends on the interaction of the motion of the nuclei and the electrons or (2) a field shift that depends on the difference in nuclear sizes and shapes of isotopes (Bigeleisen, 1996). Depending on the reaction, we can distinguish between two kinds of mechanisms: equilibrium and kinetic effects. If in a certain reaction the reaction rate of the back and forth reaction is identical, then a chemical equilibrium is reached (e.g. phase equilibrium, exchange reactions). The most important characteristics of an equilibrium fractionation are: (1) the heavier isotope favors the reaction product with the stronger bond and with atoms with a high ionic potential and low atomic mass; (2) an equilibrium fractionation usually depends on the temperature and not on other functions of state (e.g. pressure); (3) if the temperature is lower than 100 °C, then the fractionation factor is proportional to $1/T$. At higher temperatures it is proportional to $1/T^2$. A kinetic fractionation will occur if the chemical equilibrium is not reached, e.g. during diffusion, evaporation, dissolution, precipitation or biological processes. In this case, the fractionation is of kinetic origin and its magnitude is either controlled by the difference in vibrational or kinetic energy of both reagents and activated complex (Bigeleisen and Mayer, 1947; Urey, 1947; Bigeleisen, 1965; Hoefs, 2004).

The mass shift depends on quantum mechanical effects that occur during chemical reactions (e.g. translational, rotational and vibrational energy of the nuclides). However, the vibrational energy plays the largest role for the mass shift. It increases with $\delta M/M^2$ and therefore becomes negligible for elements with an atomic number of ≥ 40 (Bigeleisen, 1996).

For the heavier elements, especially uranium, the nuclear field shift is the dominant reason for an isotope fractionation, as the mass shift affect is negligible. The nuclear field shift depends on the differences in the electronic energy due to the differences in nuclear sizes and shapes of isotopes (Bigeleisen, 1996). A lighter isotope is smaller in size and has a larger surface charge density compared to a heavier isotope, which results in a lower electronic energy for the lighter isotope. The effect of the nuclear field shift depends however on two factors: (1) the electron densities at the nucleus and (2) the charge, size and shape of the nucleus and the change of the latter two factors between a chemical reaction (Bigeleisen, 1996). Due to the nuclear field shift, heavier isotopes will be located in the species where the electron density is the smallest, i.e. with the fewer number of *s* electrons in the bonding or valence orbital or where the s electrons are shielded by a larger number of *p*, *d* or *f* electrons. For heavy elements, like U, *f* electrons play a major role, when it comes to a change in the oxidation state, which usually triggers an isotope fractionation. However, *f* electrons are able to shield *s* electrons and therefore a decrease in the electronic density occurs during the reduction of U^{VI} ($[Rn]5f^0$) to U^{IV} ($[Rn]5f^2$). Thus, the two remaining *f* electrons in the U^{IV} species will shield the *s* electrons and favor the heavier isotope, ^{238}U. This result is actually in contrast to a mass shift, where the reduced species would be enriched in the lighter isotope.

CHAPTER 2

Methodology

2.1 Sample preparation

The whole sample preparation was carried out in a clean lab facility in the University of Frankfurt and the University of Hannover.

For organic-rich sediments, e.g. post-Archean shales from Australia (Chapter 3), sediments from the Kyllaren fjord (Chapter 4) and soil samples from Schneckenstein (Chapter 6), about 300 mg were ashed in ceramic vessels at 550 °C overnight to remove the organic compounds. Afterwards, these samples were, just like the granites (Chapter 3) and basalts (Chapter 5), digested with a mixture of concentrated $HF/HNO_3/HClO_4$ (3:1:1) in Parr® high-pressure vessels at 180 °C. Samples were repeatedly treated with 6 M HNO_3 and 6 M HCl to dissolve any remaining fluorides (modified after Weyer et al., 2008).

Water samples from the rivers (Chapter 3), Kyllaren fjord (Chapter 4), Baltic Sea (Chapter 4), hydrothermal fluids (Chapter 5) and a former tailing area (Chapter 6), were filtered through a 0.45 µm filter. Usually, the volume was gently reduced to about 10 mL on a hot plate. If this resulted in a clear solution (e.g. rivers), concentrated nitric acid was added to adjust acidity to 3 M HNO_3 for U purification. However, some samples formed crystals during the evaporation process and were re-dissolved with 15 M HNO_3 and 30 % H_2O_2 or additionally with 6 M HCl.

After complete digestion, the samples were finally re-dissolved in 3 M HNO_3 for the purification of U from the sample matrix, by anion exchange chromatography (based on eichrom®, now Triskem, UTEVA® resin, following the procedure, described by Weyer et al., 2008). After determining the trace element concentrations, especially U concentration, an appropriate amount of U double-spike solution (IRMM 3636-A: see description in Chapter 3 and supplementary documents within Chapter 4 for details of the spike calibration) was added to the sample solution and then U was purified from the sample matrix.

The sediment samples from the Kyllaren fjord were split into two equal aliquots after digestion to use one aliquot for U separation and the other one for Mo separation. Separation of Mo from the sample matrix was achieved by a two-step chromatographic purification (on anion and cation columns, following the procedure outlined in Anbar et al., 2001). The applied protocol for this purification can be found in the appendix of this chapter (Table A 2.1, Table A 2.2 and Table A 2.3).

As the water samples from the Kyllaren fjord and the Baltic Sea contained only a limited amount of Mo and U, we separated and purified Mo and U from the same aliquot. For this, we quantitatively collected the matrix (including the Mo fraction) from U purification (on eichrom® UTEVA® resin) to subsequently reload it on columns with anion and cation exchange resins for the purification of Mo. As we did not use a Mo double spike to monitor potential Mo isotope fractionation during sample preparation and analyzes, we performed extensive tests with synthetic seawater, in order to ensure 100 % recovery, particularly for Mo. These tests revealed overall yields of 100 % ± 5 % Mo during the procedure. In contrast, switching the order of U and Mo purification resulted in very poor and non-reproducible yields for U and was thus emerged as an unsuitable procedure.

2.2 Mass spectrometry

2.2.1 Trace element analyses

The determination of trace elements (e.g. Fe, Al, Mn, Re, Mo and U) was carried out with a Thermo Fisher Scientific Element 2 (at the Goethe University of Frankfurt), which is an inductively coupled plasma mass spectrometer (ICP-MS). Usually, a sample aliquot of ~ 5 % was taken from the digested sample and further diluted with 2 % HNO_3, which already contained 10 ng/g indium (as In was used as an internal standard). The sample was introduced with a 50 µL/min nebulizer and a glass spray chamber. The mass spectrometer was tuned to yield an intensity of $\approx 1 \cdot 10^6$ cps on ^{115}In in a 1 ng/g In solution in low resolution. Additionally, the intensity of uranium oxide was monitored to ensure that the oxide formation rate was less than 5 %. The mass spectrometer was tuned with a multi elemental standard solution and during the measurements the standard SDO-1, a certified USGS Ohio Devonian Shale, has been measured repeatedly. Trace element concentrations were determined by comparison of the blank corrected (2 % HNO_3) and ^{115}In-normalized signal intensity of an element of interest in the sample with that of the same element in the standard (e.g. USGS SDO-1 or other standards with known trace element concentrations).

2.2.2 Molybdenum and U isotope analyses

The determination of the molybdenum isotopic composition was carried out with a Thermo Fisher Scientific Neptune (at the Goethe University of Frankfurt and the Leibniz University of Hannover), which is a multicollector inductively coupled plasma mass spectrometer (MC-ICP-MS). Molybdenum has seven stable naturally occurring isotopes (with their natural abundances given in brackets): ^{92}Mo (14.77 %), ^{94}Mo (9.23 %), ^{95}Mo (15.90 %), ^{96}Mo (16.68 %), ^{97}Mo (9.56 %), ^{98}Mo (24.19 %) and ^{100}Mo (9.67 %). However, some Mo isotopes are affected by isobaric mass interferences, e.g.

^{96}Mo by ^{40}Ar^{56}Fe. Therefore, the samples were purified by a two-step chromatographic purification method. Molybdenum isotopes were analyzed at wet plasma conditions using an Elemental Scientific SSI glass spray chamber combined with a 50 µL PFA nebulizer. The instrument was equipped with aluminum skimmer and sample cones. In general, all sediment and most of the water samples were measured at mass fractions of 400 ng/g Mo, which resulted in a signal of ~ 3 V on ^{98}Mo. Prior to the isotope measurements, all standards and samples were "spiked" with a solution of natural Zr (Specpure Lot#13716055), which was used to monitor and correct for instrumental mass-bias, assuming an exponential fractionation within the mass spectrometer and applying the exponential law (Eq. 2.2. and Eq. 2.3), with $n(^{90}\mathrm{Zr}) / n(^{91}\mathrm{Zr}) = 4.58421$ (Anbar et al., 2001; Barling et al., 2001). The used cup configuration can be found in the appendix of this chapter (Table A 2.4). In addition to the measurement of six Mo isotopes ($n(^{92}\mathrm{Mo})$, $n(^{95}\mathrm{Mo})$, $n(^{96}\mathrm{Mo})$, $n(^{97}\mathrm{Mo})$, $n(^{98}\mathrm{Mo})$, $n(^{100}\mathrm{Mo})$), we also measured two Zr isotopes ($n(^{90}\mathrm{Zr})$, $n(^{91}\mathrm{Zr})$) and one ruthenium isotope ($n(^{99}\mathrm{Ru})$), as there are interferences between Zr and Ru isotopes with Mo isotopes. Therefore, we applied an interference correction with the canonical ratios from IUPAC for $n(^{92}\mathrm{Mo})$, $n(^{96}\mathrm{Mo})$, $n(^{98}\mathrm{Mo})$ and $n(^{100}\mathrm{Mo})$ (Eq. 2.1). The mass fraction of Zr was adjusted to about half of the Mo mass fraction. Samples were measured relative to the Johnson Matthey Specpure® Mo plasma standard (Lot #802309E; here called "Roch Mo2"), which was already used in previous studies (Anbar et al., 2001; Barling et al., 2001; Arnold et al., 2004; Kendall et al., 2009). The results of the isotopic measurements are expressed in the delta-notation (Eq. 2.4).

$$n\left(^{98}\mathrm{Mo}\right) = n\left(^{98}\mathrm{Mo}\right)_{\mathrm{measured}} - \frac{n\left(^{99}\mathrm{Ru}\right)_{\mathrm{measured}}}{\left(\frac{n\left(^{99}\mathrm{Ru}\right)}{n\left(^{98}\mathrm{Ru}\right)}\right)_{\mathrm{IUPAC}}} \qquad \text{Eq. 2.1}$$

$$\left(n\left(^{98}\mathrm{Mo}\right) / n\left(^{95}\mathrm{Mo}\right)\right)_{\mathrm{true}} = \left(n\left(^{98}\mathrm{Mo}\right) / n\left(^{95}\mathrm{Mo}\right)\right)_{\mathrm{measured}} \times \left(\frac{M\left(^{98}\mathrm{Mo}\right)}{M\left(^{95}\mathrm{Mo}\right)}\right)^{\beta} \qquad \text{Eq. 2.2}$$

$$\beta = \frac{\ln\left(\frac{\left(n\left(^{90}\mathrm{Zr}\right) / n\left(^{91}\mathrm{Zr}\right)\right)_{\mathrm{IUPAC}}}{\left(n\left(^{90}\mathrm{Zr}\right) / n\left(^{91}\mathrm{Zr}\right)\right)_{\mathrm{measured}}}\right)}{\ln\left(\frac{M\left(^{90}\mathrm{Zr}\right)}{M\left(^{91}\mathrm{Zr}\right)}\right)} \qquad \text{Eq. 2.3}$$

$$\delta^{98/95}\mathrm{Mo}/\,‰ = \left[\frac{\left(n(^{98}\mathrm{Mo})\,/\,n(^{95}\mathrm{Mo})\right)_{\mathrm{sample}}}{\left(n(^{98}\mathrm{Mo})\,/\,n(^{95}\mathrm{Mo})\right)_{\mathrm{standard}}} - 1\right] \times 1000 \qquad \text{Eq. 2.4}$$

Similar to Barling et al. (2001) the samples were analyzed by standard bracketing in triplicates interleaved with the Johnson Matthey Specpure® Mo plasma standard, "Roch Mo2". Occasional runs of a Devonian Ohio shale (USGS SDO-1, δ^{98}Mo = 1.1 ‰) and a gravimetrically prepared standard (Grav Rochester Mo2, δ^{98}Mo = -1.0 ‰) ensured that instrumental conditions are stable (reference values for these standards are published in Barling et al., 2001 and Kendall et al., 2009). The reproducibility of the Mo standards "Roch Mo2", "Grav Roch Mo2" and "USGS SDO-1" are shown in Fig. 2.1 and Fig. 2.2.

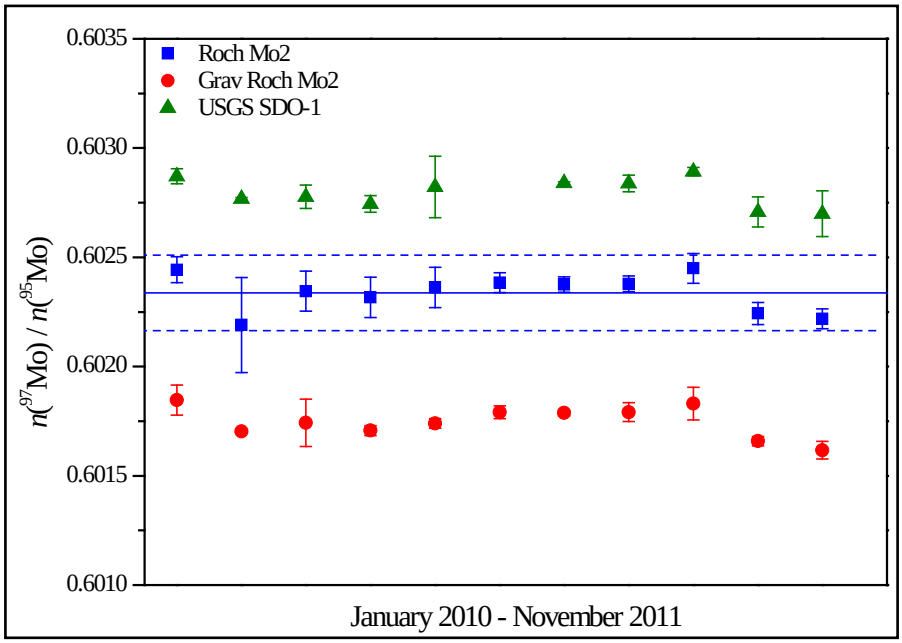

Fig. 2.1 Reproducibility of the $n(^{97}\mathrm{Mo})$ / $n(^{95}\mathrm{Mo})$ ratio of the standard "Roch Mo2", in comparison to that of other Mo standards "Grav Roch Mo2" and "USGS SDO-1" for individual measurements between January 2010 and November 2011. The blue straight line indicates the average for "Roch Mo2" ($n(^{97}\mathrm{Mo})$ / $n(^{95}\mathrm{Mo})$ = 0.6023) of all sessions and the blue dashed lines indicate the double standard deviation of 0.0002.

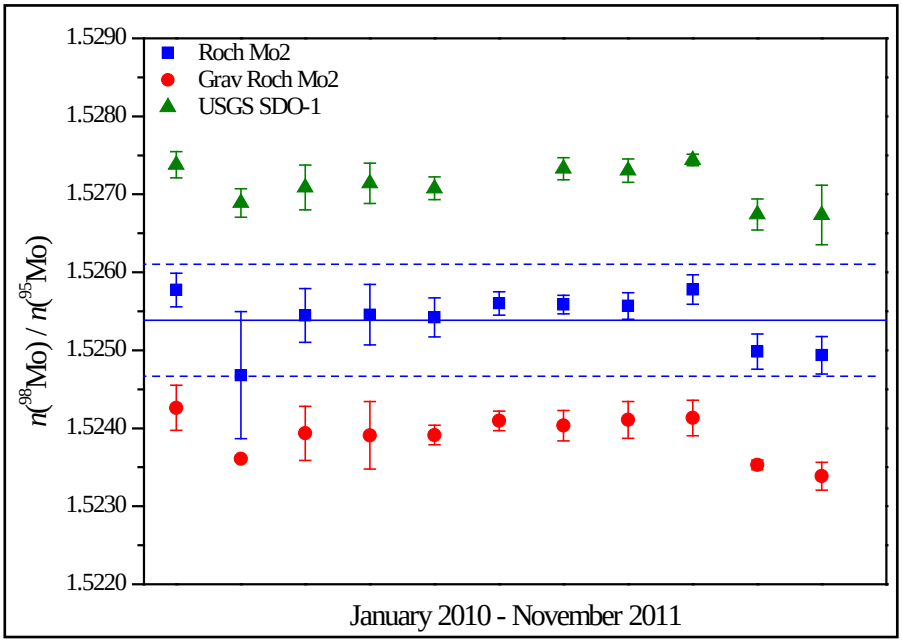

Fig. 2.2 Reproducibility of the $n(^{98}Mo)$ / $n(^{98}Mo)$ ratio of the standard "Roch Mo2", in comparison to that of other Mo standards "Grav Roch Mo2" and "USGS SDO-1" for individual measurements between January 2010 and November 2011. The blue straight line indicates the average for "RochMo2" ($n(^{98}Mo)$ / $n(^{98}Mo)$ = 1.5254) of all sessions and the blue dashed lines indicate the double standard deviation of 0.0007.

The measurements of the U isotopes (^{233}U, ^{235}U, ^{236}U and ^{238}U) were also performed on a Thermo Fisher Scientific Neptune MC-ICP-MS at the University of Frankfurt and the Leibniz University of Hannover, similar as outlined in Weyer et al. (2008). The used cup configuration can be found in the appendix of this chapter (Table A 2.5). The instrument was equipped with a nickel skimmer X cone and an aluminum sample cone. The measurements were performed using a CETAC Aridus™ desolvating nebulizer system combined with a 50 µL PFA nebulizer for sample introduction. The Aridus™ was usually adjusted to 4 L/min argon and 5 mL/min nitrogen. Sample analyses were first performed relative to the U standard NIST SRM 950-A. However, as this standard is no longer available, we obtained the U standard NBL CRM 112-A, and performed a thorough cross calibration through repeated measurements of both standards (over several months). These measurements revealed that NBL CRM 112-A

seems to be slightly offset relative to NIST SRM 950-A, by ≈ +0.04 ‰. This offset is smaller than the precision of an individual U isotope measurement, however, statistically resolvable if applying the respective standard errors of the long-term mean (2 SE) for both standards.

To calculate the actual measured isotope ratio of $n(^{238}U)$ / $n(^{235}U)$, first their individual intensities were corrected for the $n(^{235}U)$ and $n(^{238}U)$ portion, which they inherited by adding the U double spike solution, IRMM 3636-A. Additionally, there is a minor tailing from $n(^{238}U)$ on $n(^{236}U)$. Therefore, the measured $n(^{236}U)$ intensity was corrected by measuring the intensity of $n(^{233}U)$ and $n(^{236}U)$ before each measurement session in a non-spiked standard solution. This natural tail from $n(^{238}U)$ on $n(^{236}U)$ was always below 10^{-6}.

We measured the U standard in between every 3 samples and used a "3 sample-standard-bracketing (SSB)" mass bias correction method in addition to that from the double spike, similarly as reported in Weyer et al. (2008). Again, the mass bias correction was done assuming an exponential fractionation within the mass spectrometer and applying the exponential law (Eq. 2.5 and Eq. 2.6). Comparison of the double spike corrected U isotope compositions relative to the daily average of the U standard revealed identical results in almost all cases. The final results of the isotopic measurements are expressed in the delta-notation (Eq. 2.7). The instrumental U blank was insignificant. Analytical U blanks from the reagents ranged between 20 pg/g and 78 pg/g U. This is more than three orders of magnitude lower than the mass fractions of our samples.

$$\left(n\left(^{238}\mathrm{U}\right) / n\left(^{235}\mathrm{U}\right)\right)_{\mathrm{true}} = \left(n\left(^{238}\mathrm{U}\right) / n\left(^{235}\mathrm{U}\right)\right)_{\mathrm{measured}} \times \left(\frac{M\left(^{238}\mathrm{U}\right)}{M\left(^{235}\mathrm{U}\right)}\right)^{\beta} \qquad \text{Eq. 2.5}$$

$$\beta = \frac{\ln\left(\frac{\left(n\left(^{236}\mathrm{U}\right) / n\left(^{233}\mathrm{U}\right)\right)_{\mathrm{certified}}}{\left(n\left(^{236}\mathrm{U}\right) / n\left(^{233}\mathrm{U}\right)\right)_{\mathrm{measured}}}\right)}{\ln\left(\frac{\mathrm{M}\left(^{236}\mathrm{U}\right)}{\mathrm{M}\left(^{233}\mathrm{U}\right)}\right)} \qquad \text{Eq. 2.6}$$

$$\delta^{238/235}\mathrm{U} \,/\, ‰ = \left[\frac{\left(n\left(^{238}\mathrm{U}\right) / n\left(^{235}\mathrm{U}\right)\right)_{\mathrm{sample}}}{\left(n\left(^{238}\mathrm{U}\right) / n\left(^{235}\mathrm{U}\right)\right)_{\mathrm{standard}}} - 1\right] \times 1000 \qquad \text{Eq. 2.7}$$

The reproducibility of the U standards "NIST SRM 950-A", "REIMEP 18-A" and "NBL CRM 112-A" are shown in Fig. 2.3 and Fig. 2.4. The overall variations of $n(^{238}U) / n(^{235}U)$ are within the error of recently published data (Richter et al., 2010). The average for NIST SRM 950-A is $n(^{238}U) / n(^{235}U) = 137.878 \pm 0.013$, NBL CRM 112-A: $n(^{238}U) / n(^{235}U) = 137.850 \pm 0.023$ and REIMEP 18-A: $n(^{238}U) / n(^{235}U) = 137.844 \pm 0.028$.

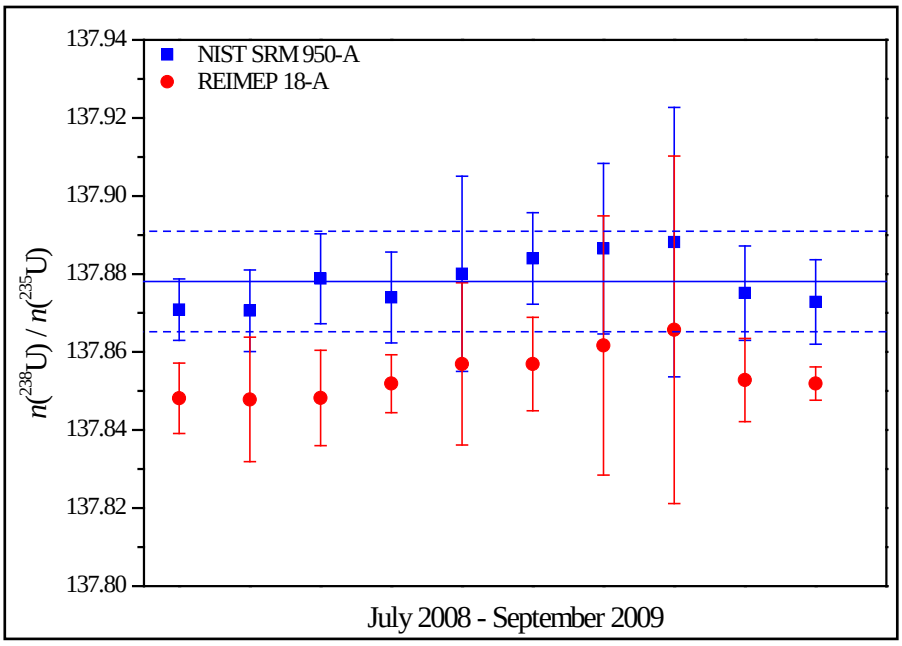

Fig. 2.3 Reproducibility of the $n(^{238}U) / n(^{235}U)$ ratio of the standard "NIST SRM 950-A", in comparison to that of the U standard "REIMEP 18-A" for individual measurements between July 2008 and September 2009. The blue straight line indicates the average for "NIST SRM 950-A" ($n(^{238}U) / n(^{235}U) = 137.878$) of all sessions and the blue dashed lines indicate the double standard deviation of 0.0129. In June 2009, we switched from the in-house prepared U spike ($n(^{236}U) / n(^{233}U) = 0.65917$) to the commercially available IRMM 3636-A ($n(^{236}U) / n(^{233}U) = 0.98130$). In addition, we also switched the U standard from "NIST SRM 950-A" to "NBL CRM 112-A", which has a slightly lighter U isotope composition.

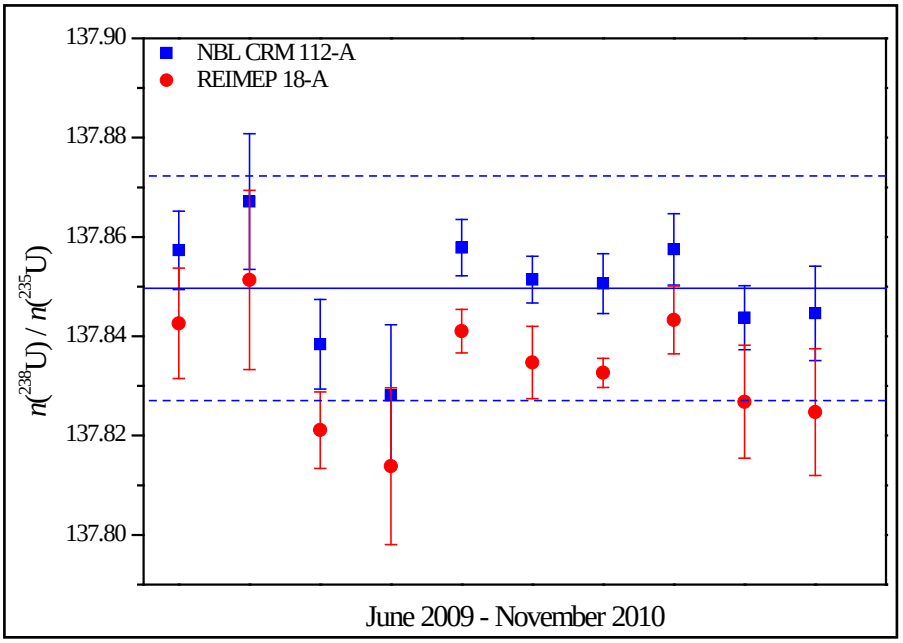

Fig. 2.4 Reproducibility of the $n(^{238}U) / n(^{235}U)$ ratio of the standard "NBL CRM 112-A", in comparison to that of the U standard "REIMEP 18-A" for individual measurements between June 2009 and November 2010. The blue straight line indicates the average for "NBL CRM 112-A" ($n(^{238}U) / n(^{235}U) = 137.850$) of all sessions and the blue dashed lines indicate the double standard deviation of 0.023.

2.3 Appendices

Table A 2.1 First step for separating Mo from the matrix with an anion exchange resin, DOWEX® 1X8 (100-200 mesh), according to the following method. Samples were loaded in 6 M HCl.

Fraction	Eluent	V / mL	Step
1	Milli-Q® H_2O	10	washing of the resin
	Milli-Q® H_2O	10	
	1 M HCl	10	
	1 M HCl	10	
2	6 M HCl	10	conditioning of the resin
	6 M HCl	10	
3	-	2	loading of the samples
4	6 M HCl	10	wash-out of the matrix
	6 M HCl	10	
	6 M HCl	10	
5	1 M HCl	0.5	collect Mo-fraction, possibly with Fe
	1 M HCl	0.5	
	1 M HCl	0.5	
	1 M HCl	0.5	
	1 M HCl	1	
	1 M HCl	1	
	1 M HCl	1	
	1 M HCl	5	
	1 M HCl	10	
	1 M HCl	10	
	1 M HCl	10	

Table A 2.2 Second and final step for separating Mo from the matrix with a cation exchange resin, Bio-Rad AG® 50W-X8 (200-400 mesh), according to the following method. Samples were loaded in a solution containing 0.5 M HCl and 0.01 % H_2O_2.

Fraction	Eluent	V / mL	Step
1	Milli-Q® H_2O	10	washing of the resin
	0.5 M HCl	10	
	0.5 M HCl*	10	
2	0.5 M HCl + 0.01 % H_2O_2	10	conditioning of the resin
3	-	2	loading of the samples
4	0.5 M HCl + 0.01 % H_2O_2	0.5	collect Mo-fraction
	0.5 M HCl + 0.01 % H_2O_2	0.5	
	0.5 M HCl + 0.01 % H_2O_2	0.5	
	0.5 M HCl + 0.01 % H_2O_2	0.5	
	0.5 M HCl + 0.01 % H_2O_2	1	
	0.5 M HCl + 0.01 % H_2O_2	1	
	0.5 M HCl + 0.01 % H_2O_2	1	
	0.5 M HCl + 0.01 % H_2O_2	5	
	0.5 M HCl + 0.01 % H_2O_2	10	
	0.5 M HCl + 0.01 % H_2O_2	10	
	0.5 M HCl + 0.01 % H_2O_2	10	

* columns were sealed after this step for at least 14 hours, before letting HCl elute

Table A 2.3 Purification of U from the sample matrix with an anion exchange resin, eichrom® (now TRISKEM) UTEVA® (particle size: 100-150 µm), according to the following method. Samples were loaded in 3 M HNO_3.

Fraction	Eluent	V / mL	Step
1	0.05 M HCl	5	washing of the resin
	0.05 M HCl	5	
	0.05 M HCl	5	
2	3 M HNO_3	5	conditioning of the resin
3	-	1	loading of the samples
4	3 M HNO_3	1	wash-out of the matrix
	3 M HNO_3	5	
	3 M HNO_3	5	
	3 M HNO_3	5	
5	7.5 M HCl	3	HCl conditioning
6	0.05 M oxalic acid in 5 M HCl	5	Thorium wash-out
7	7.5 M HCl	5	wash-out of oxalic acid
8	0.05 M HCl	1	collect U-fraction
	0.05 M HCl	1	
	0.05 M HCl	1	
	0.05 M HCl	3	
	0.05 M HCl	5	

Table A 2.4 Cup configuration for molybdenum isotope measurements with interfering isotopes (natural abundance according to De Laeter et al., 2003).

Faraday cup	L4	L3	L2	L1	C	H1	H2	H3	H4
Nominal mass	90	91	92	95	96	97	98	99	100
Element of interest	Zr	Zr	Mo	Mo	Mo	Mo	Mo	Ru	Mo
Natural abundance / %	51.45	11.22	14.77	15.90	16.68	9.56	24.19	12.76	9.67
Interfering isotopes			92Zr		96Zr				
Natural abundance / %			17.15		2.80				
Interfering isotopes					96Ru		98Ru		100Ru
Natural abundance / %					5.54		1.87		12.60

Table A 2.5 Cup configuration for uranium isotope measurements (natural abundance according to De Laeter et al., 2003).

Faraday cup	L3	L2	L1	H1
Nominal mass	233	235	236	238
Element of interest	U	U	U	U
Natural abundance / %	-	0.72	-	99.28
Spike abundance / %	50.1355	-	49.8324	-

CHAPTER 3

The uranium ($n(^{238}U) / n(^{235}U)$) isotope composition of rivers and the continental crust

Abstract

Recent studies revealed subtle but significant fractionation of the primordial U isotopes ^{238}U and ^{235}U during Earth surface processes, such as U reduction in anoxic oceanic basins or U adsorption to ferromanganese crusts (on the order of 0.1 ‰ to 1 ‰). This study was undertaken to address the question, whether U isotope fractionation occurs during the weathering of the continental crust and riverine transport. Therefore, we determined the $n(^{238}U) / n(^{235}U)$ isotope ratio of the continental crust (the major U source to the oceans) by analyzing granitic rocks with different ages from Greenland, Japan, Germany and Swaziland and three post-Archean shales from Australia. We also analyzed the U isotope composition in the dissolved load of major- and tributary rivers, i.e. from Venezuela (Rio Portuguesa), India (Alaknanda, Bhagirathi, Ganges, Brahmaputra), Pakistan (Indus), Germany (Main, Nidda) and Switzerland (Ticino, Birs, Saane).

All analyzed rock samples fall into a range of $\delta^{238}U$ between -0.45 ‰ and -0.21 ‰ (relative to NBL CRM 112-A), with an average of -0.30 ‰ ± 0.04 ‰ (2 SE). Their U isotope variations are independent of the U concentration, age, sample locality or degree of differentiation as measured by their La/Yb ratio. The analyzed rivers have U isotope compositions ranging between -0.32 ‰ and +0.01 ‰. However, despite

differences in catchment lithologies, all major rivers define a narrow range between -0.31 ‰ and -0.13 ‰ and can barely be resolved from the estimate for the upper continental crust (-0.30 ‰). In comparison to the major rivers, tributary rivers from the Swiss Alps display a larger range in $\delta^{238}U$ (-0.29 ‰ to +0.01 ‰), and they also have lower U concentrations (0.87 nmol/kg to 3.08 nmol/kg) compared to the investigated major rivers (5.19 nmol/kg to 11.69 nmol/kg).

The shift towards higher than crustal $\delta^{238}U$ of several rivers indicates that U isotope fractionation does occur during weathering and/or riverine transport. As the heaviest U isotope compositions are displayed by rivers with low U concentrations, we infer that most of the observed isotope fractionation occurs between dissolved and particulate U in the rivers. Rivers with high U concentrations (including the investigated major rivers) have a higher fraction of dissolved U and are thus less affected by U isotope fractionation. Some of their U isotope variations may also mirror the isotopic variations of the respective river catchments. As large rivers are the major U source to the oceans, we infer from our findings that the U input to the ocean is barely (if at all) fractionated relative to the U isotope composition of the continental crust.

For mass balance consideration, we propose to use the average $\delta^{238}U$ of major rivers from this study (-0.23 ‰) as best estimate for the oceans U source.

3.1 Introduction

Uranium is a redox-sensitive trace metal which commonly occurs in two redox states in nature, U^{IV} and U^{VI}, respectively. Its speciation in aqueous solutions depends on the redox potential, pH and the amount of dissolved complexing agents. Oxygenated ocean water contains U^{VI}, predominantly as uranyl ($U^{VI}O_2^{2-}$) that forms in the presence of carbonate soluble and non-reactive complexes, e.g. $[UO_2(CO_3)_3]^{4-}$. Under more reducing conditions, U forms insoluble and more reactive U^{IV} compounds ($U(OH)_4$, $U(OH)_5^-$), which precipitate as uraninite (UO_2).

The isotopic composition of $n(^{238}U) / n(^{235}U)$ in nature was generally assumed to be invariant and equal to 137.88 (Rosman and Taylor, 1998; De Laeter et al., 2003). However, several recent studies revealed significant U isotope variations in both, meteorites and terrestrial samples; while $n(^{238}U) / n(^{235}U)$ variations in meteorites (by ~4 ‰) were likely produced by the decay of extant ^{247}Cm in the early Solar System (Brennecka et al., 2010a), such on Earth (~1.3 ‰) are the result of U isotope fractionation during chemical reactions (e.g. Stirling et al., 2007; Weyer et al., 2008; Bopp et al., 2009; Brennecka et al., 2010b; Montoya-Pino et al., 2010). The latter appear to be the strongest between oxidized and reduced depositional environments and are likely related to nuclear volume effects (Schauble, 2007; Weyer et al., 2008). Sediments formed in oxic environments, e.g. manganese crusts, display slightly lighter U isotope compositions (by ~ 0.2 ‰, Weyer et al., 2008; Brennecka et al., 2011a,b) than seawater ($\delta^{238}U_{seawater}$ = -0.37 ‰, relative to NBL CRM 112-A, recalculated from Weyer et al., 2008)[1]. However, sediments from reducing environments display heavy U isotope compositions with $\delta^{238}U$ of up to +0.47 ‰ (relative to NBL CRM 112-A, recalculated from Weyer et al., 2008)[1].

Recently, U isotopes were used as a paleo-redox proxy, to quantify the expansion of ocean anoxia during oceanic anoxic events (i.e. OAE-2; Montoya-Pino et al., 2010), similarly as previously modeled with Mo isotopes (e.g. Arnold et al., 2004; Kendall et al., 2009). However, for such modeling, detailed knowledge on the isotopic mass balance, i.e. the isotope composition of all modern oceanic sources and sinks, is essential (assuming that this modern mass balance can then be projected to modified conditions in the past). There are two major and two minor sinks for U from the ocean (Klinkhammer and Palmer, 1991; Morford and Emerson, 1999): the two major sinks are organic-rich suboxic sediments at continental margins and altered oceanic crust through hydrothermal circulation at mid-ocean ridges (Fig. 3.1). The two minor sinks are euxinic sediments (e.g. Black shales from the Black Sea) and oxic sediments (e.g. ferromanganese crust). However, the only (major) source of U are rivers, which

[1] The original values of Weyer et al. (2008) were analyzed relative to NIST SRM 950-A, resulting in a shift of +0.04 ‰, compared to our measurements relative to NBL CRM 112-A (see Chapter 3.3. U isotope measurements).

transport the weathered U from the continental crust to the oceans (Sarin et al., 1990). Weyer et al. (2008) provided a first estimate on the U isotope composition of the continental crust by analyzing several granites and basalts. They speculated that rivers will likely not display large U isotope fractionation (compared to granites and basalts), due to the relatively quantitative mobilization of U during weathering and the conservative behavior of U during transport in rivers. Still, isotope analyses of Mo (a chemically similar element) in rivers revealed highly variable isotope compositions, indicating that significant isotope fractionation during weathering and transport may occur, though some of the observed isotope variations reflect those of the river catchments (Archer and Vance, 2008; Neubert et al., 2011).

To assess whether U isotope fractionation occurs between the continental crust and rivers, we analyzed water samples from three major rivers and eight tributary rivers of different climatic conditions. Those tributary rivers included three rivers from Switzerland, which were sampled four times throughout the year, to quantify if any seasonal variations affect the isotopic composition of U. Furthermore, we analyzed several granites from different localities and of different ages and three post-Archean shales, to expand the very limited data set and to obtain a better estimate for the U isotope composition of the continental crust.

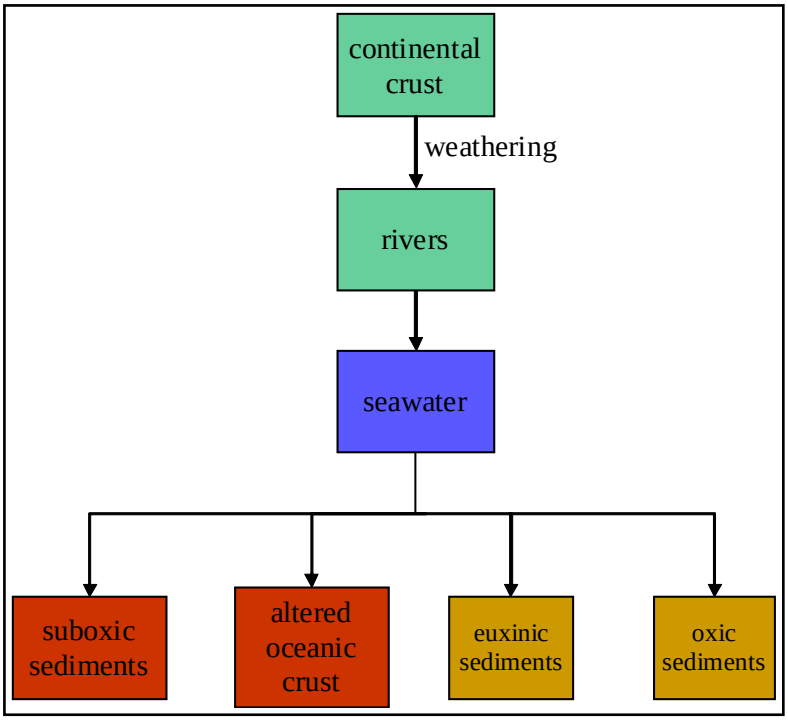

Fig. 3.1 Sources and sinks for the global oceanic uranium cycle (Chen et al., 1986; Morford and Emerson, 1999). The main source for dissolved U in the ocean is the riverine input of the weathered continental crust. U is removed from seawater into four sinks: The two major sinks are suboxic sediments, together with metalliferous sediments, and hydrothermal altered oceanic crust and the two minor sinks are anoxic/euxinic sediments and oxic sediments.

3.2 Sample description

3.2.1 Rocks

The rock samples include: (1) Two international standards from Japan: a Rhyolite (JR-2) from Shimosuwa, Nagano Prefecture and a Cretaceous Naegi biotite granite (JG-2) from Hirukawa-mura, Gifu Prefecture (Ando et al., 1987). (2) The

samples RGd 23-84, RbG 17-54, Wb 11-94, Wb 68-94 are granites from Weinsberg (South Bohemian massive, Germany) and between 327 Ma and 329 Ma old. A detailed description of the sampling can be found in Gerdes (2001). (3) Two granitic samples from the Isukasia terrane (Greenland) were also analysed (Hoffmann et al., 2011): the first one (jeh-SG-01) is a homogeneous tonalite with magmatic texture (Nutman et al., 1999) and was collected close to a crosscutting Ameralik dyke in the vicinity of the Isua supracrustal belt (ISB, Greenland, ~3.80 Ga). The second one (sample 229403) is a mafic grey gneiss with quartzdioritic composition (Baadsgard et al., 1986) and about 3.72 Ga old. (4) Further, we analyzed four granitic samples from Swaziland: AG7 (3.64 Ga) and SW25 (3.32 Ga) are tonalitic gneisses (Zeh et al., 2011). SIN23 (3.07 Ga) is a (gneissic) Sinceni granite and SIC19 (2.72 Ga) is a Sicunusa granite (Zeh et al., 2011). A detailed description for the samples can be found in Zeh et al. (2011). (5) Additionally, three post-Archean shales from Australia were measured (Nance and Taylor, 1976; McLennan and Taylor, 1981); PW5 is a Kockatea shale from the Perth Basin (Western Australia) with an age between 250 Ma to 200 Ma (Triassic), sample SC-8 is a Silurian State Circle Shale (440 Ma) and MI-5 was taken from the Mount Isa Groupe and has an age of 1.5 Ga.

3.2.2 Rivers

Water samples are taken from the rivers Rio Portuguesa (Venezuela), Ganges, Bhagirathi, Alaknanda, Brahmaputra (all India), Indus (Pakistan), Main and Nidda (Germany), Ticino, Birs and Saane (Switzerland). The sampling of the Rio Portuguesa is described in detail in Chen et al. (2006). Briefly, the Rio Portuguesa drainage basin contains a diverse mixture of evaporites, limestones, shales, sandstones, metamorphics, granites and calc-alkaline volcanics, but exposures of shales and limestones dominate (Palmer and Edmond, 1992). A detailed description of the sampling and geologic setting of the Ganges, the Brahmaputra and the Indus are given in (Sharma et al., 1999). Briefly, the Ganges sample was collected near the city of Patna and the Brahmaputra sample was taken upstream of the city of Guwahati. The Indus sample originates from

Besham along the Karakoram highway in Pakistan. The Ganges drainage basin contains carbonates, shales (pyritous at places), quartzites, and low- to high-grade gneisses (Sarin et al., 1992). Although, the Brahmaputra flows along the ophiolitic assemblage along the Indus-Tsangpo suture zone, its drainage basin is dominated by the weathering and erosion of felsic paragneisses of rapidly exhuming Namche Barwa massif in the eastern syntaxis of the Himalaya (Stewart et al., 2008; Enkelmann et al., 2011; Guilmette et al., 2011). Similarly the drainage basin of the Indus upstream of Besham is dominated by weathering and erosion of high grade gneisses of rapidly exhuming Nanga Parbat Massif and adjacent South Karakorum Belt in the western syntaxis of the Himalaya (Garzanti et al., 2005). The Bhagirathi River is the source stream for the Ganges. After it meets the Alaknanda River in Devprayag, the River is called Ganges.

Sampling of the rivers Main and Nidda was done in Frankfurt (Germany) before the Nidda flows into the Main. The catchment of River Main contains primary of sandstone and some magmatic rocks (including granitoids and basalts). It has its origin by the confluence of River Red Main and River White Main. The River Red Main has its source in the hills of Franconian Switzerland and the Red Main arises in the Fichtelgebirge (mountain area in Northern Bavaria). River Nidda has its source in a volcanic region (Vogelsberg) and the catchment is dominated by basaltic rocks.

A detailed description of the sampling sites and geological setting of all investigated Swiss-rivers (Ticino, Birs, Saane) is given in Georg et al. (2006). Briefly, the catchment of Ticino consists mainly of crystalline gneisses. The Birs River is surrounded by shallow marine carbonate deposits and the Saane River by a diversity of sedimentary lithologies, including predominantly marine siliciclastic rocks, but also carbonate-sandstones, mudstones and limestones. We analyzed four samples from Ticino and Birs and two samples from Saane (Ticino was sampled in May 2004, August 2004, June 2005 and July 2005; Birs was sampled in August 2004, October 2004, February 2005 and May 2005; Saane was sampled in January 2005 and May 2005).

3.3 Analytical methods

3.3.1 Sample preparation

For granites and shales about 0.3 g of rock powder was digested with a mixture of concentrated $HF/HNO_3/HClO_4$ (3:1:1) in Parr® high-pressure vessels at 180 °C. Samples were repeatedly treated with 6 M HNO_3 and 6 M HCl to dissolve any remaining fluorides (modified after Weyer et al., 2008). The samples were finally re-dissolved in 3 M HNO_3 for the purification of U from the sample matrix, by anion exchange chromatography (based on eichrom® UTEVA® resin, following the procedure, described by Weyer et al., 2008).

River waters were filtered after sampling through a 0.45 µm filter and acidified. For analyses, the volume of 50 mL to 100 mL of river water was gently reduced to about 10 mL on a hot plate. Subsequently, concentrated nitric acid was added to adjust acidity to 3 M HNO_3 for U purification. Prior to chromatographic separation of U, an Aliquot of 5 % was taken from the rock and river samples for the analyses of trace element- and (in particular) U-concentrations with ICP-MS (Thermo Finnigan Element 2, HR-ICP-MS in Frankfurt), in order to optimize the addition of the U double spike.

3.3.2 Preparation of the spike-solution

Before U was purified from the sample matrix, a double-spike-solution (IRMM 3636-A) was added to correct for instrumental mass bias during measurement on the MC-ICP-MS. The double-spike-solution, IRMM 3636-A (provided by the Institute for Reference Material and Measurements, Belgium), consists of a ~1:1 mixture of ^{236}U and ^{233}U (Richter et al., 2008). We diluted an aliquot of the original stock to a mass fraction of 20.32 ng/g. The mass fraction of this working solution was determined by isotope

dilution relative to U metal solutions and cross-calibrated relative to a previously calibrated $n(^{236}U) / n(^{233}U)$ double spike (Weyer et al., 2008). IRMM 3636-A was prepared gravimetrically (using highly enriched ^{233}U and ^{236}U) and certified with an uncertainty on $n(^{236}U) / n(^{233}U)$ of only 0.16 ‰. This uncertainty is smaller than the uncertainty on $n(^{238}U) / n(^{235}U)$ of most available standard solutions. Thus, we directly used the certified ratio for $n(^{236}U) / n(^{233}U)$ (= 0.98130). However, analyses of the minor isotope ratios revealed significant differences between our diluted spike aliquot ($n(^{238}U) / n(^{233}U) = 0.00152695$, $n(^{235}U) / n(^{233}U) = 0.00005640$, $n(^{234}U) / n(^{233}U) = 0.00037729$) and the certified values ($n(^{238}U) / n(^{233}U) = 0.00152695$, $n(^{235}U) / n(^{233}U) = 0.00004463$, $n(^{234}U) / n(^{233}U) = 0.00035921$). This difference can be explained by contamination of our spike aliquot (likely during preparation of the working solution) with ± natural U. This contamination did not affect the ratio of the major spike isotopes ($n(^{236}U) / n(^{233}U)$, as these isotopes do not occur in nature). The "dilution effect" of this contamination is insignificant. We corrected for the contribution of the minor spike isotopes ($n(^{238}U)$, $n(^{235}U)$) to the natural abundances during our double spike calculations. This correction was precise enough that the contamination of the samples with these minor spike isotopes did not affect the precision of the $n(^{238}U) / n(^{235}U)$ isotope analyses of the samples (even for high spike/sample ratios of $n(^{236}U)/ n(^{235}U) \approx 10$). The spike calibration and performance of our method has been tested by the contribution of our laboratory to a comparative inter-laboratory study in which various international U standards have been analyzed (Richter et al., 2010). We also analyzed these and other international U-standards (NBL CRM 112-A = NBS SRM 960, IRMM-184 and NIST SRM 950-A, REIMEP 18-A) repeatedly and our results agree with those of other laboratories, within uncertainties (Richter et al., 2010). Spike/sample ratios were optimized to $n(^{236}U)/ n(^{235}U) \approx 3$, to minimize tailing effects from $n(^{238}U)$ on $n(^{236}U)$ and from $n(^{236}U)$ on $n(^{235}U)$, respectively.

3.3.3 Uranium isotope measurements

The measurements of the U isotopes (^{233}U, ^{235}U, ^{236}U and ^{238}U) were performed on a Thermo Scientific Neptune MC-ICP-MS (Weyer and Schwieters, 2003) at the University of Frankfurt. The instrument was equipped with nine Faraday collectors and amplifiers with one $10^{10}\ \Omega$, seven $10^{11}\ \Omega$ and two $10^{12}\ \Omega$ resistors. The measurements were performed using a CETAC Aridus™ combined with a 50 µL PFA nebulizer for sample introduction. Sample analyses were performed relative to two different standard solutions: River water samples were measured relative to NIST SRM 950-A, which was already used in previous studies (e.g. Weyer et al., 2008; Brennecka et al., 2010a,b; Montoya-Pino et al., 2010). All rock samples were performed relative to NBL CRM 112-A (as NIST SRM 950-A is no longer available). Weyer et al. (2008) reported within errors identical $n(^{238}U) / n(^{235}U)$ for a limited number of analyses of NIST SRM 950-A and NBL CRM 112-A. A thorough cross calibration, however, through repeated measurements of both standards (over several months), revealed that NBL CRM 112-A seems to be slightly offset relative to NIST SRM 950-A, by ≈ +0.04 ‰. This offset is smaller than the precision of an individual U isotope measurement, however, statistically resolvable if applying the respective standard errors of the long-term mean (2 SE) for both standards. Accordingly, we applied this offset to the river samples, to achieve the most accurate comparison between the crustal samples and the rivers.

The rock samples and all water samples from the major rivers were measured at mass fractions of 100 ng/g U. The tributary rivers have generally low U contents and were measured at mass fractions between 20 ng/g and 50 ng/g U (the mass fraction of the U standard NIST SRM 950-A was ± adjusted to the sample mass fractions). Both analyses of the rock and the water samples were performed using a CETAC Aridus™ combined with a 50 µL PFA nebulizer for sample introduction. In general, ^{238}U was measured on a $10^{10}\ \Omega$ resistor; ^{236}U, ^{233}U and ^{235}U on $10^{11}\ \Omega$ resistors. For intensities lower than 50 mV, we used a $10^{12}\ \Omega$ resistor. With this setup, we achieved for a solution, containing 100 ng/g U, a signal of 30-40 V for ^{238}U, 220-300 mV for ^{235}U and 600-800 mV for ^{233}U and ^{236}U. The results of the isotopic measurements are expressed in the delta-notation (Eq. 3.1).

$$\delta^{238/235}\mathrm{U} \,/\, ‰ = \left[\frac{\left(n(^{238}\mathrm{U}) \,/\, n(^{235}\mathrm{U})\right)_{\mathrm{sample}}}{\left(n(^{238}\mathrm{U}) \,/\, n(^{235}\mathrm{U})\right)_{\mathrm{standard}}} - 1\right] \times 1000 \qquad \text{Eq. 3.1}$$

We measured the U standards (i.e. NIST SRM 950-A for the rivers and NBL CRM 112-A for the crustal samples, respectively) in between every 3 samples and used a "3 sample-standard-bracketing (SSB)" mass bias correction method in addition to that from the double spike, similarly as reported in Weyer et al. (2008). However, comparison of the double spike corrected U isotope compositions relative to the daily average of the U standard revealed identical results in almost all cases. The instrumental U blank was insignificant. Analytical U blanks from the reagents ranged between 20 pg and 78 pg U. This is more than three orders of magnitude lower than the mass fractions of our samples.

3.4 Results

All samples were analyzed for the U concentration by isotope dilution (ID) and the U isotope composition (δ^{238}U; Table 3.1 and Table 3.2, Fig. 3.2, Fig. 3.4, **Fehler! Verweisquelle konnte nicht gefunden werden.**). Further, analyzes of REE in the granites and major cations in the Swiss-Rivers (both measured by ICP-MS) are presented in Fig. 3.3, Fig. 3.5 and Fig. 3.6, respectively.

Table 3.1 Uranium isotope and selected trace element results for the analyzed rock samples relative to the uranium standard NBL CRM 112-A are given (2 SD represents the double standard deviation for $\delta^{238}U$ and n the number of measurements). The concentrations for the REE (La, Eu, Yb) are normalized to CI chondrites (values from McDonough and Sun, 1995). The calculations for the REE (e.g. La_N, Eu_N, Eu_N*) were done according to Eq. 3.2 and Eq. 3.3.

Sample	Location	Material	Age Ga	La_N	Eu_N	Eu_N*	$(Eu/Eu^*)_N$	Yb_N	$(La/Yb)_N$	*w* (Mo) µg/g	*w* (U) µg/g	$\delta^{238}U$ ‰	2 SD ‰	n
jeh-SG-01	Greenland	Tonalite	3.80	48.59	12.63	13.87	0.91	5.10	9.53	0.06	0.91	-0.37	0.02	4
229403	Greenland	Gneiss	3.72	73.13	16.53	20.50	0.81	6.57	11.13	0.08	0.62	-0.39	0.08	4
JR2	Japan	Rhyolite	n.a.	50.07	1.27	23.71	0.05	25.72	1.95	1.30	9.13	-0.45	0.08	4
JG2	Japan	Granite	n.a.	80.90	1.25	45.83	0.03	41.82	1.93	0.16	9.27	-0.27	0.06	4
RGd 23-84	Germany	Granite	0.38	257.43	27.01	30.57	0.88	6.16	41.77	1.33	3.73	-0.29	0.05	3
RbG 17-54	Germany	Granite	0.38	115.83	30.44	51.78	0.59	12.96	8.94	0.87	11.77	-0.25	0.03	4
Wb 11-94	Germany	Granite	0.38	131.20	36.90	56.30	0.66	17.41	7.54	1.83	2.21	-0.26	0.07	3
Wb 68-94	Germany	Granite	0.38	233.97	20.32	46.05	0.44	7.77	30.11	2.08	1.27	-0.25	0.08	4
SW-AG7	Swaziland	Gneiss	3.64	159.51	24.45	47.75	0.51	20.41	7.81	0.39	2.78	-0.26	0.05	4
SW-SIN23	Swaziland	Granite	3.07	126.26	4.69	26.71	0.18	26.74	4.72	0.15	4.66	-0.21	0.03	3
SW-SIC19	Swaziland	Granite	2.72	475.86	19.62	70.60	0.28	32.82	14.50	2.15	2.71	-0.28	0.04	4
PW-5	Australia	Shale	0.23	185.21	17.99	29.16	0.62	10.08	18.37	0.17	8.43	-0.39	0.00	4
SC-8	Australia	Shale	0.44	144.06	12.44	21.02	0.59	7.48	19.26	0.05	2.78	-0.34	0.06	3
MI-5	Australia	Shale	1.50	160.10	17.31	33.30	0.52	14.45	11.08	6.50	10.60	-0.26	0.08	4

Table 3.2 U isotope, selected trace element results and specific characteristics for all analyzed water samples are given (n.d. = not determined, the double standard error (2 SE) is calculated after the student t-distribution, based on the standard deviation (SD), the number of sample analyses n and the student *t*-factor for a confidence level of 95 %). If the sample amount was only sufficient for a single measurement (e.g. Indus, Birs, Ticino, Saane), we used the daily standard deviation from the U standard, NBL CRM 112-A.

River	Sampled	Nature of River	Length km	Discharge m^3/s	*w* (Ca) µg/g	*w* (Mg) µg/g	*w* (Na) µg/g	*c* (Mo) nmol/kg	*c* (U) nmol/kg	$\delta^{238}U$ ‰	2 SD ‰	2 SE ‰	n
Ganges	near the city of Patna	Major	2510	12015	n.d.	n.d.	n.d.	16.01	11.69	-0.31	0.08	0.06	4
Brahmaputra	upstream of the city Guwahati	Major	2900	19300	n.d.	n.d.	n.d.	9.78	5.19	-0.27	0.09	0.08	3
Indus	Besham	Major	3200	6600	n.d.	n.d.	n.d.	18.19	7.18	-0.13	0.07	0.11	2
Bhagirathi	source of the Ganges	Tributary	205	156	n.d.	n.d.	n.d.	13.77	9.09	-0.20	0.03	0.02	4
Alaknanda	source of the Ganges	Tributary	200	552	n.d.	n.d.	n.d.	16.48	7.75	-0.32	0.08	0.07	3
Main	in the city of Frankfurt	Tributary	529	200	n.d.	n.d.	n.d.	11.40	4.47	-0.31	0.05	0.03	5
Rio Portuguesa		Tributary	600	n.a.	n.d.	n.d.	n.d.	10.54	1.76	-0.05	0.07	0.07	3
Nidda	in the city of Frankfurt	Tributary	98	13	n.d.	n.d.	n.d.	9.51	3.11	-0.18	0.06	0.03	5
Birs	August 2004	Tributary	73	7	96.4	5.0	7.0	4.93	1.77	-0.19	0.06	0.09	2
	October 2004	Tributary		4	93.7	5.8	10.0	7.23	1.82	-0.21	0.06	0.09	2
	February 2005	Tributary		11	100.7	5.3	14.8	4.00	1.91	-0.10	0.06	0.09	2
	May 2005	Tributary		15	94.3	4.8	6.1	3.96	1.55	0.01	0.06	0.09	2
Ticino	August 2004	Tributary	248	112	37.8	5.4	2.0	9.64	2.98	-0.21	0.06	0.09	2
	June 2005	Tributary		88	34.4	5.1	1.7	11.63	2.93	-0.29	0.06	0.09	2
	July 2005	Tributary		27	52.2	8.8	2.3	14.28	3.08	-0.28	0.06	0.09	2
	May 2004	Tributary		97	23.4	3.1	1.5	9.38	1.64	-0.19	0.06	0.09	2
Saane	May 2005	Tributary	126	91	74.9	6.7	5.4	1.75	0.87	-0.21	0.11	0.10	3
	January 2005	Tributary		34	84.2	9.7	9.7	1.80	1.64	-0.05	0.05	0.08	2

The concentrations for Ca, Mg and Na were measured for R. B. Georg at ACME Analytical Laboratories Ltd. in Vancouver, Canada. The values for length and discharge were obtained from several sources (Ganges, Brahmaputra, Indus: Sarin et al., 1989; Bhagirathi and Alaknanda: Yadav and Chakrapani, 2011; Birs, Ticino, Saane: Georg et al., 2006; Nidda and Main: Schulz and Bischoff, 2008).

3.4.1 Rocks

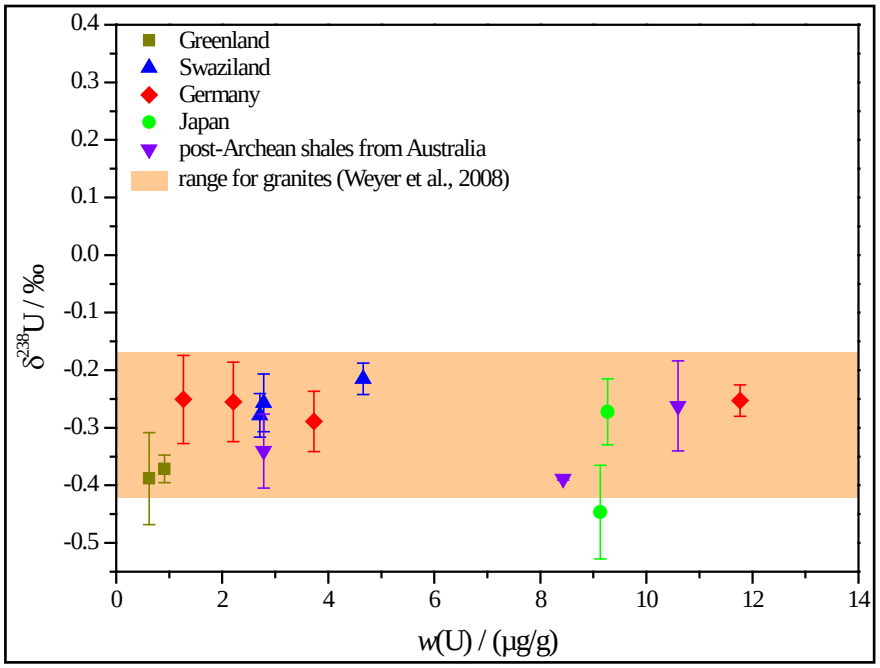

Fig. 3.2 $\delta^{238}U$ in ‰ vs. mass fraction *w* of U in µg/g in the analyzed granites, rhyolites and shales, representing the continental crust, compared to the range for the continental crust measured by Weyer et al. (2008), orange field.

We analyzed granites from different localities, e.g. Japan, Germany, Greenland, Swaziland, and of different ages (3.80 Ga to 328 Ma). The granites from Germany display variable U mass fractions (11.8 µg/g to 1.3 µg/g), though all of them have indistinguishable U isotopic compositions ($\delta^{238}U$ = -0.25 ‰ to -0.29 ‰). The samples

from Greenland (one gneiss and one tonalite) represent the oldest of the investigated samples (3.7 Ga to 3.8 Ga) and have very low U mass fractions (0.6 µg/g to 0.9 µg/g), and also slightly lower U isotope compositions ($\delta^{238}U$ = -0.37 ‰ to -0.39 ‰) relative to the younger granites from Germany. Other Archean samples from Swaziland (two granites and one gneiss, slightly younger than the samples from Greenland) display a very similar range of $\delta^{238}U$ (-0.21 ‰ to -0.28 ‰) as the relatively young granites from Germany (~ 380 Ma). The lightest U isotope composition is displayed by a rhyolithe from Japan ($\delta^{238}U$ = -0.45 ‰).

To investigate whether the degree of differentiation within the granitic rocks impacts their U isotope composition, we determined the mass fractions for the rare earth elements (REE) in the rocks. Then the mass fractions of the REE were normalized to the mass fractions of the reference values for CI chondrites (e.g. Eq. 3.2; values for CI condrites taken from McDonough and Sun, 1995). Additionally, Eu_N^* has been calculated after Eq. 3.3 to infer a further degree of differentiation. However, none of the investigated rocks show correlations between $\delta^{238}U$ and the $(La/Yb)_N$ or the $(Eu/Eu^*)_N$ value (Fig. 3.3).

$$Eu_N = \frac{w(Eu)_{sample}}{w(Eu)_{CI}} \qquad \text{Eq. 3.2}$$

$$Eu_N^* = \frac{(Sm_N + Gd_N)}{2} \qquad \text{Eq. 3.3}$$

The post-Archean shales from Australia are from three different time periods, Triassic, Silurian, Mesoproterozoic. Their U mass fractions and isotope compositions overlap with those of the investigated magmatic and metamorphic rocks ($\delta^{238}U$ = -0.26 ‰ to -0.39 ‰, and *w*(U) = 2.78 µg/g to 10.60 µg/g, respectively).

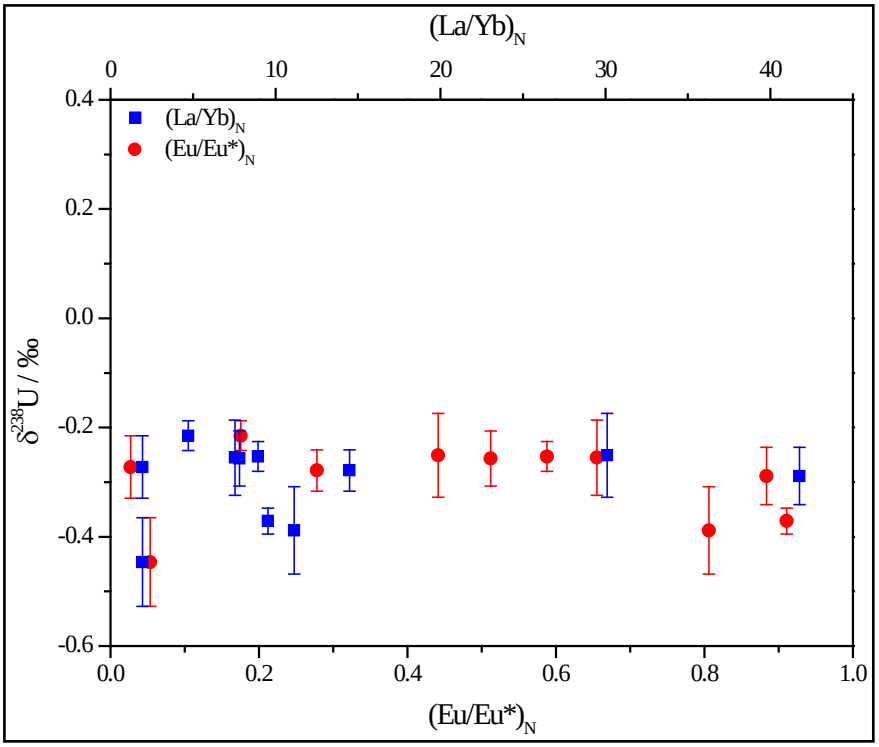

Fig. 3.3 $\delta^{238}U$ in ‰ relative to the $(La/Yb)_N$ ratio and relative to the $(Eu/Eu^*)_N$ content, both normalized to CI chondrites (McDonough and Sun, 1995).

3.4.2 Rivers

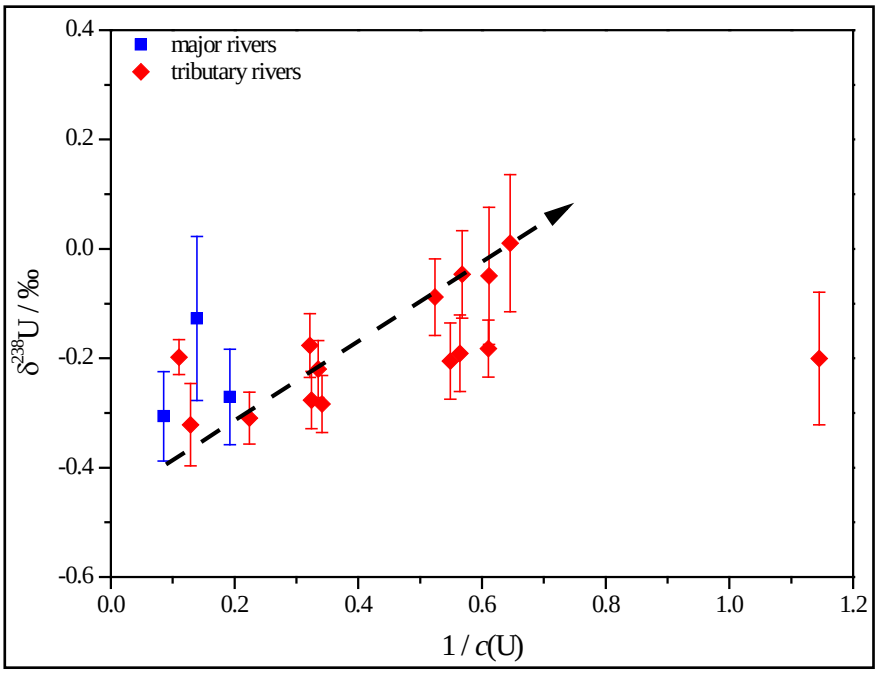

Fig. 3.4 $\delta^{238}U$ in ‰ vs. 1 / *c*(U) in 1/(nmol/kg) in the analyzed rivers, divided into major and tributary rivers, according to their discharge. Almost all rivers display a correlation between $\delta^{238}U$ and the reciprocal value of the U concentration. Therefore, just the rivers with a high U concentration display a $\delta^{238}U$ similar to the average of their sources ($\delta^{238}U_{\text{average of the crust}}$ = -0.3 ‰).

The rivers were divided into two groups: (i) major and (ii) tributary rivers. Due to their high discharge (more than 1000 m^3/s), the rivers Ganges, Brahmaputra and Indus were defined as major rivers. Due to their small discharge and catchment size, the source streams for the Ganges, Bhagirathi and Alaknanda, are considered as tributary rivers. Also, the Swiss-rivers (Ticino, Birs and Saane) are characterized by a much smaller catchment size, compared to the major rivers, e.g. areas are between $0.9 \cdot 10^3$ km^2 (Birs) and $1.9 \cdot 10^3$ km^2 (Saane) compared to $1.1 \cdot 10^6$ km^2 for the Ganges. Additionally, the discharge in the Swiss-rivers is at least a factor of 100 lower than in the Ganges (Table 3.2). Accordingly, the rivers Bhagirathi, Alaknanda, Main, Rio Portuguesa, Nidda, Ticino, Birs and Saane were defined as tributary rivers (Table 3.2).

The Ganges and the Brahmaputra have $\delta^{238}U$ of around -0.3 ‰ and U concentrations of 5 nmol/kg to 12 nmol/kg, while the river Indus (also a major river) has a heavier $\delta^{238}U$ of -0.13 ‰ (Table 3.2). The tributary rivers display lower U concentrations, ranging between 0.87 nmol/kg (Saane, May 2005) and 9.09 nmol/kg (Bhagirathi) and in average a heavier $\delta^{238}U$, which varies between -0.32 ‰ (Alaknanda) and 0.01 ‰ (Birs, May 2005).

3.5 Discussion

The results of this study can be used to address the following questions: (a) what is the U isotope composition of the continental crust? (b) what are the sources of U isotope variations in rivers? (c) what is the average U isotopic composition of rivers? and (d) what is the extent of U isotope fractionation between the continental crust and rivers?

3.5.1 Uranium isotope composition of the continental crust

The main source for U in the rivers is the weathered (upper) continental crust, which in average has a granitic composition. Granites and gneisses comprise primarily of quartz, feldspar and biotite or amphibole. However, the bulk inventory of U in granitic rocks is located in a variety of accessory phases, e.g. zircon, sphene, apatite, allanite, monazite, magnetite and ilmenite (Bajo et al., 1983). The granites analyzed in this study show variable U mass fractions, ranging between 0.62 µg/g (quartz-diorite from Greenland) and 11.77 µg/g (granite from Germany), and isotope compositions ranging between -0.39 ‰ and -0.21 ‰ (Fig. 3.2 and Table 3.1). There is no correlation between the U isotope composition and the U mass fraction (Fig. 3.2) or the age of the samples (Table 3.1). Additionally, there is no correlation between $\delta^{238}U$ and $(La/Yb)_N$ or $(Eu/Eu^*)_N$ (Fig. 3.3), implying that there is no direct link between U isotope

fractionation and the differentiation of the crust. This is also indicated by the fact that all investigated granites have similar U isotope compositions to basalts ($\delta^{238}U$ = -0.29 ‰ to -0.21 ‰) reported in Weyer et al. (2008), although granites show larger U isotopic variations and show a tendency towards isotopically lighter values. In particular, the light isotope composition of a rhyolite ($\delta^{238}U$ = -0.45 ‰) indicates that in some cases U isotope fractionation during crustal differentiation may occur. The $\delta^{238}U$ of all analyzed granites, gneisses, the tonalite and the rhyolite fall into the previously observed range for granites by Weyer et al. (2008; $\delta^{238}U$ = -0.42 ‰ to -0.16 ‰), within uncertainties.

The three investigated post-Archean shales have U isotope compositions ranging between -0.26 ‰ and -0.39 ‰, which is within the range observed for magmatic and metamorphic rocks. As these shales sample large areas, they have been previously used for estimations of the composition of the continental crust. However, with respect to U mass fractions and isotope compositions they may be non-representative of the average crust, as authigenic U enrichment, and with that, U isotope fractionation may occur. In essentially anoxic/euxinic past oceans, they may mirror the U isotope composition of their source (rivers), as likely most of the dissolved U was quantitatively removed into such shales. The oldest post-Archean shale, MI-5 (1.5 Ga), with an isotopic composition of $\delta^{238}U$ = -0.26 ‰, similar as observed for the major rivers in this study (average $\delta^{238}U$ = -0.23 ‰) may represent such an example. The relatively high U mass fraction of 10.6 µg/g indicates that U was already mobilized during that time to a similar extent than today. In overall oxidized oceans of the Phanerozoic, the U isotope compositions of seawater appears to be slightly fractionated relative to that of rivers (Weyer et al., 2008; this study), depending on the relative mass balance of oxic and anoxic sinks (Montoya-Pino et al., 2010). Further, the U isotope composition of sediments may represent a mixture of fractionated authigenic U and a detrital component, representing the continental crust. Such processes may have affected U mass fractions and isotope compositions of the Devonian shale SC-8 (with an age of 440 Ma, and U mass fraction of 2.8 µg/g and $\delta^{238}U$ = -0.34 ‰) and the Triassic shale PW-5 (with a high U mass fraction of 8.4 µg/g and $\delta^{238}U$ = -0.39 ‰), which have U isotope compositions like

modern seawater or suboxic sediments (Weyer et al., 2008), but also fall into the range of granites from this study.

Using the granites and shales analyzed in this study and granites measured by (Weyer et al., 2008), we estimate an average U isotope composition for the upper crust to be -0.30 ‰ ± 0.04 ‰ (average and double standard error of the mean). We did not investigate the U isotope composition of carbonates, which may also contribute to the dissolved U in rivers. This may particular be the case for rivers from mountain belts, such as the here investigated alpine rivers, since their catchments contain a significant carbonate fraction which becomes easily weathered. Preliminary results from Herrmann et al. (2010) revealed that non-biogenic carbonates display an average $\delta^{238}U$ of -0.22 ‰ (relative to NBL CRM 112-A), i.e. somewhat heavier than the crustal average of this study.

3.5.2 Possible sources of U isotope variation in rivers

A study by Palmer and Edmond (1993) about the sources of U in major river systems, e.g. Orinoco, Amazon, Ganges, revealed that a large fraction of U is derived from non-silicate weathering. In many cases, organic rich sediments, e.g. black shales, seem to play an important role (Colodner et al., 1995; Singh et al., 2003), especially for rivers, which originate from the Himalayan (Indus, Brahmaputra, Bhagirathi, Alaknanda and Ganges) (Rahaman et al., 2010). However, granites and basalts also have to be considered as important U sources to the rivers (Borole et al., 1982; Pradeepkumar et al., 2008).

U isotope variations in rivers may reflect (a) contributions from various U sources with different isotope ratios within a river system and (b) U isotope fractionation during weathering and transport, e.g. through adsorption of U onto the surface of oxides or during dissolution processes within the river system.

To gain information, whether distinct U sources may dominate the U isotope composition of the rivers we investigated the relation between the major element composition (e.g. Ca, Na) and $\delta^{238}U$ of the rivers. This relationship is shown for the Swiss-rivers in Fig. 3.5. Among these rivers, Ticino shows the highest U concentrations, the lightest U isotope composition and also the highest Ca content of all Swiss-Rivers. The high Ca/Na ratios may be the result of mainly dolomitic and limestone weathering, occurring in the northern part of Ticino (Georg et al., 2006). Additionally, Ticino contains the highest discharge of all Swiss-Rivers (Table 3.1), which results in a larger diversity of different rocks and minerals. Compared to Ticino, Birs and Saane display lower U concentrations, slightly heavier $\delta^{238}U$, and lower Ca/Na ratios. Together, the Swiss rivers (in particular Ticino and Saane) display an anti-correlation between the U isotope composition and Ca/Na. These findings together indicate that carbonates, although potentially slightly heavier than granites (Herrmann et al., 2010; this study), are not the source of heavy U isotope compositions in rivers. Rather, the carbonate-dominated Ticino has a similar U isotope composition than the average of granites and carbonates, while the two other Swiss rivers (Birs and Saane) both display heavier U isotope compositions. As black shales, the only known source for heavy U isotopes (Weyer et al., 2008) are not frequent in the catchment of Birs and Saane, we conclude that the heavier U isotope composition of these rivers is generated by U isotope fractionation during weathering and transport. Fractionation could take place in the vadose zone during weathering, e.g. via incomplete dissolution and/or selective adsorption of U isotopes on Fe-oxyhydroxides/clays. Alternatively, it could occur within the rivers via interaction with suspended sediment, if isotopically light U is preferentially adsorbed on oxide particles (Brennecka et al., 2011a). Our data show that the tributary rivers, i.e. the dissolved river load, have low U concentration and somewhat higher $\delta^{238}U$ values. In comparison, larger rivers have higher U concentrations, with their U isotope composition virtually identical to that of the average of their sources (Fig. 3.4). These observations may indicate that a larger fraction of the U content of small rivers is adsorbed or incorporated by particles, assuming, that the total river load of small rivers, has not generally lower U contents than that of large rivers. In this case, U isotope fractionation may take place between the

dissolved and the particulate river load (i.e. within the vadose zone in case of the here investigated Swiss rivers). Confirmation of this assumption requires further detailed investigation and is beyond the scope of this study.

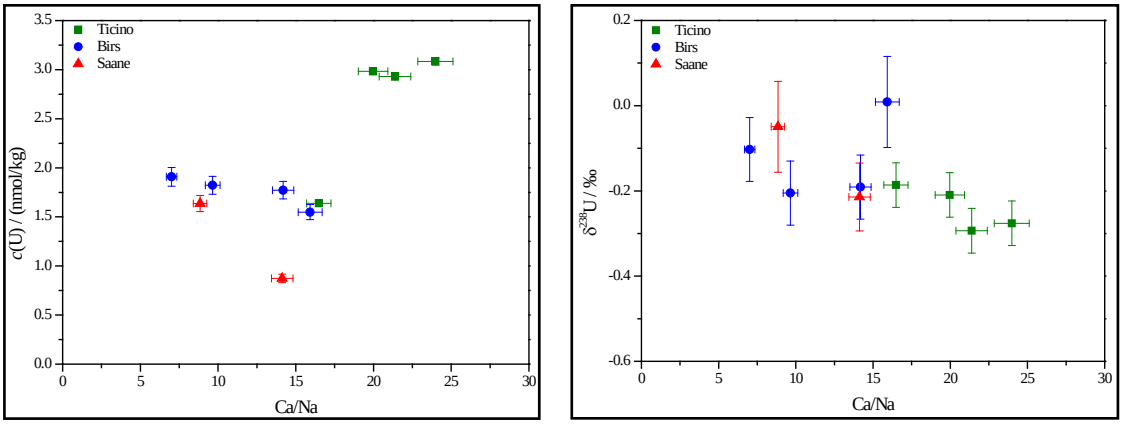

Fig. 3.5 Relationship between $\delta^{238}U$ in ‰ and *c*(U) in nmol/kg and the Ca/Na ratio in the Swiss-Rivers. All rivers together (in particular Ticino and Saane) show a negative correlation between Ca/Na and $\delta^{238}U$. The Ca/Na ratios were corrected for wet depositional inputs, according to the correction factors given by (Georg et al., 2006).

3.5.3 The U isotope composition of rivers

Ganges, Brahmaputra, and Indus, were defined as major rivers. Due to their high discharge and U concentration, they provide a large portion of the U input to the ocean. The confluence of the tributary rivers Bhagirathi and Alaknanda marks the beginning of the Ganges River. Comparing the U isotope composition of those three rivers may thus provide information, if U isotope fractionation takes place during the transport of U in rivers. In fact, Bhagirathi displays a slightly heavier isotopic signal ($\delta^{238}U$ = -0.23 ‰) than Alaknanda and Ganges ($\delta^{238}U$ = -0.32 ‰ and -0.31 ‰), although they all agree within their analytical uncertainties. Uranium isotope fractionation in rivers may occur, if isotopically light U is preferentially adsorbed on oxide particles (Brennecka et al.,

2011a), which would result in isotopically heavy U in rivers (in agreement with observations for Bhagirathi). Alternatively, isotopically heavy U may preferentially dissolve, e.g. from oxides, also resulting in a heavier U isotope signature of river water. Potentially, the effect of U isotope fractionation in rivers decreases, as most U becomes dissolved downstream the Ganges, also resulting in the high U concentration of the Ganges sample. Furthermore, the Ganges sample was taken shortly before the river flows into the Bay of Bengal, after it drained a catchment size of $1 \cdot 10^6$ km^2. In contrast, Bhagirathi only drains an area of $4 \cdot 10^3$ km^2 (Yadav and Chakrapani, 2011), respectively. Accordingly, Ganges is more representative as U input into the ocean, as it samples a large catchment area, averaging out potential U isotope heterogeneities in the catchment.

Additionally, we investigated how seasonal changes affect U concentrations and δ^{238}U in the Swiss-Rivers (Ticino, Birs and Saane). Fig. 3.6 displays how the U concentration changes throughout the year. The variations in the U concentration in Birs and Saane are rather small, just Ticino displays some noticeable changes, especially between March 2004 and May 2004, where the U concentration drops from 5.1 nmol/kg to 1.8 nmol/kg. Despite this change in the U concentration, Ticino displays no resolvable variation in the U isotopic composition (Fig. 3.7). Birs and Saane show larger seasonal U isotope variations and also the heaviest U isotope compositions of all analyzed rivers (i.e. δ^{238}U = 0.01 ‰ to -0.21 ‰ and -0.05 ‰ to -0.21 ‰, respectively). Their U concentrations are relatively constant throughout the year. Hence, individual Swiss-Rivers display no direct correlation between the U content and δ^{238}U. Potentially, the variations in δ^{238}U are the result of variable U isotope fractionation between the dissolved- and the particulate river load. One may speculate that U isotope fractionation is the largest during seasons of high discharge (e.g. in May), resulting in high physical weathering and high particulate river load, although the data set of this study is insufficient to resolve this relationship.

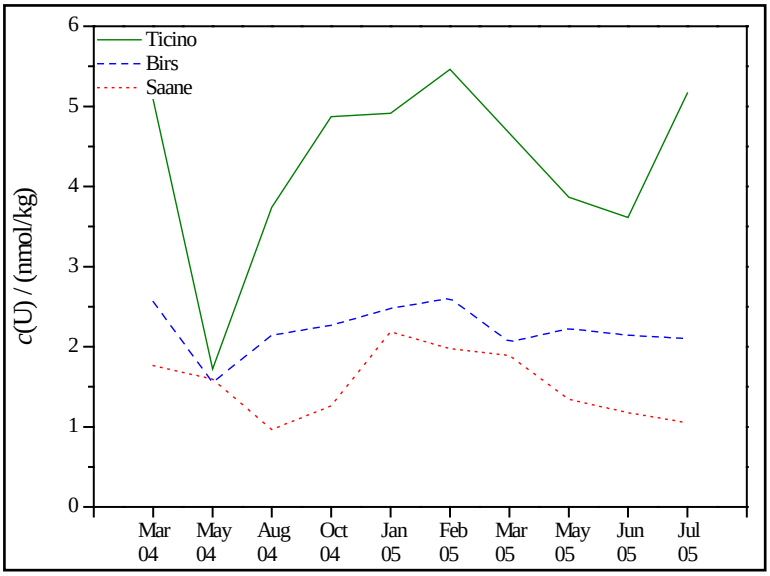

Fig. 3.6. U concentration in the Swiss-Rivers observed over a time period of 16 month. Ticino is the only Swiss-River, which shows significant variations throughout the year.

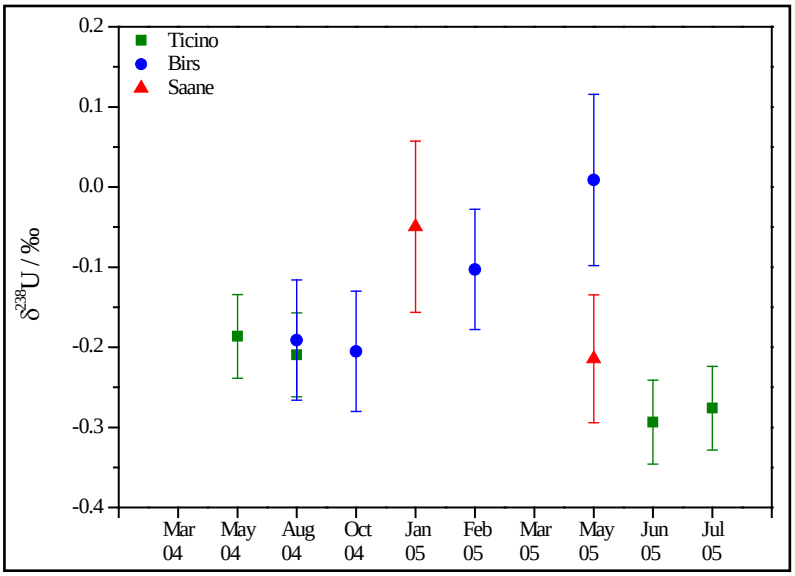

Fig. 3.7. $\delta^{238}U$ versus time in the Swiss-Rivers. Birs and Saane display the largest seasonal U isotope variations.

As Birs and Saane show large seasonal U isotope variations, likely generated by variable U isotope fractionation and as these small rivers contribute only little to the global river discharge, we excluded these rivers from an estimation of the average U isotope composition of rivers. Most representative may be the three investigated major rivers (Indus, Ganges and Brahmaputra), all of which display an average $\delta^{238}U$ of -0.23 ‰ ± 0.11 ‰ (2 S.E.). However, the major rivers studied here drain the Himalayan and the catchments may sample a significant proportion of black shales (Sarin et al., 1992; Sharma et al., 1999); potentially, such sources may be responsible for the heavy U isotope composition of Indus which differs outside analytical uncertainties from those of Ganges and Brahmaputra. Nevertheless, the average of these major rivers agrees, within analytical uncertainties, with the average value for the upper crust ($\delta^{238}U$ of -0.30 ‰ ± 0.04 ‰ (2 S.E.)) obtained by this study. This finding indicates that only minor U isotope fractionation occurs between the continental crust and major rivers.

Table 3.3 Average values obtained in this study, relative to the uranium standard NBL CRM 112-A.

Average values for the different input materials	$\delta^{238}U$ ‰	Uncertainty	
		2 SD	2 SE
granites (this study)	-0.30	0.14	0.04
granites (Weyer et al., 2008)	-0.31	0.21	0.10
post-archean shales	-0.33	0.13	0.07
average crust (this study)[a]	-0.30	0.15	0.04
basalts (Weyer et al., 2008)	-0.25	0.07	0.03
average rivers (this study)	-0.23	0.19	0.11

[a]The value for the average crust (this study) includes the data of all crustal samples of this study and the granites analyzed by Weyer et al. (2008).

3.6 Conclusion

We conclude that in average only minor U isotope fractionation occurs during weathering and transport of the continental crust to the ocean. An essentially

quantitative transfer of the soluble uranyl complex may explain this limited fractionation during oxidative weathering. Only tributary rivers display larger U isotope variations likely generated by U isotope fractionation between the dissolved and the particulate U. Additionally, isotopically heavy U sources in the river catchment (e.g. black shales) may be mirrored by the U isotope composition of rivers in some cases.

In average, major rivers show a slightly lighter U isotopic composition compared to tributary rivers, and less U isotope variations. $\delta^{238}U_{average}$ of rivers is slightly heavier than that of granites (~0.07 ‰). However, they display an identical U isotopic signature to basalts (Weyer et al., 2008) and carbonates (Herrmann et al., 2010). Based on our measurements of major rivers, we obtained a new estimate for the U input to the modern ocean ($\delta^{238}U$ = -0.23 ‰) and we recommend to use this value for further mass balance calculations.

Acknowledgments

Sampling of the Swiss Rivers was supported by ETH Zurich and the Swiss National Funds (No.: 2000 20/101 780). We are grateful to Axel Gerdes, Armin Zeh, Elis Hoffmann and Carsten Münker for providing samples. We thank Anna K. Neumann and Michael Seitz for laboratory assistance. Funding was provided by the Deutsche Forschungsgemeinschaft (DFG, WE 2850/6).

3.7 Appendix

Table A 3.1 Additional results for the analyzed rock samples.

Sample	Sampled	Material	*w*(La) (µg/g)	*w*(Ce) (µg/g)	*w*(Pr) (µg/g)	*w*(Nd) (µg/g)	*w*(Sm) (µg/g)	*w*(Eu) (µg/g)	*w*(Gd) (µg/g)	*w*(Tb) (µg/g)	*w*(Dy) (µg/g)	*w*(Ho) (µg/g)	*w*(Er) (µg/g)	*w*(Tm) (µg/g)	*w*(Yb) (µg/g)	*w*(Lu) (µg/g)
jeh-SG-01	Greenland	Tonalite	48.59	35.14	44.70	33.01	17.09	12.63	10.64	8.17	6.56	5.97	5.30	5.62	5.10	4.93
229403	Greenland	Gneiss	73.13	64.97	52.56	46.44	25.39	16.53	15.62	11.82	9.34	8.38	7.31	7.44	6.57	6.18
JR2	Japan	Rhyolite	50.07	44.79	40.79	32.98	26.98	1.27	20.44	21.47	21.37	21.95	21.87	26.22	25.72	26.12
JG2	Japan	Granite	80.90	76.88	68.14	57.00	52.26	1.25	39.39	41.89	41.50	42.14	40.50	45.68	41.82	40.53
RGd 23-84	Germany	Granite	257.43	175.31	123.34	87.32	38.61	27.01	22.53	14.91	10.97	9.95	8.90	8.59	6.16	5.47
RbG 17-54	Germany	Granite	115.83	120.63	116.32	107.82	68.74	30.44	34.82	24.63	18.24	15.88	13.62	14.43	12.96	12.35
Wb 11-94	Germany	Granite	131.20	110.09	97.50	86.34	69.65	36.90	42.95	33.70	26.67	23.65	20.30	20.21	17.41	16.29
Wb 68-94	Germany	Granite	233.97	177.63	140.59	106.33	57.42	20.32	34.68	24.33	17.48	14.49	11.40	9.85	7.77	7.60
SW-AG7	Swaziland	Gneiss	159.51	126.05	98.81	78.02	57.14	24.45	38.37	32.27	27.28	24.66	21.61	22.53	20.41	19.35
SW-SIN23	Swaziland	Granite	126.26	90.81	71.62	48.60	28.86	4.69	24.56	27.54	31.15	34.90	33.84	33.80	26.74	23.32
SW-SIC19	Swaziland	Granite	475.86	354.41	248.13	165.87	84.78	19.62	56.42	45.04	38.64	36.81	34.37	36.24	32.82	31.55
PW-5	Australia	Shale	185.21	106.65	93.97	68.97	36.78	17.99	21.54	17.35	13.92	12.75	10.77	11.37	10.08	10.28
SC-8	Australia	Shale	144.06	82.32	72.19	50.71	26.98	12.44	15.06	12.25	9.55	8.74	7.56	8.18	7.48	7.75
MI-5	Australia	Shale	160.10	120.05	89.44	66.09	36.48	17.31	30.11	20.96	17.14	15.22	14.64	14.19	14.45	13.86

CHAPTER 4

Uranium and molybdenum isotope systematics in modern euxinic basins: Case studies from the central Baltic Sea and the Kyllaren fjord (Norway)

Janine Noordmann, Stefan Weyer, Carolina Montoya-Pino, Olaf Dellwig, Nadja Neubert, Sebastian Eckert, Matthias Paetzel, Michael E. Böttcher

Published in Chemical Geology (2015) 396, 182-195,
doi:10.1016/j.chemgeo.2014.12.012

Abstract

Recent investigations have revealed significant fractionation of $^{238}U/^{235}U$ between organic-rich sediments of anoxic marginal seas and seawater, indicating redox-dependent U isotope fractionation. This study explores the conditions controlling U isotope fractionation in selected modern anoxic basins (Baltic Sea: Landsort and Gotland Deeps and the Kyllaren fjord in Norway) and compares U with Mo isotope fractionation. Therefore, the concentrations and isotope compositions of dissolved U and Mo from the water column and organic-rich sediments from three currently anoxic basins have been analysed.

The water column samples from the Kyllaren fjord display a moderate depletion of U and a strong depletion of Mo with increasing depth. These variations are associated with a decrease in $\delta^{238}U$ and an increase in $\delta^{98}Mo$ with depth, from -0.35 ‰ to -0.70 ‰ and from 2.4 ‰ to 2.6 ‰, respectively. From the U isotope composition of the deep euxinic water column of the Kyllaren fjord, a minimum value of $\Delta^{238}U_{red} \approx 0.7$ ‰ for the U isotope fractionation during reduction is inferred. Due to the high sedimentation rate in the Kyllaren fjord, surface sediment samples are only moderately enriched in U and Mo (~ 4 µg/g and 6 µg/g to 37 µg/g, respectively) and display $\delta^{238}U$ and $\delta^{98}Mo$ averages of -0.26 ‰ ± 0.10 ‰ and 2.18 ‰ ± 0.21 ‰, respectively.

Water column samples from the Baltic Sea display a minor decrease in the U and Mo concentrations and only negligible U and Mo isotope fractionation compared to open seawater. The sediment layers from the Baltic Sea (Landsort Deep), which were deposited under mostly anoxic conditions, are moderately enriched in U (up to 8 µg/g) and highly enriched in Mo (up to 222 µg/g). However, U and Mo isotopic compositions are significantly lighter (with $\delta^{238}U$ of -0.36 ‰ ± 0.08 ‰ and $\delta^{98}Mo$ of -0.04 ‰ ± 0.11 ‰) than those of typical organic-rich sediments from anoxic basins.

These findings reveal that compared to Mo, the U isotopic composition of sediments in restricted and strongly euxinic basins like the Kyllaren fjord is significantly more dependent on (1) the extent of U removal from the water column, which is lower than that of Mo, and on (2) the sedimentation rate (i.e., the fraction of

authigenic U relative to detrital U in the sediment), which is also lower compared to that of Mo. In more open and only temporarily euxinic basins such as the investigated basins of the Baltic Sea, strong Mo is coupled with weak U isotope fractionation between water and sediment. These signatures were likely the result of isotope fractionation under weakly sulfidic conditions and the generation of isotopically light Mo during frequently occurring flushing events with oxygen-rich water from the open sea. This implies that Mo and U isotope signatures of sediments only record paleo-water column redox conditions of restricted basins if the water column was permanently stratified.

4.1 Introduction

Uranium and Mo are redox-sensitive trace elements with long ocean residence times (0.5 Ma and 0.8 Ma, respectively; Morford and Emerson, 1999; Dunk et al., 2002) and with similar redox behaviour in the ocean. Under oxidizing conditions (e.g. $\geq 10^{-4}$ mol O_2 L^{-1}), they occur in a valence state of +VI and as soluble uranyl complexes (e.g. $UO_2(CO_3)_3^{4-}$) and soluble molybdate (MoO_4^{2-}; Morford and Emerson, 1999). Under these conditions, both Mo and U are assumed to typically display conservative behaviour in the water column, with only a few exceptions (e.g., observed for Mo in coastal waters in the Wadden Sea of NW Germany; Dellwig et al. (2007) and Kowalski et al. (2009)). Under suboxic (e.g. 10^{-5} to 10^{-4} mol O_2 L^{-1}) to anoxic ($< 10^{-6}$ mol H_2S L^{-1}, $< 10^{-5}$ mol O_2 L^{-1}) conditions (e.g., at continental margins), both Mo and U become non-conservative and enriched in the sediments (McManus et al., 2006). Under highly euxinic conditions ($H_2S > 11$ µM; 0 mol O_2 L^{-1}, Erickson and Helz, 2000), which occur in the deep water columns of some stratified isolated basins (e.g., Black Sea), Mo is quantitatively transformed to particle-reactive thiomolybdate (MoS_4^{2-}) and therefore, almost quantitatively removed from the water column into organic-rich sediments (Helz

et al., 1996; Erickson and Helz, 2000; Neubert et al., 2008). In such cases, sediments can essentially record the original seawater Mo isotopic composition due to a closed-system reservoir effect (Barling et al., 2001; Nägler et al., 2005; Neubert et al., 2008; Nägler et al., 2011); however, the overall transformation to thiomolybdate is associated with Mo isotope fractionation between seawater and sediment (on the order of $\Delta^{98}Mo_{sed\text{-}water}$ = -0.5 ‰; Nägler et al., 2011). In contrast to Mo, U is assumed to occur as soluble and chemically labile U(VI), even under highly euxinic conditions such as the deep water column of the Black Sea (Anderson et al., 1989). Reduction and removal of U in such environments is assumed to occur in the sediment or within the pore water rather than by scavenging from the water column. This process appears to be associated with significant U isotope fractionation of approximately 0.4 ‰ to0.7 ‰ relative to seawater (Weyer et al., 2008), resulting in sediments with a high $\delta^{238}U$ of up to 0.4 ‰ (Weyer et al., 2008; Bopp et al., 2010; Montoya-Pino et al., 2010; Andersen et al., 2014). Under such conditions, the direction of U isotope fractionation during reduction appears to be opposite that of Mo, probably due to volume-dependent isotope effects (i.e. "nuclear field shift", Bigeleisen, 1996; Schauble, 2007; Abe et al., 2008) dominating U isotope fractionation.

Adsorption of Mo to pelagic clays, ferromanganese oxides or Mo removal to reducing sediments (e.g., at continental margins) results in significant isotope fractionation (on the order of 1 ‰ to 3 ‰; Goldberg et al., 2009; Poulson et al., 2009; Goldberg et al., 2012) towards a light Mo isotopic composition compared to the mean ocean water value ($\delta^{98}Mo$ = 2.3 ‰; Siebert et al., 2003; Barling and Anbar, 2004; Siebert et al., 2006). Uranium displays only minor U isotope fractionation under oxic conditions towards lower $\delta^{238}U$, relative to the mean ocean water value of -0.4 ‰ (e.g., that occurs during adsorption to ferromanganese oxides) (Stirling et al., 2007; Weyer et al., 2008; Brennecka et al., 2011a).

Although modern anoxic basins (e.g. the Black Sea, deeps in the Baltic Sea, and Cariaco Basin) account for only 0.3 % of the modern oceans (Bertine and Turekian, 1973), they play a significant role as a sink for Mo and U from ocean water. This results from the low solubility behaviour of Mo and U in the water column under anoxic

conditions and their high enrichment in the organic-rich sediments of such basins. As Mo and U display significant isotope fractionation between oxic and anoxic sinks, both isotope systems have the potential to record the redox evolution of the oceans (e.g., Arnold et al., 2004; Wille et al., 2007; Pearce et al., 2008; Wille et al., 2008; Kendall et al., 2009; Dahl et al., 2010; Montoya-Pino et al., 2010; Brennecka et al., 2011b; Nägler et al., 2011, Asael et al., 2013; Dahl et al., 2014). However, sedimentary records of ancient seawater Mo and U isotopic compositions, such as black shales, should be used with caution as variable isotope fractionation may occur depending on the local redox conditions during their deposition (Nägler et al., 2005; Poulson et al., 2006; Neubert et al., 2008; Gordon et al., 2009; Dahl et al., 2010; Montoya-Pino et al., 2010; Nägler et al., 2011; Goldberg et al., 2012). In contrast to Mo, whose isotopic composition in seawater may be directly reflected by black shales accumulated under strong euxinic conditions with concentrations of total dissolved sulphide > 100 µmol/L (Barling et al., 2001; Neubert et al., 2008; Nägler et al., 2011), U isotopes generally display large fractionation between organic-rich sediments and seawater (Weyer et al., 2008; Montoya-Pino et al., 2010). However, little is currently known about the parameters and environmental conditions that control the extent of U isotope fractionation.

In this study, U and Mo concentrations and isotope compositions of the water columns and the sediments of recent anoxic basins (including the Kyllaren fjord and the Landsort and Gotland Deeps of the Baltic Sea) are presented. The findings for U isotopes have been compared with the better understood Mo isotope systematics. A particular focus of the study was on the effect of the degree and persistence of water column stratification on the U and Mo isotope signatures observed in the sediments and on their liability to be affected by detrital components.

4.2 Sampling locations

4.2.1 Kyllaren fjord

The Kyllaren fjord is a 29 m deep basin that is located on the west coast of Norway (Fig. 4.1a, 61°25´N, 5°10´E) and connected to the Norwegian Sea by a narrow 5 km long and 1-2 m deep tidal channel. The water column of the Kyllaren fjord is strongly stratified. The salinity increases with depth from 14 g/kg to 25 g/kg, which is similar to the Black Sea. The oxygen concentration decreases to undetectable levels at approximately 4 m depth, while the H_2S concentration increases to ~ 4000 µmol/L at a depth of approximately 6 m, which is an order of magnitude higher than H_2S_{total} in the Black Sea water column (Neretin et al., 2001; Fig. 4.1b; Smittenberg et al., 2004; van Breugel et al., 2005a,b). The chemocline (the area with the strongest increase in salinity and the strongest decrease in oxygen concentration) in the Kyllaren fjord is usually located at a depth of approximately 3.5 m (van Breugel et al., 2005a). In 1954 and 1988, dams were built in Straume and Askvika (Fig. 4.1a), which reduced the connection to the open sea from 400 m to two connections of 15 m width each (Smittenberg et al., 2004). In 1993, another 2 m wide opening was built into the dam at Straume (Smittenberg et al., 2004; van Breugel et al., 2005a). As a result of the anthropogenic restriction, anoxic degassing events have frequently occurred since 1993.

The water samples for this study were collected using a tube, a winch and a vacuum pump; all parts are composed of plastic components, which were intensively cleaned with 2 % HNO_3 and Milli-Q® H_2O. The two 40 cm deep sediment cores (KY09-1 und KY09-3) were collected from two different stations in the fjord (at 28 m below sea level and 10 m below sea level, respectively) using a gravity corer deployed from a raft in May 2009.

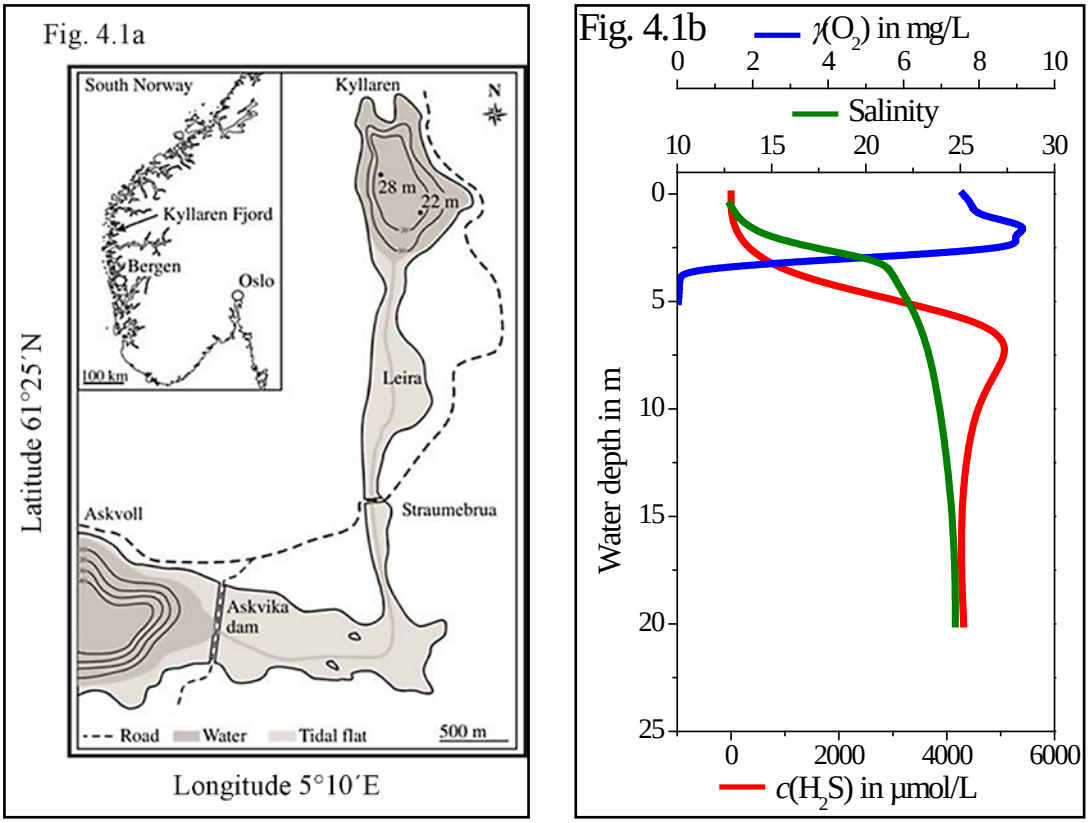

Fig. 4.1a Location of the Kyllaren fjord on the west coast of Norway (61°25´N, 5°10´E, Smittenberg et al., 2004); 4.1b) Depth profile for the salinity content, H_2S and oxygen concentrations in the Kyllaren fjord. The H_2S, oxygen and salinity data were taken from van Breugel et al. (2005a).

4.2.2 The Baltic Sea

The Baltic Sea is the largest brackish water basin worldwide (Fig. 4.2a), displaying a salinity increase with depth from 7 g/kg to 13 g/kg (Jost et al., 2008). The average depth is approximately 50 m, while several deeper basins, such as the Gotland Deep and Landsort Deep, reach maximum depths of 249 m and 459 m, respectively. These basins differ in their spatial extent with the Landsort Deep being much smaller but deeper than the Gotland basin. Both basins are affected by temporary redox stratification and currently have a euxinic deep water column due to limited water exchange between the deeper and shallower parts of the water column resulting from

density stratification (Matthäus and Franck, 1992). This water column stratification results in a shuttling of Fe and Mn into the Gotland- and Landsort Deep (Huckriede and Meischner, 1996; Dellwig et al., 2010; Scholz et al., 2013). The chemocline is positioned at an approximate water depth of 90 m in the Landsort Deep and 120 m in the Gotland Deep (Fig. 4.2b and 4.2c; Dellwig et al., 2012). The euxinic conditions in the Baltic Sea are not stable, as periodical flushing events, usually on a decadal time scale, contribute salty and oxygenated waters from the North Sea (e.g., Matthäus and Franck, 1992; Huckriede and Meischner, 1996; Schinke and Matthäus, 1998; Reissmann et al., 2009). Accordingly, deep water renewal times are variable and difficult to estimate. However, recent measurements of the salt content suggest that the current deep water renewal time is on the order of 100 years (Reissmann et al., 2009).

The Baltic Sea water samples were recovered during the R/V “Prof. A. Penck” cruise in July 2008 (station 342390 for Landsort Deep and station 342370 for Gotland Deep) with a CTD pumpcast system (Conductivity-temperature-depth profiler). On board, all samples were filtered with a 0.45 µm polycarbonate filter, acidified to a pH < 2 with HNO_3 and stored in PE bottles.

The organic-rich sediments were obtained with multicoring devices during the R/V “Prof. A. Penck” cruise in 2007. A downcore profile (core 342390-2-7) from the Landsort Deep (58° 34.91´ N/ 18° 13.71´ E) was collected at a water depth of 450 m.

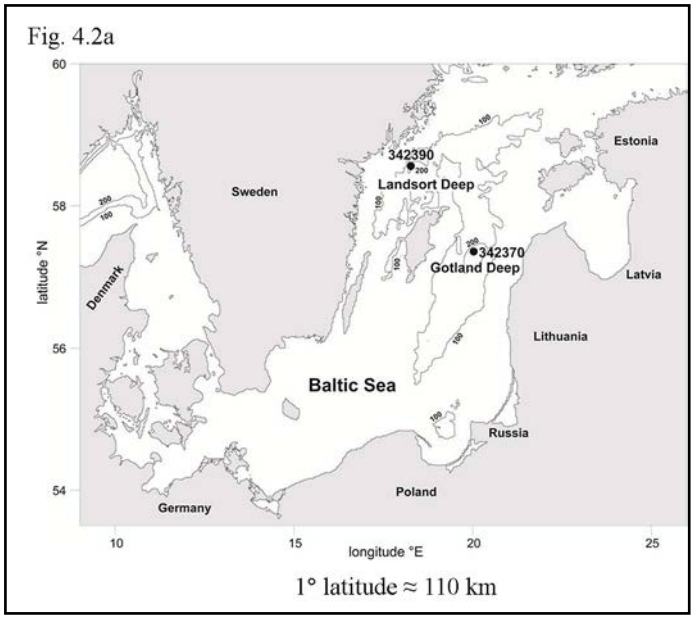

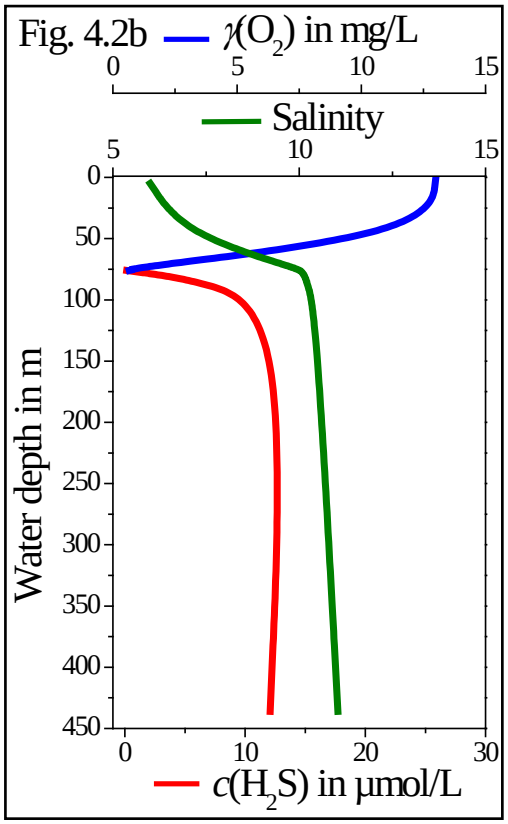

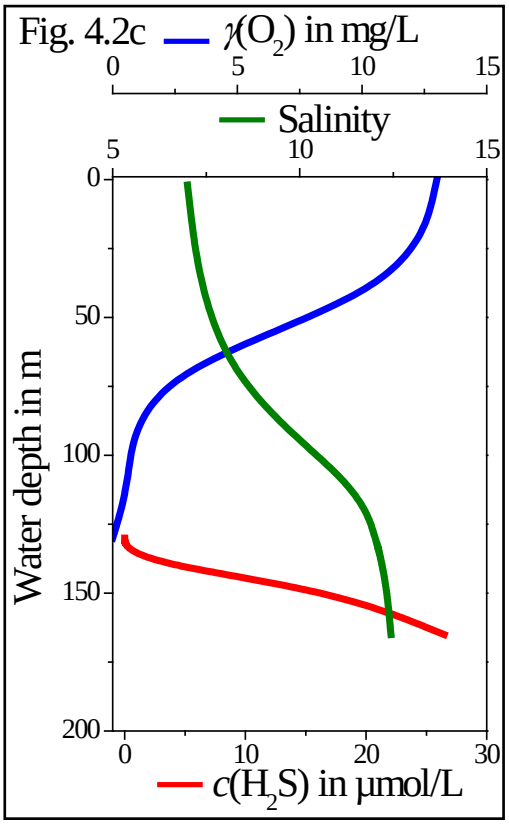

Fig. 4.2 Location of the Baltic Sea and the Gotland and Landsort Deep basins within the Baltic Sea (Dellwig et al., 2012); b) and c) are depth profiles for the salinity content and H_2S and oxygen concentrations for the Landsort Deep and Gotland Deep, respectively. The H_2S, oxygen and salinity data were taken from Dellwig et al. (2012).

4.3 Analytical methods

4.3.1 Sample preparation

For organic-rich sediments, approximately 200 mg was ashed in ceramic vessels at 550 °C overnight. The residue was digested with a mixture of concentrated $HF/HNO_3/HClO_4$ (3:1:1) in Parr® high-pressure vessels at 180 °C. The samples were repeatedly treated with 6 M HNO_3 and 6 M HCl to dissolve any remaining fluorides (modified according to Weyer et al., 2008). The samples were finally re-dissolved in 6 M HCl and split into two equal aliquots, intended for Mo and U purification. Prior to chromatographic separation, an aliquot of 5 % was taken from the samples for the analyses of element concentrations (including Fe, Al, Mn, Re, Mo and U) with ICP-MS (Thermo Scientific Element 2 in Frankfurt). The U double-spike IRMM 3636-A (which consists of a ~ 1:1 mixture of ^{236}U and ^{233}U; Richter et al., 2008) was added to the remaining sample solution prior to separation of U from the sample matrix by anion exchange chromatography (based on Eichrom UTEVA resin, following the procedure described by Weyer et al., 2008). The separation of Mo from the sample matrix was achieved by a two-step chromatographic purification (on anion and cation columns without previous addition of a Mo double spike, following the procedure outlined in Anbar et al., 2001).

To analyse the water samples, approximately 100 mL was gently evaporated to dryness. Subsequently, nitric acid was added to re-dissolve and prepare the samples for U and Mo purification, according to the method described in Weyer et al. (2008) and Barling et al. (2001). Prior to Mo and U purification from the sample matrix, a small aliquot was taken from the samples for the determination of trace element concentrations (including Mo and U) with ICP-MS. Subsequently, the U double-spike IRMM 3636-A was added to the remaining sample solution. According to the limited amount of Mo and U in the water samples, we separated and purified Mo and U from the same aliquot. To this end, we quantitatively collected the matrix (including the Mo fraction) from U purification (on Eichrom UTEVA resin) to subsequently reload it on columns with anion and cation exchange resins for the purification of Mo. As we did

not use a Mo double spike to monitor potential Mo isotope fractionation during sample preparation and analysis, we performed extensive tests with synthetic seawater to ensure 100 % recovery, particularly for Mo. These tests revealed overall yields of 100 % ± 5 % Mo during the procedure. In contrast, switching the order of U and Mo purification resulted in very poor and non-reproducible yields for U, which thus emerged as an unsuitable procedure.

4.3.2 Molybdenum and U isotope analyses

Both Mo and U isotope measurements were performed on a MC-ICP-MS (Thermo Scientific Neptune; Weyer and Schwieters, 2003) at the Goethe University of Frankfurt and the Leibniz University of Hannover. Molybdenum isotopes were analysed at wet plasma conditions using an Elemental Scientific SIS glass spray chamber combined with a 50 µL PFA nebuliser. In general, all sediment and most of the water samples were measured at concentrations of 400 ng/g Mo, which resulted in a signal of ~ 3 V on ^{98}Mo. Prior to the isotopic measurements, all standards and samples were "spiked" with a solution of natural Zr (Specpure Lot#13716055), which was used to monitor and correct for instrumental mass-bias, assuming ^{90}Zr/^{91}Zr = 4.58421 (Anbar et al., 2001; Barling et al., 2001). The concentration of Zr was adjusted to approximately half of the Mo concentration. The samples were measured relative to the Johnson Matthey Specpure® Mo plasma standard (Lot #802309E; "RochMo2"), which has already been used in previous studies (Anbar et al., 2001; Barling et al., 2001; Arnold et al., 2004; Kendall et al., 2009). The results of the isotope analyses are expressed in the delta-notation:

$$\delta^{98}\text{Mo in ‰} = [(^{98}\text{Mo}/^{95}\text{Mo})_{\text{sample}}/(^{98}\text{Mo}/^{95}\text{Mo})_{\text{standard}} - 1] \times 1000 \qquad \text{Eq. 4.1}$$

Similar to Barling et al. (2001), the samples were analysed by standard bracketing in triplicate and interleaved with the Johnson Matthey Specpure® Mo plasma standard. Occasional runs of a Devonian Ohio shale (USGS SDO-1, δ^{98}Mo = 1.1 ‰) and a gravimetrically prepared standard (Grav Rochester Mo2, δ^{98}Mo = -1.0 ‰)

ensured that instrumental conditions were stable (reference values for these standards were published in Barling et al., 2001 and Kendall et al., 2009).

The U isotope composition and concentration for the sediments and water samples were determined according to the method described in detail in Weyer et al. (2008) and Montoya-Pino et al. (2010). Briefly, all U isotopes (^{233}U, ^{235}U, ^{236}U and ^{238}U) were measured on a MC-ICP-MS (Thermo Scientific Neptune) at the Goethe University of Frankfurt and the Leibniz University of Hannover, using a Cetac Aridus combined with a 50 µL PFA nebulizer for sample introduction. The ^{238}U was measured on a 10^{10} Ω resistor and ^{233}U, ^{235}U and ^{236}U were measured on a 10^{11} Ω resistor due to their lower intensities. The samples were analysed at concentrations of 100 ng/g U, resulting in a signal of at least 35 V on ^{238}U and 250 mV on ^{235}U. Uranium isotope analyses were obtained by standard bracketing, as described for Mo isotope analyses, relative to the U standard NBL CRM 112-A. The results of the isotope measurements are provided in the delta-notation:

$$\delta^{238}U \text{ in } ‰ = [(^{238}U/^{235}U)_{sample}/(^{238}U/^{235}U)_{standard} - 1] \times 1000 \qquad \text{Eq. 4.2}$$

The U double spike, IRMM 3636-A, was used to correct for instrumental mass bias during U isotope analyses with MC-ICP-MS. The spike/sample ratios were optimized to $n(^{236}U)/n(^{235}U) \approx 3$, to minimise tailing effects from $n(^{238}U)$ on $n(^{236}U)$ and from $n(^{236}U)$ on $n(^{235}U)$, respectively. As the contribution of the $n(^{238}U)$ tail on $n(^{236}U)$ was typically smaller than $1 \cdot 10^{-6}$, it did not significantly affect the precision of the analyses. Nevertheless, we routinely monitored the tail of $n(^{238}U)$ on mass $n(^{236}U)$.

The performance of this double spike method was tested by the contribution of our laboratory to a comparative inter-laboratory study in which various international U standards have been analysed (Richter et al., 2010). Furthermore, several international U standards (NBL CRM 112-A = NBS SRM-960, IRMM-184, NIST SRM 950-A and REIMEP 18-A) have been analysed and the results are in agreement with those published previously (Weyer et al., 2008; Richter et al., 2010; Basu et al., 2014).

4.4 Results

Water and sediment samples from the Kyllaren fjord and the Baltic Sea (Landsort and Gotland Deep) have been analysed for selected major and trace element concentrations (including Fe, Al, Mn, Re, Mo and U for the sediments and only Mo and U for the water samples) and for their U and Mo isotope compositions ($\delta^{238}U$ and $\delta^{98}Mo$). The results are presented in Tables 4.1 and 4.2 and Figs. 4.3 to 4.6. The water samples were collected and presented at the given water depth (Table 4.1), while sediment samples were collected and presented as averaged values across a certain sediment section (Table 4.2). The accuracy and precision are better than 1 % for the determination of the U concentrations (with ID) and approximately 5 % for the other element concentrations, which were determined by ICP-MS. The uncertainties for $\delta^{238}U$ and $\delta^{98}Mo$, as determined by three replicate measurements of each sample, are typically 0.05 ‰ and 0.1 ‰ (2 SD).

Table 4.1 Analyses of the water column samples from the Kyllaren fjord and the Landsort and Gotland Deeps (both localities within the Baltic Sea)

Locality	Water depth m	Salinity	*c* (Oxygen) µmol/L	*c* (H_2S) µmol/L	*c* (Mo) nmol/kg	δ^{98}Mo ‰	2 SD ‰	*c* (U) nmol/kg	δ^{238}U ‰	2 SD ‰
Kyllaren fjord										
	2	13.9	387.5	1.1	38	2.44	0.14	5.1	-0.35	0.01
	3	20.5	375.0	n.d.	71	2.59	0.14	7.4	-0.37	0.02
	3.5	21.3	212.5	n.d.	n.d.	n.d.	n.d.	7.4	-0.41	0.02
	4	21.6	18.8	1015.5	42	2.58	0.11	7.3	-0.44	0.08
	4.6	22.0	6.3	n.d.	57	2.42	0.12	7.3	-0.49	0.08
	7	23.5	0.0	5022.1	22	n.d.	n.d.	7.2	-0.60	0.03
	15	24.7	0.0	4228.4	7	n.d.	n.d.	6.3	-0.73	0.01
	20	24.7	0.0	4316.0	8	n.d.	n.d.	5.3	-0.70	0.04
Landsort Deep										
	45	6.9	398.1	0.0	17	2.24	0.14	3.0	-0.33	0.03
	73	9.8	33.1	0.1	19	2.37	0.22	3.5	-0.39	0.08
	76	10.1	20.5	0.1	21	2.36	0.09	3.5	-0.43	0.11
	85	10.2	0.0	6.9	22	2.38	0.24	3.5	-0.36	0.01
	112	10.5	0.0	13.5	21	2.49	0.02	3.6	-0.39	0.04
	436	11.0	0.0	12.1	24	2.42	0.08	3.9	-0.41	0.02
Gotland Deep										
	110	11.6	21.3	0.0	26	2.32	0.14	4.4	-0.36	0.07
	130	12.1	0.0	0.0	25	2.39	0.10	4.5	-0.40	0.01
	134	12.1	0.0	0.0	27	2.34	0.19	4.5	-0.43	0.08
	140	12.2	0.0	3.4	29	2.22	0.07	4.5	-0.44	0.04
	150	12.3	0.0	18.0	28	2.37	0.18	4.5	-0.50	0.07
	165	12.4	0.0	26.5	28	2.27	0.16	4.5	n.d.	n.d.

Table 4.2 Analyses of sediment cores from the Kyllaren fjord (KY09-1: 28 mbsl and KY09-3: 10 mbsl) and the Landsort Deep (Baltic Sea)

Average depth cm	Sediment section cm	*w* (Fe) mg/g	*w* (Al) mg/g	*w* (Mn) mg/g	*w* (Re) ng/g	*w* (Mo) µg/g	δ^{98}Mo ‰	2 SD ‰	*w* (U) µg/g	δ^{238}U ‰	2 SD ‰
Kyllaren fjord											
KY09-1											
1.20	1.0 - 1.4	26	49	0.4	4.8	6.0	2.00	0.14	4.8	-0.20	0.06
3.60	3.4 - 3.8	28	53	0.5	6.1	8.2	2.11	0.14	5.1	-0.26	0.03
5.60	5.4 - 5.8	30	51	0.5	6.4	19.8	2.34	0.07	5.4	-0.21	0.07
7.60	7.4 - 7.8	33	46	0.5	2.5	8.4	2.16	0.11	4.5	-0.23	0.09
16.20	16.0 - 16.4	31	45	0.5	5.3	9.3	2.17	0.15	6.0	-0.23	0.06
19.30	18.8 - 19.8	30	46	0.5	3.5	17.3	2.12	0.12	4.9	-0.31	0.05
22.30	21.8 - 22.8	29	50	0.5	2.6	9.8	2.12	0.12	4.6	-0.34	0.07
30.30	30.3 - 32.8	27	52	0.5	3.9	12.6	2.28	0.05	4.2	-0.32	0.08
35.30	35.3 - 37.8	26	54	0.5	2.7	10.7	2.24	0.11	4.7	-0.33	0.09
37.80	37.8 - 40.3	25	50	0.4	3.1	16.5	2.18	0.06	4.9	-0.27	0.05
KY09-3											
1.20	1.0 - 1.4	30	41	0.4	6.3	13.6	2.14	0.08	4.0	-0.22	0.05
4.80	4.6 - 5.0	31	43	0.4	6.8	32.9	2.30	0.05	4.1	-0.18	0.05
9.20	9.0 - 9.4	34	42	0.5	5.1	6.9	1.93	0.06	4.2	-0.30	0.09
11.20	11.0 - 11.4	36	45	0.5	3.8	8.9	2.08	0.05	3.8	-0.30	0.10
16.80	16.6 - 17.0	31	42	0.4	5.5	37.1	2.23	0.10	4.9	-0.22	0.14
18.50	18.0 - 19.0	32	42	0.5	5.9	28.8	2.15	0.09	4.7	-0.31	0.07
30.25	29.0 - 31.5	30	47	0.5	7.8	27.6	2.19	0.06	5.5	-0.25	0.04
35.25	34.0 - 36.5	28	44	0.4	7.6	20.3	2.28	0.13	6.0	-0.22	0.09
42.00	41.5 - 42.5	30	47	0.5	8.0	21.9	2.30	0.14	5.4	-0.28	0.02
Landsort Deep											
0.5	0 - 1	29	39	113.1	3.1	103.4	-0.08	0.10	6.0	-0.39	0.06
1.5	1 - 2	22	29	162.4	2.8	98.7	0.00	0.10	5.0	-0.33	0.06
2.5	2 - 3	37	35	123.1	3.5	152.2	-0.24	0.10	7.0	-0.18	0.06
3.5	3 - 4	18	20	187.6	2.0	163.8	0.25	0.10	6.5	-0.38	0.06
4.5	4 - 5	51	53	29.9	4.0	222.4	0.26	0.10	8.1	-0.13	0.06
5.5	5 - 6	54	64	22.8	3.1	81.1	0.13	0.10	6.4	-0.23	0.06
6.5	6 - 7	52	69	10.8	2.2	43.3	1.00	0.10	5.4	-0.36	0.06
7.5	7 - 8	52	73	9.1	2.1	25.6	1.12	0.10	5.0	-0.36	0.06
8.5	8 - 9	48	78	6.1	2.3	25.0	0.29	0.10	5.2	-0.30	0.06
9.5	9 - 10	56	67	24.4	2.2	19.7	0.66	0.10	4.4	-0.33	0.06
10.5	10 - 11	53	69	21.1	1.8	11.2	0.19	0.10	4.4	-0.31	0.06
11.5	11 - 12	57	74	5.2	1.7	15.5	0.00	0.10	4.4	-0.28	0.06
12.5	12 - 13	48	77	5.3	1.5	11.2	0.27	0.10	4.4	n.d.	n.d.
13.5	13 - 14	52	76	5.4	1.4	7.2	0.29	0.10	4.6	-0.26	0.06
14.5	14 - 15	48	78	4.7	1.9	5.7	0.09	0.10	4.5	n.d.	n.d.

4.4.1 Kyllaren fjord

The Mo concentration, *c*(Mo), in the water column of the Kyllaren fjord decreases with depth (below 3 m) from 71 nM to 8 nM, and δ^{98}Mo slightly increases from 2.4 ‰ to 2.6 ‰ until reaching a depth of 4.6 m (Table 4.1; Fig. 4.3a). Due to the low Mo concentration in the bottom water and the limited amount of sample we had available for analysis, we were only able to measure δ^{98}Mo up to a depth of 4.6 m (i.e., ≈ 1 m below the chemocline in the fjord).

In contrast to Mo, the U concentrations, *c*(U), in the water column display only a slight decrease with depth (below 3 m) from 7 nM to 5 nM. However, δ^{238}U values significantly decrease from -0.35 ‰ to -0.70 ‰ (Table 4.1; Fig. 4.3b).

The two investigated sediment cores (KY09-1: 28 mbsl and KY09-3: 10 mbsl) from the Kyllaren fjord display similar patterns for major and trace elements and also for δ^{98}Mo and δ^{238}U (Table 4.2, Figs. 4.4a and 4.4b). Both sediment cores represent the last approximately 400 years, based on ^{210}Pb dating (Smittenberg et al., 2004). Molybdenum and U are only moderately enriched (6 to 37 µg/g and 4 to 6 µg/g, respectively; Table 4.2) and display minor variations in the mass fractions, *w*(Mo) and *w*(U), respectively (Figs. 4.4a and 4.4b). Both sediment cores show Mo isotopic compositions that are close to seawater (δ^{98}Mo = 2.3 ‰; Siebert et al., 2003), with an average of 2.17 ‰ ± 0.19 ‰ (double standard deviation) and 2.18 ‰ ± 0.24 ‰, respectively. Only one sample in the core KY09-3 (9.2 cm depth) has a slightly lower δ^{98}Mo value (1.93 ‰). Uranium isotopic compositions range between -0.18 ‰ and -0.34 ‰ (Figs. 4.4a and 4.4b). Surface sediments display ~ 0.5 ‰ higher δ^{238}U than deep water samples. However, they have lower δ^{238}U than those typically observed for organic-rich sediments from the seafloor of the Black Sea.

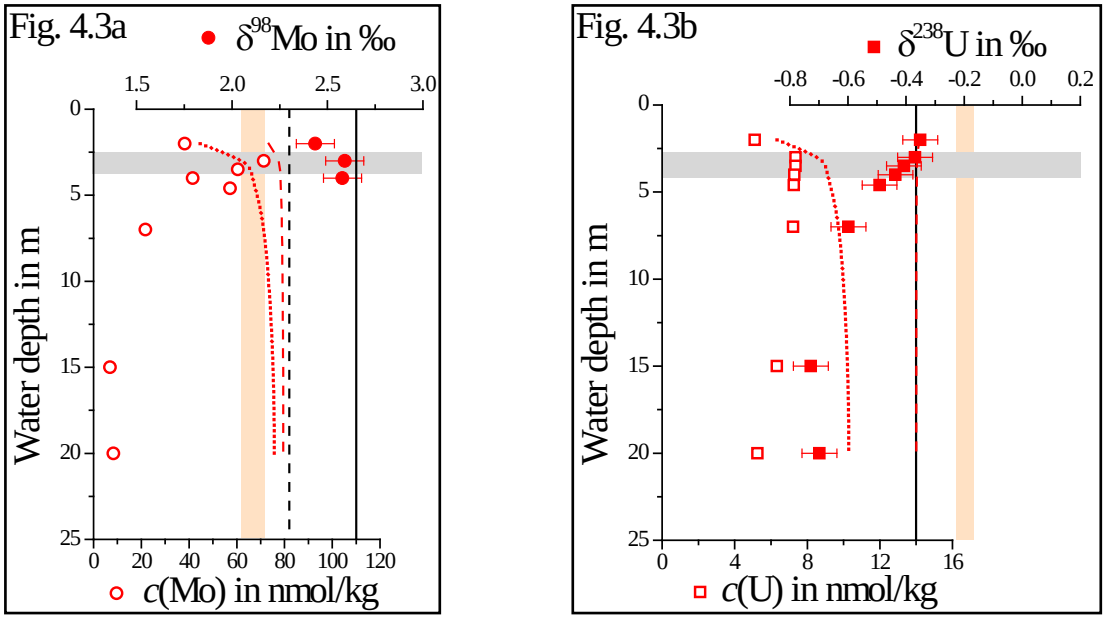

Fig. 4.3a: Mo and U concentrations and isotopic compositions in the water column of the Kyllaren fjord. The grey bar indicates the range for the chemocline, the black dashed line displays the mean ocean water isotope composition for Mo (δ^{98}Mo of 2.3 ‰; Siebert et al., 2003), and the black straight line is the mean ocean concentration for Mo (*c*(Mo) = 110 nmol/kg; Collier, 1985; Siebert et al., 2003). In Fig. 4.3b, the black straight line indicates both the mean ocean concentration and isotope composition for U (δ^{238}U of -0.37 ‰; and *c*(U) = 14 nmol/kg; Ku et al., 1977; Weyer et al., 2008), and the orange bar describes the measured isotope composition of the upper sediments. The dotted and dashed red lines are modelled seawater-freshwater mixing lines (dotted = concentration; dashed = isotope composition), as described in detail in the discussion section.

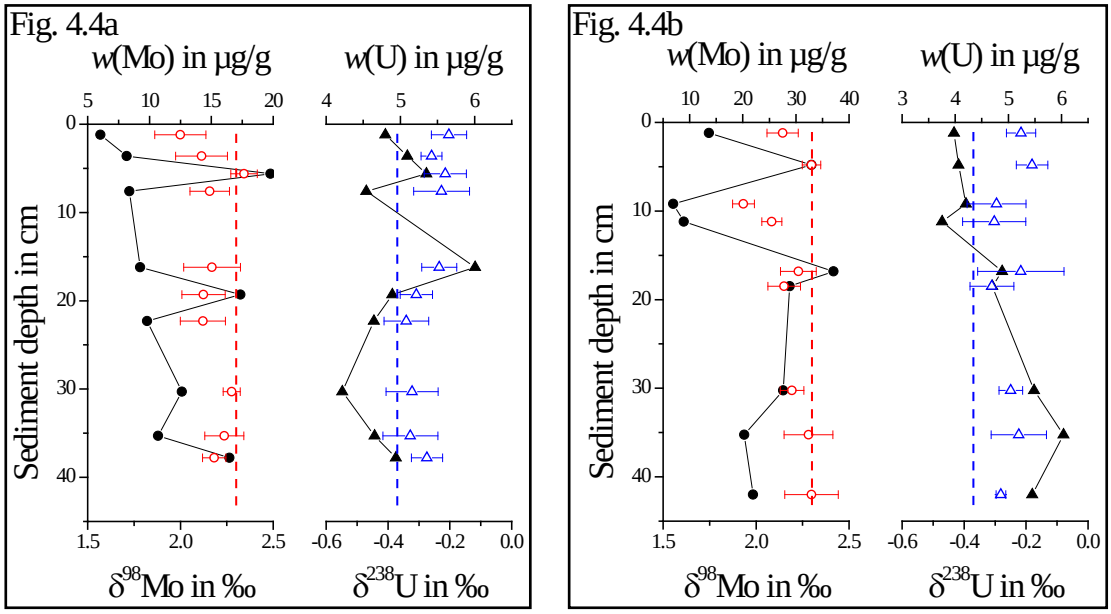

Fig. 4.4 Sediment depth profiles of core KY09-1 collected at 28 m water depth (a), and core KY09-3, collected at 10 m water depth (b) from the Kyllaren fjord; shown are selected mass fractions, *w*, of Mo and U, and isotope compositions of U ($\delta^{238}U$) and Mo ($\delta^{98}Mo$). Red and blue dashed lines: $\delta^{98}Mo$ and $\delta^{238}U$ of mean ocean water, respectively (Siebert et al., 2003; Weyer et al., 2008).

4.4.2 The Baltic Sea

The water column samples from the Baltic Sea, Landsort and Gotland Deep, display an increase in Mo and U concentrations with increasing depth (*c*(Mo) from 17 nM to 28 nM and *c*(U) from 3.0 nM to 4.5 nM, respectively) (Figs. 4.5a and 4.5b). Molybdenum isotopic compositions slightly increase (from $\delta^{98}Mo$ = 2.3 ‰ to 2.5 ‰, Fig. 4.5a), while $\delta^{238}U$ slightly decreases with depth (from -0.33 ‰ above the chemocline to values mostly between -0.41 ‰ and -0.50 ‰; Fig. 4.5b). The molybdenum isotope results are similar to those previously reported by Nägler et al. (2011).

The sediment core from the Landsort Deep was subdivided into an upper segment (up to a depth of 6 cm) and a lower segment (below 6 cm), according to

significant changes in the dominating redox conditions between the lower and upper segment (Fig. 4.6). The upper segment is characterised by low *w*(Re)/*w*(Mo) and high *w*(Fe)/*w*(Al) ratios and a high content of redox-sensitive trace elements (mass fraction of Mn up to 188 mg/g, *w*(Mo): up to 222 µg/g and *w*(U): up to 8 µg/g), an average δ^{98}Mo of 0.05 ‰ ± 0.39 ‰ (2 SD) and variable δ^{238}U ranging between -0.13 ‰ and -0.39 ‰. The lower segment displays no strong enrichment of redox-sensitive trace metals (with *w*(Mn)/w(Al) < 0.4 g/g, *w*(Mo) < 43 µg/g and *w*(U) < 5 µg/g). Molybdenum isotope compositions in the lower segment increase from values of approximately 0.2 ‰ (similar to those in the upper segment) below a depth of 10 cm to significantly heavier values of approximately 1 ‰ at a depth of 7 cm. In contrast, the U isotopic composition in the lower segment is relatively constant, with a similar average δ^{238}U (-0.31 ± 0.08 ‰) but less variable than sediments of the upper segment (Fig. 4.6).

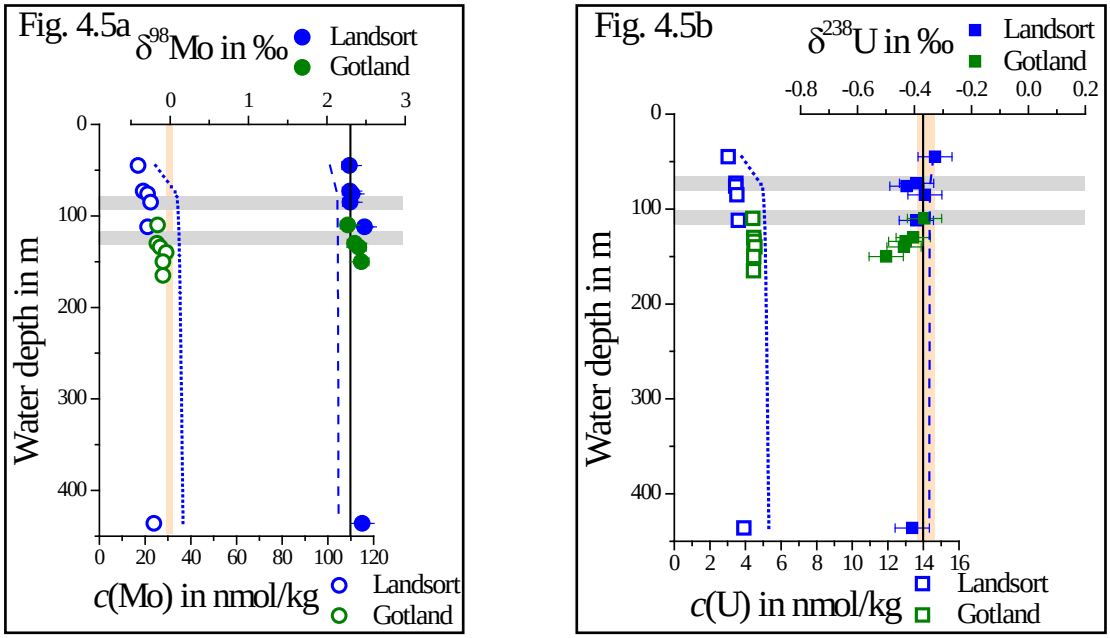

Fig. 4.5 Depth profiles for the Mo and U concentrations and isotopic compositions in the water column of the Baltic Sea (Landsort and Gotland Deeps combined). The grey bars indicate the position of the chemoclines of both deeps, the black straight lines represent the Mo and U isotope compositions and concentrations of mean ocean water (δ^{98}Mo of 2.3 ‰ and δ^{238}U of -0.37 ‰; *c*(Mo) = 110 nmol/kg and *c*(U) = 14 nmol/kg;

Ku et al., 1977; Collier, 1985; Siebert et al., 2003; Weyer et al., 2008), and the orange bars represent the measured isotope composition of the uppermost sediments analysed for the Landsort Deep. The dotted and dashed blue lines are modelled seawater-freshwater mixing lines (dotted = concentration; dashed = isotope composition), as described in detail in the discussion section.

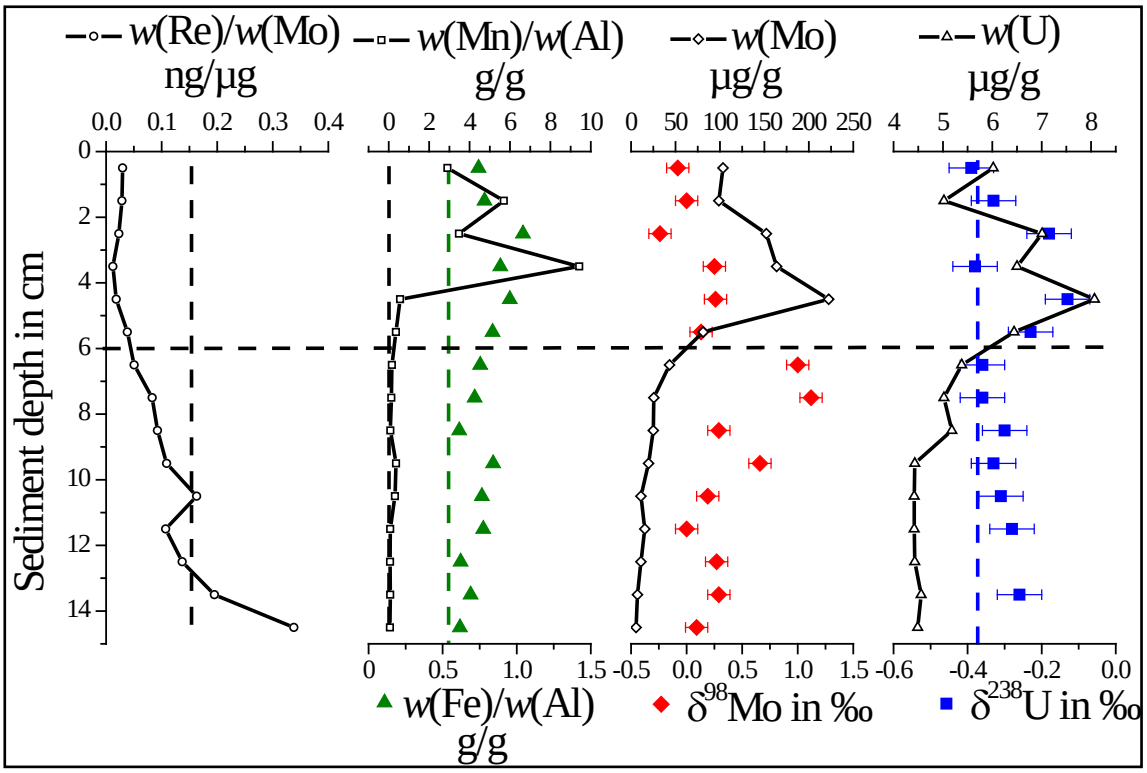

Fig. 4.6 Sediment depth profiles of core MUC 342390-2-7 from the Landsort Deep (Baltic Sea). The profiles shown are for selected major and trace elements (e.g., mass fractions, *w*, of Re, Mn, Fe, Mo and U), and isotope compositions of U ($\delta^{238}U$) and Mo ($\delta^{98}Mo$). The mass fractions of Mn and Fe are normalised to the Al mass fraction, and the Re mass fraction is normalised to the Mo mass fraction. Green dashed line: *w*(Fe)/*w*(Al) of average shale of 0.54 g/g according to Wedepohl (2004). The vertical black dashed lines represent the average shale for *w*(Re)/*w*(Mo) = 0.15 ng/µg (Turekian and Wedepohl, 1961; Esser, 1991) and *w*(Mn)/*w*(Al) = 0.0097 g/g (Turekian and Wedepohl, 1961; Bowen, 1979). The blue dashed line: mean ocean water $\delta^{238}U$ (Weyer et al., 2008). The mean ocean Mo isotopic composition for $\delta^{98}Mo$ = 2.3 ‰

according to Siebert al., 2003. The black dashed line at a depth of 6 cm separates the upper segment from the lower segment (see explanation in the text).

4.5 Discussion

The Mo and U isotopic compositions of sediments are frequently used as (paleo) redox tracers. For example, high, seawater-like δ^{98}Mo (of ~ 2.3 ‰) and high δ^{238}U (approximately 0 ‰) are assumed to indicate euxinic conditions in the water column during sediment deposition (Anbar, 2004; Weyer et al., 2008). However, in the past few years, several studies have shown that the Mo isotope composition in sediments can be highly variable, even though deposition occurred in a euxinic environment (Neubert et al., 2008; Nägler et al., 2011). The discussion focuses on the behaviour of U isotopes deposited under variable euxinic conditions in comparison with that of Mo isotopes. These results can be used to discuss the parameters and environmental conditions that affect the extent of U and Mo isotope fractionation between the water column and the sediments in different anoxic basins.

4.5.1 Uranium and Mo isotope fractionation in the water column of the Kyllaren fjord compared to the basins of the Baltic Sea

Two processes may explain the variability in Mo and U concentrations and isotope compositions we observed in the water columns for the Baltic Sea and the Kyllaren fjord. These are: 1) non-conservative behaviour of Mo and U under euxinic conditions in the deep water column and 2) mixing of fresh water and seawater (which have vastly different Mo and U concentrations and isotope compositions).

Under strongly euxinic conditions, as observed in the lower water column of the Kyllaren fjord (4000 µmol/L H_2S_{total} at a depth of 6 m), molybdate (MoO_4^{2-}) is quantitatively reduced and transformed via different species of thiomolybdates (MoO_xS_{4-x2-}; x = 0-3) to tetrathiomolybdate (MoS_4^{2-}; Erickson and Helz, 2000). The

latter is readily removed from the water column, resulting in a strong decrease of Mo concentration in the water column of the fjord (Fig. 4.3a), as was similarly observed in the modern Black Sea (Nägler et al., 2011). Uranium also shows non-conservative behaviour in euxinic water, although it is not as quantitatively removed from the water column as Mo. In contrast to Mo, U removal is assumed to occur mainly via diffusion of seawater U into sediment pore waters and subsequent U reduction and accumulation in the sediment (Anderson, 1989; Barnes and Cochran, 1990; Klinkhammer and Palmer, 1991). This process appears to result in only a moderate decrease of U concentrations with depth, while U isotopes of the deep water column are significantly fractionated (Fig. 4.3b). This observation is in agreement with previous findings from the Black Sea (Romaniello et al., 2009; Andersen et al., 2014), indicating partial U reduction in the pore water and diffusion back into the water column. The depositional conditions in the Baltic Sea are less euxinic and not as constant as those in the Kyllaren fjord. The Baltic Sea is influenced by periodically occurring flushing events transporting oxygenated waters from the North Sea into the Baltic Sea. Accordingly, the water column of the Gotland and Landsort Deeps suffers more fluctuations that affect the values of the oxygen- and H_2S-concentration, and therefore, the salinity stratification (Fig. 4.2b and Fig. 4.2c), *c*(Mo), *c*(U), $\delta^{238}U$ and $\delta^{98}Mo$ is less pronounced (Figs. 4.5a and 4.5b). The redox boundary that separates the water columns of the Gotland and Landsort Deeps from oxygenated surface water, also results in a Mn-Fe shuttling into these basins, which may also control Mo burial via adsorption to Mn and Fe oxides (Dellwig et al., 2010; Jilbert and Slomp, 2013; Scholz et al., 2013).

In the following, we apply a salinity-based conservative mixing model of seawater with fresh water for the Baltic Sea and the Kyllaren fjord to evaluate the effect and extent of redox-related Mo and U removal from the deep euxinic water columns (see supplementary text for equations used in this modelling; Figs. 4.3a, 4.3b, 4.5a and 4.5b).

Relative to the expected concentrations from such a mixing model, the whole water column of the Baltic Sea is depleted in *c*(Mo) by ≈ 30 % (Fig. 4.5a). Furthermore, the measured $\delta^{98}Mo$ in the Baltic Sea is constantly ~ 0.2 ‰ heavier than the modelled

δ^{98}Mo. The Kyllaren fjord also shows a depletion compared to a conservative mixing model; however, in this case, the amount of depletion in *c*(Mo) is depth dependent, due to the increase in the H_2S_{total} concentration. While the surface water in the Kyllaren fjord is only weakly depleted, the deep water displays 90 % Mo depletion (Fig. 4.3a). Likewise, the δ^{98}Mo measured across the chemocline of the Kyllaren fjord is slightly higher than that expected from conservative mixing (up to 0.4 ‰). Similar systematics are observed when applying this mixing model to U. The water column of the Baltic Sea displays a constant U depletion (of ~ 20 %, Fig. 4.5b), while the water column of the Kyllaren fjord shows increasing U depletion with depth of up to 50 % (Fig. 4.3b). The minor U depletion in the Baltic Sea resulted in only limited U isotope fractionation, which can barely be resolved from the modelled $\delta^{238}U_{mix}$ or the U isotopic composition of seawater (with one exception from the Gotland Deep). In contrast, the measured δ^{238}U of the Kyllaren fjord deep water column exceeds the modelled $\delta^{238}U_{mix}$ by up to 0.33 ‰.

These findings for the deep water column are consistent with the non-conservative behaviour of both Mo and U in the water columns of the Baltic Sea and the Kyllaren fjord (i.e., removal of Mo and U from the water column into the sediments as a consequence of Mo and U reduction). As recently observed in the Black Sea (Nägler et al., 2011), reduction and removal of Mo from the water column is also associated with minor Mo isotope fractionation (i.e., the remaining Mo in the deep water column is slightly heavier isotopically than the homogeneous surface water Mo). In the Kyllaren fjord, δ^{98}Mo increases to values of ~ 2.6 ‰ below the chemocline, indicating minor Mo isotope fractionation of ~ 0.3 ‰ to 0.5 ‰ during Mo reduction. The δ^{238}U decreases to values of ~ -0.70 ‰ in the deep water column of the fjord, indicating strong U isotope fractionation as a result of the reduction and removal of U from sulphidic water into the sediments. These findings are in agreement with theoretical models of U isotope fractionation during U reduction (Bigeleisen, 1996; Schauble, 2007; Abe et al., 2008) and with data from Romaniello et al. (2009) for the water column of the Black Sea combined with the observation of heavy U isotope compositions in sediments of euxinic basins (Black Sea: Weyer et al., 2008; Andersen et al., 2014). Furthermore, these results show that relative to the total range of isotope fractionation observed in nature, U

isotope fractionation in euxinic water columns is significantly stronger than that observed for Mo isotopes.

In contrast to Mo, the isotopic composition of the authigenic U is not equivalent to the seawater value (or that of the respective basin), as U removal from the water column is non-quantitative, even under strongly euxinic conditions. If the U isotopic composition of the original water reservoir is known prior to U reduction, , the magnitude of isotope fractionation during U reduction may be estimated either from the isotopic composition of the authigenic U in the sediment (Andersen et al., 2014) or from that of the deep water column (or a combination of both). The isotope composition of the authigenic U may be difficult to determine as the sedimentary U signature is frequently modified by other U sources (e.g., detrital or carbonate-bounded U). Assuming a closed system, the deep water column essentially consists of back-diffused pore water that has experienced a variable degree of U reduction. Assuming equilibrium isotope fractionation during U reduction, the $\delta^{238}U$ of the pore water will decrease linearly during progressive U reduction. In such a scenario, the deep water column provides an integrated isotope composition of the pore water U and a simple mass balance may be used to estimate the integrated U isotope composition of the authigenic U:

$$\delta^{238}U_{sw} = [U]_{pw}\,\delta^{238}U_{pw} + [U]_{auth}\,\delta^{238}U_{auth} \qquad \text{Eq. 4.3}$$

Where $[U]_{pw}$ is the relative (integrated) amount of U left over in pore water after reduction, $\delta^{238}U_{pw}$ its isotope composition, $[U]_{auth}$ is the relative (integrated) amount of U deposited in the sediment after reduction (= 1- $[U]_{pw}$) and $\delta^{238}U_{auth}$ is its isotope composition.

Applying this model to the U concentrations and U isotope composition of the deep water column of the Kyllaren fjord implies that approximately 50 % of U was reduced in the pore water resulting in authigenic U with $\delta^{238}U_{auth}$ of ~ 0.0 ‰ and $\Delta^{238}U_{water\text{-}sediment}$ of ~ 0.7 ‰. According to this model, the isotope composition of authigenic U in the sediments will strongly depend on the fraction of U that was reduced and removed from the water column.

However, in a more realistic scenario, some mixing occurred in the deep water column between the depleted pore water and the unmodified surface water, which is also indicated by the slightly isotopically lighter surface water compared to that expected by conservative mixing between seawater and fresh water. In this case, the $\delta^{238}U$ would be higher compared to the value expected for the depleted pore water. Furthermore, a Rayleigh model for U reduction may generate even lower $\delta^{238}U$ in the pore water, which is only significant for very high degrees of U reduction. Accordingly, the deep water column only provides maximum values for the U concentration and the $\delta^{238}U$ of the pore water and the inferred values for $\delta^{238}U_{auth}$ in the sediment (using equation 4.3 above) and the isotope fractionation between water and sediment ($\Delta^{238}U_{water\text{-}sediment}$) are minimum values. However, as detrital U has a strong contribution to the bulk U in the sediments of the Kyllaren fjord, $\delta^{238}U_{auth}$ is difficult to determine from the U isotope composition of the sediments (see below). Moreover, the minimum values for $\delta^{238}U_{auth}$ and $\Delta^{238}U_{water\text{-}sediment}$ determined from the deep water column of the Kyllaren fjord are very similar to those determined from the deep water column of the Black Sea (applying data from Romaniello et al., 2009) and those determined from the sediments of the Black Sea (Andersen et al., 2014). In the latter case, $\delta^{238}U$ values of the corresponding sediments are much less affected by detrital U, although they are potentially affected to some extent by carbonate-hosted U (Weyer et al., 2008; Andersen et al., 2014). Within uncertainties, the $\delta^{238}U$ of the top Black Sea sediments agrees with the $\delta^{238}U_{auth}$ inferred from the deep water column. Thus, we may consider a value of $\Delta^{238}U_{water\text{-}sediment} \sim 0.7$ ‰ to 0.8 ‰ as inferred from the deep water columns of the Kyllaren fjord and the Black Sea and the Black Sea sediments, with typical U isotope fractionation that occurs during U reduction in the pore water of a strongly stratified basin with highly euxinic conditions in the deep water column. This value is in accord with theoretical and recent experimental findings (Abe et al., 2008; Basu et al., 2014).

In contrast to the Kyllaren fjord, the depletion and isotopic shifts of Mo and U in the deeps of the Baltic Sea are rather constant, i.e., almost identical in the oxidized upper and the euxinic deep water column, where Mo and U removal is expected to

occur. These findings imply that Mo and U removal from the water column occurred over a long period of time, exceeding the time of deep water renewal in the Gotland and Landsort Deep (Feistel et al., 2006; Reissmann et al., 2009).

Slightly lower Mo concentrations and heavier Mo isotope compositions in the surface water of the Baltic Sea, compared to those expected from conservative mixing of fresh water and seawater, were also observed by Nägler et al. (2011). However, these authors observed a stronger trend towards heavier δ^{98}Mo with increasing depth in the water column of the Gotland and Landsort Deeps, which was barely resolvable in the samples investigated in this study. The samples of this study are from a different sample period, i.e., from 2008, two years later than the sampling of Nägler et al. (2011). It is possible that continuous upwelling resulted in a more complete re-mixing of Mo and U from deep and surface water.

4.5.2 The U and Mo isotopic signatures of sediments from anoxic basins

The Mo and U concentrations and isotope compositions of redox-sensitive trace metals in sediments that were deposited in restricted basins with anoxic or euxinic deep water are essentially a mixture of two sources: a detrital input and authigenic metal enrichment. In some cases (e.g., the Black Sea), carbonate-hosted U may represent a third U source, which is less significant for the sediments of the Kyllaren fjord and Baltic Sea considered in this study. The Mo or U fraction from a detrital component may be monitored, e.g., by the Al (or Ti, Zr, and Th) concentration of the sediment and determined by the following equation:

$$c(\mathrm{M})_{\mathrm{det}} = (c(\mathrm{M})/\, c(\mathrm{Al}))_{\mathrm{crust}} \times c(\mathrm{Al})_{\mathrm{tot}} \qquad \text{Eq. 4.4}$$

where c(M) is the concentration of Mo or U and the indices “det” and “tot” indicate the detrital fraction and the total concentration of an element. For the continental crust we assumed concentrations as (e.g., given by Taylor and McLennan

(1985)) c(Mo) = 1.1 µg/g, c(U) = 2.5 µg/g and c(Al) = 8 wt%, if not otherwise indicated. The authigenic metal fraction is then given by equation 4.5:

$$c(M)_{auth} = c(M)_{tot} - c(M)_{det} \quad \text{Eq. 4.5}$$

The isotopic mass balance is given by equation 4.6 for the example of U:

$$\delta^{238}U_{tot} = (\delta^{238}U_{auth} \times c(U)_{auth} + \delta^{238}U_{det} \times c(U)_{det}) \div c(U)_{tot} \quad \text{Eq. 4.6}$$

Therefore, the isotope compositions of the authigenic metal fraction can be calculated by equation 4.7, given the example of U:

$$\delta^{238}U_{auth} = (\delta^{238}U_{tot} \times c(U)_{tot} - \delta^{238}U_{det} \times c(U)_{det}) \div c(U)_{auth} \quad \text{Eq. 4.7}$$

For the isotope composition of the detrital component, we used $\delta^{98}Mo_{det}$ = 0.3 ‰, (Voegelin et al., 2014) and $\delta^{238}U_{det}$ of -0.30 ‰ (Weyer et al., 2008; Noordmann et al., 2011), if not otherwise indicated.

In the following, we used this mixing model to evaluate the parameters that control authigenic enrichment and the effect of "detrital dilution" on the Mo and U concentrations and isotope signatures of the sediments. We also discuss how depositional conditions may have changed with time within the record of the investigated sediment cores.

The Kyllaren fjord

The extent of authigenic Mo and U enrichment in the sediment is essentially driven by the redox conditions in the water column (i.e., Mo is particularly and strongly depleted under euxinic conditions in the water column). Notably, the analysed δ^{98}Mo of the sediments is generally high (> 2.1 ‰, with only two exceptions) throughout the analysed core, indicating relatively constant euxinic conditions in the water column during its deposition. Applying equations 4.4, 4.5 and 4.7 (supplementary Table A 4.1) reveals that the contribution of detrital Mo to the Mo budget of the sediments does not

exceed 0.7 µg/g (i.e., > 90 % of the Mo in the sediment was always of authigenic origin). Accordingly, the effect of the detrital component on the Mo isotopic composition of the sediment is generally small (≤ 0.2 ‰; suppl. Table A 4.1). After a correction for detrital Mo, the lowermost sediment samples resemble the mean ocean value of 2.3 ‰. The surface sediments (with δ^{98}Mo of 2.2 ‰ after correction) are identical to uncertainties with the initial value (before Mo reduction ≈ 2.1 ‰ to 2.2 ‰) assumed for the current water column of the fjord. Therefore, the data for the Kyllaren fjord are in accord with quantitative Mo removal from the water column, resulting in no significant Mo isotope fractionation into the sediments, which is very similar to observations from the Black Sea (Barling et al., 2001; Neubert et al., 2008; Nägler et al., 2011) or a euxinic lake in Switzerland (Dahl et al., 2010). These findings demonstrate (1) the dominance of authigenic Mo in these sediments (suppl. Table A 4.1), although according to the high sedimentation rate proposed by Smittenberg et al. (2004), Mo is only moderately enriched in the sediments of the fjord; (2) they aso indicate the continuous existence of a significant water column H_2S (> 20 µmol/L; Neubert et al., 2008; Arnold et al., 2012) even at a depth of only 10 m (i.e., the redox conditions in the fjord were constantly euxinic throughout the last 400 years).

Uranium isotope compositions of the sediments are generally heavier than those of seawater (average δ^{238}U = -0.25 ‰ ± 0.1 ‰); however, they are light compared to those observed for euxinic sediments from the Black Sea that were deposited under similar conditions (unit I: δ^{238}U = 0.04 ‰ ± 0.1 ‰, Weyer et al., 2008; Montoya-Pino et al., 2010; Andersen et al., 2014). Compared to the sediments from the Black Sea (with an average U concentration of 15 µg/g), U is only moderately enriched in fjord sediments (approx. 4 to 6 µg/g), i.e., only by a factor of ≈ 2 compared to typical U concentrations of the continental crust. Accordingly, the effect of a detrital component on the U concentration and isotope composition of the sediment was stronger than that observed for Mo. We applied equations 4 to 6 to estimate this effect. For authigenic U, we assumed a value of $\delta^{238}U_{auth}$ = 0.0 ‰, as inferred from the U isotope composition of the deep water column. Notably, this value is a minimum value (see above), and thus, the light U isotope composition of at least the uppermost sediments cannot be explained by a lower $\delta^{238}U_{auth}$. Assuming $c(U)_{det}$ = 2.5 µg/g (average continental crust, Taylor and

McLennan, 1985) and applying equation 4.5 would give values for $c(U)_{auth}$ of approximately 3.3 µg/g (supplementary Table A 4.2).

However, neither the U concentration nor the U isotope composition of the detrital component is well defined. Both values may easily vary within a range as defined by granites (likely a major contributor for detrital U in the Baltic Sea sediments), which display a large range in U concentration (1 µg/g to 10 µg/g) and U isotope composition (-0.21 ‰ to -0.51 ‰; Weyer et al., 2008; Noordmann et al., 2011; Telus et al., 2012). These large variations and the commonly lower enrichment factor of U (compared to that of Mo and Re) generate a large uncertainty in the determination of the concentration and isotope composition of authigenic U (Fig. 4.7a and Fig. 4.7b). The modelled curves in Fig. 4.7a show that a detrital sediment component will significantly affect the U isotope composition of a sediment (with $\delta^{238}U_{auth}$ = 0.0 ‰) if the ratio of the mass fractions of U and Al is below 1 or even 10, depending on the U concentration and U isotope composition of the detritus. Likewise, the position of the sediment data in Fig. 4.8 shows that the detritus likely had $w(U)_{det}$ > 2.5 µg/g and/or $\delta^{238}U_{det}$ < -0.30 ‰ (the average crustal values: Taylor and McLennan, 1985; Weyer et al., 2008; Noordmann et al., 2011).

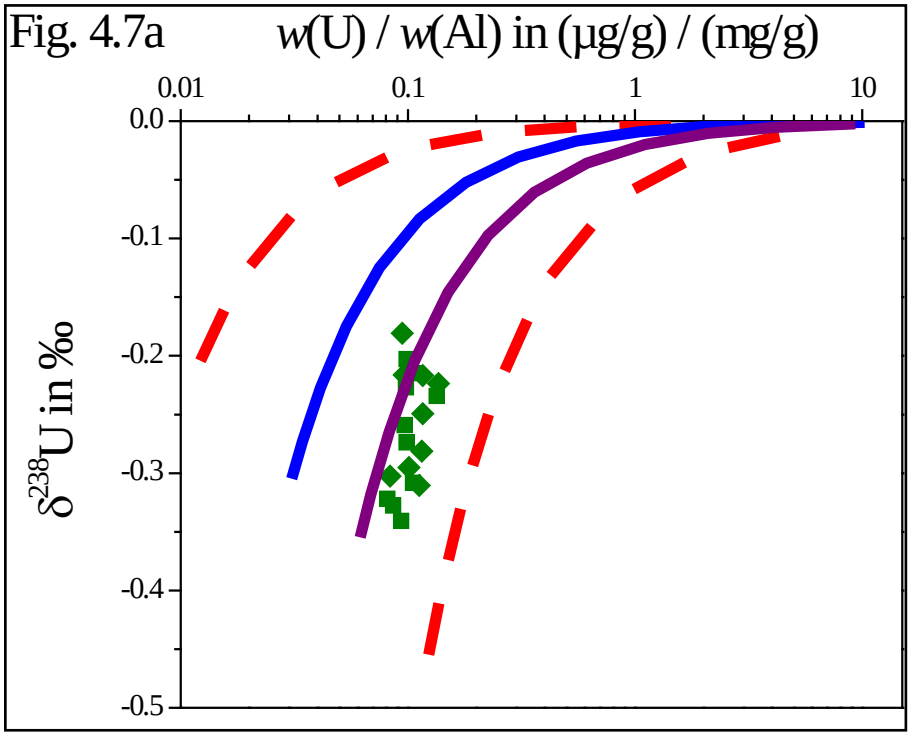

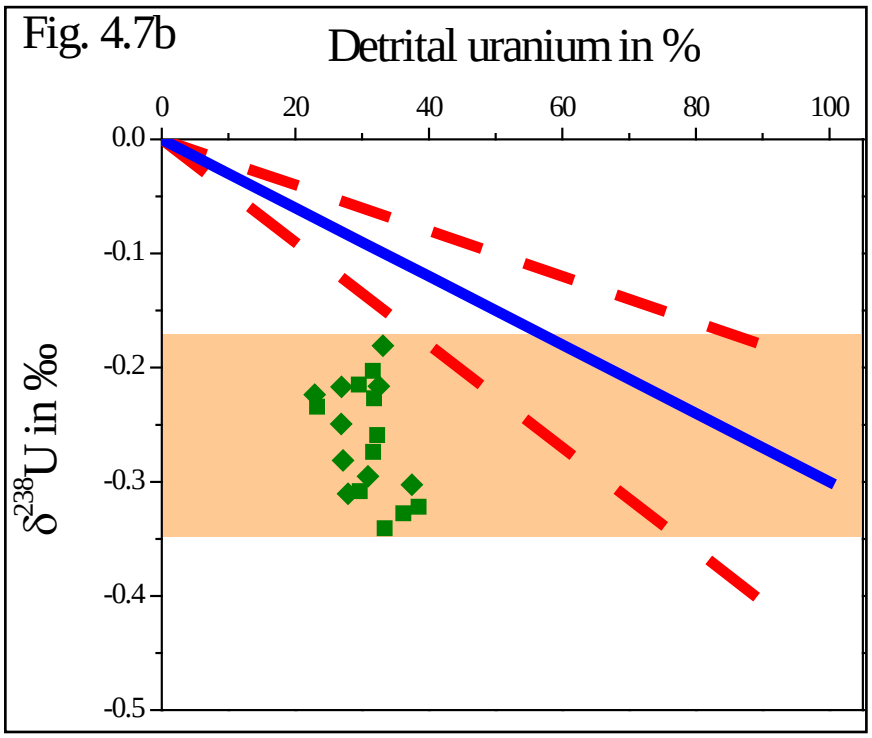

Fig. 4.7 Plot of w(U) / w(Al) (a) and the fraction of detrital U (b) vs. U isotopic composition, δ^{238}U, of a sediment; green squares represent data for sediment core KY09-1 and green diamonds for KY09-3. The position of the sediment data in Fig. 4.7b assumes that the detrital sediment component has $c(U)_{det}$ = 2.5 µg/g (= average crust: Taylor

and McLennan, 1985). The modelled curves and lines assume that authigenic U has $\delta^{238}U_{auth}$ = 0.0 ‰ and is mixed with detrital U of various compositions. In Fig. 4.7a, the blue curve is modelled for mixing with an average crust, i.e., $c(U)_{det}$ = 2.5 µg/g and $\delta^{238}U$ = -0.30 ‰ (Taylor and McLennan, 1985; Weyer et al., 2008; Noordmann et al., 2011). The red dashed lines are modelled for mixing with extremely crustal endmembers of $c(U)_{det}$ = 1 µg/g, $\delta^{238}U_{det}$ = -0.20 ‰, $c(U)_{det}$ = 10 µg/g, and $\delta^{238}U_{det}$ = -0.46 ‰, respectively. The purple line is modelled for mixing with $c(U)_{det}$ = 5 µg/g and $\delta^{238}U_{det}$ = -0.35 ‰, and those values have been chosen to match the composition of the uppermost fjord sediments. In Fig. 4.7b, the blue line is modelled for mixing of $\delta^{238}U_{auth}$ with $\delta^{238}U_{det}$ = -0.30 ‰ (= average crust: Weyer et al., 2008; Noordmann et al., 2011), and the red dashed lines are modelled for mixing with extremely crustal endmembers of $\delta^{238}U_{det}$ = -0.20 ‰ and $\delta^{238}U_{det}$ = -0.46 ‰, respectively. The orange box indicates the range of isotopic compositions observed in the fjord sediments.

In Fig. 4.7b, the fraction of detrital U to the total U in the sediments of the Kyllaren fjord has been estimated by assuming a mixing of authigenic U with $\delta^{238}U_{auth}$ = 0.0 ‰. Assuming a detrital U concentration of 2.5 µg/g, none of the samples fall into the isotopic field expected for detrital U as defined by the red dashed lines in Fig. 4.7b. This implies that the detrital U concentration was > 2.5 µg/g. For the top sediments, a detrital contribution of at least 60 % would be required if the detritus had $\delta^{238}U_{det}$ = -0.30 ‰ (average crust: Weyer et al., 2008; Noordmann et al., 2011). If the detritus had a lighter U isotopic composition, less detrital U would be required to explain the uppermost sediments, e.g., only 40 % if $\delta^{238}U_{det}$ = -0.46 ‰ (the lowest value observed for granites by Noordmann et al., 2011). Likewise, assuming a slightly lighter detrital component, with a $\delta^{238}U$ of approximately -0.35 ‰, combined with a slightly higher detrital U concentration of approximately 5 µg/g (both are well within the observed range for granites) corresponding to a detrital contribution of ≈ 50 % to the sedimentary U budget, the modelled U isotopic composition (using equation 4.6) would match that observed for the top sediments (Fig. 4.8). Thus, a simple mixing model of authigenic and detrital U may explain the U concentrations and isotopic compositions of the

uppermost fjord sediments, which were deposited under conditions similar to those now displayed by the lower water column.

However, the lower sediments of the Kyllaren fjord cannot be explained by mixing with detrital U, unless its isotopic composition was extremely light. By applying the same parameters that match the uppermost sediments to the lower sediments of the Kyllaren fjord, an offset results between the analysed and the modelled $\delta^{238}U$ values, as indicated by the green dashed line in Fig. 4.8 (and supplementary Table A 4.3). These findings imply that the isotopic composition of authigenic U has likely changed with time, either due to different conditions during U reduction in the ancient water column of the fjord, or if the fraction of U that was removed from the water column had changed with time. The latter model assumes that U removal from the water column may have been more quantitative ~ 200 years ago in the Kyllaren fjord, resulting in a lighter $\delta^{238}U$ of the deep water column and, correspondingly, also in a lower $\delta^{238}U_{auth}$ in the sediments.

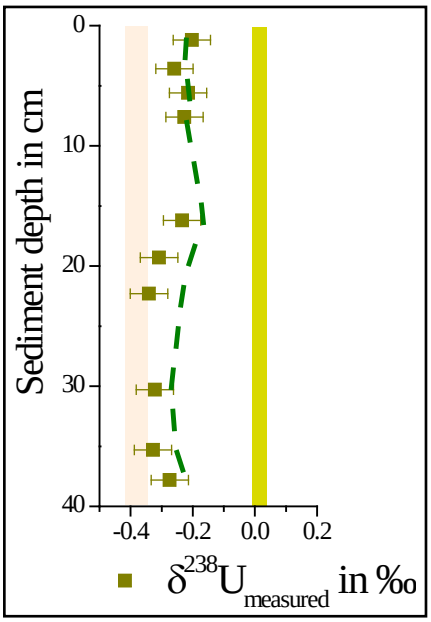

Fig. 4.8 Depth profile for the sediment core from the Kyllaren fjord (KY09-1): the green dashed line shows the modelled values for $\delta^{238}U$ of the sediment, assuming a mixing of authigenic U (as inferred from the current deep water column, shown as a green bar at

$\delta^{238}U$ = 0 ‰) with detrital U, using a slightly U-enriched and isotopically lighter detrital component (c(U) = 5 µg/g and $\delta^{238}U$ = -0.35 ‰). The light red bar between $\delta^{238}U$ = -0.41 ‰ and -0.34 ‰ indicates the range for the mean ocean water, according to Weyer et al. (2008). This model results in $\delta^{238}U$ values that match the measured $\delta^{238}U$ of the uppermost 10 cm of the sediment profile. However, the sediments below 15 cm show a small offset towards isotopically lighter values.

This simplified model shows that U isotopic compositions of anoxic sediments are (1) more strongly affected by a detrital component than Mo isotopes (enrichment factors for U in these sediments are not as high as for Mo) and (2) are likely sensitive to the conditions and/or extent of U removal from the water column. If the fraction of U that is scavenged from the water column is small, respective sediments may display very heavy U isotope compositions. This relationship may explain the heavy isotopic signatures (up to 0.4 ‰) of some sediments (e.g., from the Black Sea unit II) (Weyer et al., 2008; Montoya-Pino et al., 2010).

Uranium and Mo isotope fractionation in the sediment core of Landsort Deep

The lower segment of the sediment profile from the Landsort Deep displays a slightly upward increasing w(Fe)/w(Al), decreasing w(Re)/w(Mo), an increase in $\delta^{98}Mo$ from values of approximately 0 ‰ to values up to 1.12 ‰ and slightly increasing w(Mo) and w(U) (Fig. 4.6). This may indicate a progressive redox change from suboxic towards more anoxic conditions during the depositions of these sediments. The light Mo isotope signatures, particularly in the lowermost sediments, are likely explained by incomplete Mo scavenging and isotope fractionation during the formation of thiomolybdate species (Neubert et al., 2008; Nägler et al., 2011). Alternatively, dissolution of Mn-oxides may have resulted in the release of isotopically light Mo into the pore water (Wasylenki et al., 2008; Goldberg et al., 2012; Scholz et al., 2013). Although Mo is only moderately enriched in the lowermost sediment profile, detrital

Mo only has a minor contribution and thus cannot explain the low Mo isotope composition of these sediments (supplementary Table A 4.4). In contrast to Mo, U shows a trend towards slightly lighter isotopic compositions towards the top of the lower segment. Uranium isotopic compositions are usually heavier, rather than lighter, in sediments that formed under anoxic conditions compared to those that formed under suboxic conditions (Weyer et al., 2008). However, U isotope fractionation in suboxic environments is not yet well understood.

The correlation between decreasing Re/Mo and increasing δ^{98}Mo is disrupted at the onset of the upper segment (Fig. 4.6), where Mo isotope compositions are shifted by approximately 1 ‰ towards lower values (from δ^{98}Mo of ~ 1 ‰ to ~ 0 ‰). This shift is remarkable, as other proxies, including Fe/Al and Re/Mo, indicate more anoxic or euxinic conditions during the deposition of sediments from the upper segment, which is similar to the present conditions in the water column. The low δ^{98}Mo values of surface sediments from the Baltic Sea have previously been described as the result of incomplete reduction of molybdate to thiomolybdate under moderately euxinic conditions, followed by strong Mo isotope fractionation during incomplete Mo removal from the water column (Neubert et al, 2008; Nägler et al., 2011). However, as already argued by Nägler et al. (2011), other factors may additionally affect the Mo isotopic composition of these sediments. Manganese contents are remarkably high in the sediments of the upper segment (Fig. 4.6). During flushing events with oxygen-rich water, ferromanganese oxides may have formed and subsequently re-dissolved under anoxic conditions, resulting in the release of isotopically light Mo (Wasylenki et al., 2008; Scheiderich et al., 2010; Goldberg et al., 2012; Jilbert and Slomp, 2013; Scholz et al., 2013).

Accordingly, the sharp shift towards light Mo isotopic compositions may mark the onset of the repeated occurrence of oxygen flushing events in the investigated basins (Feistel et al., 2003; Zillen et al., 2008). Interestingly, the Mn content and δ^{98}Mo are slightly decoupled in the sediments of the upper segment, i.e. the shift towards low δ^{98}Mo occurred already before the sharp increase in Mn concentrations. Potentially, Mo became decoupled from Mn by subsequent diffusion in the sediment pore water or

repeated precipitation (e.g. on Fe oxides) and re-mobilization of Mo resulted in light Mo isotope signatures without significant contribution of manganese oxides (Scheiderich et al., 2010; Goldberg et al., 2012).

Such remobilization events may also generate a shift in the isotope composition of U towards light values. However, $\delta^{238}U$ in the upper segment sediments is rather variable. The isotope composition of U may be partially affected by the precipitation of U^{+IV} in association with $MnCO_3$, which is likely the major Mn carrier under high alkaline reducing conditions (e.g. Ca-rhodochrosites: $(MnCa)CO_3$; Suess, 1979; Sternbeck and Sohlenius, 1997; Böttcher, 1998; Lenz et al., 2014). Abiotic carbonates can incorporate significant amounts of U under anoxic conditions. The literature data display a range of carbonates for $\delta^{238}U$, which is identical or slightly heavier than the mean ocean value (Weyer et al., 2008; Romaniello et al., 2013). The observed range of $\delta^{238}U$ for sediments from the upper segment (-0.39 ‰ and -0.13 ‰) falls into the range defined by abiotic carbonates and suboxic sediments. Alternatively, the more variable U isotopic composition of sediments from the upper segment may indicate that U was not always as strongly affected by remobilization as Mo and that some of the sediments preserved relatively high $\delta^{238}U$ ($\geq$ -0.2 ‰), which is typical for deposits of anoxic settings.

4.6 Conclusion

Although the Kyllaren fjord is much smaller in size compared to the Black Sea, Mo and U concentrations and isotopic compositions display a very similar behaviour in the deep euxinic water column and sediments:

(1) Molybdenum is strongly and U only moderately removed from the water column.

(2) Both Mo and U isotopes of the deep water column are fractionated towards a heavier and a lighter composition, respectively. Accordingly, heavy U isotopes are enriched in the sediments. For Mo, no isotope fractionation between the original water mass and the sediment was observed due to the almost quantitative Mo removal from the water column.

(3) The deep water column of the Kyllaren fjord indicates a minimum value for the U isotopic composition of authigenic U in the sediments of $\delta^{238}U_{auth}$ = 0.0 ‰, which is very similar to that of the recently deposited Black Sea unit I sediments. The U isotopic compositions of the Black Sea and Kyllaren fjord deep water and that of the Black Sea sediments indicate similar U isotope fractionation during U reduction in pore water sediments of $\Delta^{238}U_{pore\ water - sediments} \approx 0.7\text{-}0.8$ ‰.

Due to the high sedimentation rate in the Kyllaren fjord (~ 1 mm/yr compared to ~0.1 mm/yr in the Black Sea), the scavenged U is significantly diluted with a detrital component, which also significantly affected the U isotopic composition of the sediments. As authigenic enrichment of Mo is higher than that of U, dilution with a detrital component has only a minor effect on the Mo isotopic composition of the sediments.

The Baltic Sea water column displays only a weak depletion of Mo and U by scavenging and negligible Mo and U isotope fractionation. Variations of the Mo and U concentrations within the water column can essentially be explained by conservative mixing of seawater with fresh water, i.e., surface water is similarly depleted in Mo (20 % to 40 %) and U (0 % to 20 %) as the deep water column. Accordingly, reduction and removal of Mo and U from the water column into authigenic sediments resulted in a general depletion of these elements in Baltic Sea water, indicating that the current deep water renewal time in the Landsort and Gotland Deep is significantly shorter than the water mass exchange between the Baltic Sea and open ocean water.

The sediment core shows increasing anoxic conditions during the deposition of the lower segment (below 6 cm), in accord with increasing Fe/Al, Mo/Al, U/Al and δ^{98}Mo. However, the shift towards lower δ^{98}Mo and variable low δ^{238}U in sediments

from the upper segment is not in accord with the predominantly anoxic to euxinic conditions during the deposition of these sediments. Rather, it infers that during frequently occurring flushing events with oxygenated water, the originally anoxic Mo and U isotopic signatures of the sediments were significantly modified, likely induced by the re-mobilization of Mo that was previously bonded to ferromanganese oxides. These findings demonstrate that only sediments that were deposited under strong and persistently euxinic conditions record high $\delta^{238}U$ and seawater-like $\delta^{98}Mo$, which are typically used as an indicator of euxinic conditions.

Acknowledgements

We thank two anonymous reviewers for their helpful comments and suggestions and Klaus Mezger for editorial handling. Funding for this study was provided by the Deutsche Forschungsgemeinschaft (DFG, WE 2850/6).

4.7 Appendix

Table A 4.1 Results for the calculation of the detrital and authigenic Mo concentration ($w(Mo_{det})$ and $w(Mo_{auth})$) and isotopic composition of authigenic Mo ($\delta^{98}Mo_{auth}$), after Eq. 4.6, Eq. 4.7 and Eq. 4.9.

Sediment depth cm	$w(Mo_{measured})$ µg/g	$w(Mo_{det})$ µg/g	$w(Mo_{auth})$ µg/g	$\delta^{98}Mo_{auth}$ ‰	$\delta^{98}Mo_{measured}$ ‰	2 SD ‰
Kyllaren Fjord						
KY09-1						
1.20	6.03	0.61	5.42	2.21	2.00	0.14
3.60	8.15	0.66	7.50	2.29	2.11	0.14
5.60	19.78	0.63	19.14	2.42	2.34	0.07
7.60	8.37	0.58	7.79	2.31	2.16	0.11
16.20	9.25	0.56	8.69	2.30	2.17	0.15
19.30	17.35	0.58	16.77	2.19	2.12	0.12
22.30	9.81	0.62	9.19	2.26	2.12	0.12
30.30	12.62	0.65	11.97	2.39	2.28	0.05
35.30	10.70	0.67	10.03	2.38	2.24	0.11
37.80	16.47	0.63	15.84	2.26	2.18	0.06
KY09-3						
1.20	13.63	0.52	13.12	2.22	2.14	0.08
4.80	32.91	0.54	32.37	2.33	2.30	0.05
9.20	6.92	0.52	6.40	2.08	1.93	0.06
11.20	8.89	0.56	8.32	2.22	2.08	0.05
16.80	37.08	0.53	36.55	2.26	2.23	0.10
18.50	28.81	0.52	28.28	2.19	2.15	0.09
30.25	27.61	0.59	27.02	2.24	2.19	0.06
35.25	20.29	0.55	19.74	2.34	2.28	0.13
42.00	21.95	0.59	21.35	2.36	2.30	0.14

Table A 4.2 Results for the calculation of the authigenic U concentration ($w(U_{auth})$) and the modeled isotopic composition of the sediments ($\delta^{238}U_{sed}$), after Eq. 4.7 and Eq. 4.8, using $w(U_{det})$ = 2.5 µg/g and $\delta^{238}U_{det}$ = -0.30 ‰.

Sediment depth cm	$w(U_{measured})$ µg/g	$w(U_{auth})$ µg/g	$\delta^{238}U_{sed}$ ‰	$\delta^{238}U_{measured}$ ‰	2 SD ‰
Kyllaren Fjord					
KY09-1					
1.20	4.80	2.30	-0.09	-0.20	0.06
3.60	5.10	2.60	-0.08	-0.26	0.03
5.60	5.35	2.85	-0.07	-0.21	0.07
7.60	4.54	2.04	-0.11	-0.23	0.09
16.20	6.01	3.51	-0.05	-0.23	0.06
19.30	4.89	2.39	-0.09	-0.31	0.05
22.30	4.64	2.14	-0.10	-0.34	0.07
30.30	4.22	1.72	-0.12	-0.32	0.08
35.30	4.65	2.15	-0.10	-0.33	0.09
37.80	4.94	2.44	-0.09	-0.27	0.05
KY09-3					
1.20	3.98	1.48	-0.14	-0.22	0.05
4.80	4.06	1.56	-0.13	-0.18	0.05
9.20	4.20	1.70	-0.13	-0.30	0.09
11.20	3.76	1.26	-0.16	-0.30	0.10
16.80	4.88	2.38	-0.09	-0.22	0.14
18.50	4.70	2.20	-0.10	-0.31	0.07
30.25	5.48	2.98	-0.07	-0.25	0.04
35.25	6.04	3.54	-0.05	-0.22	0.09
42.00	5.45	2.95	-0.07	-0.28	0.02

Table A 4.3 Results for the calculation of the authigenic U concentration ($w(U_{auth})$) and the modeled isotopic composition of the sediments ($\delta^{238}U_{sed}$), after Eq. 4.7 and Eq. 4.8, using $w(U_{det})$ = 3 µg/g and $\delta^{238}U_{det}$ = -0.35 ‰.

Sediment depth cm	$w(U_{measured})$ µg/g	$w(U_{auth})$ µg/g	$\delta^{238}U_{sed}$ ‰	$\delta^{238}U_{measured}$ ‰	2 SD ‰
Kyllaren Fjord					
KY09-1					
1.20	4.80	1.80	-0.22	-0.20	0.06
3.60	5.10	2.10	-0.20	-0.26	0.03
5.60	5.35	2.35	-0.19	-0.21	0.07
7.60	4.54	1.54	-0.23	-0.23	0.09
16.20	6.01	3.01	-0.17	-0.23	0.06
19.30	4.89	1.89	-0.21	-0.31	0.05
22.30	4.64	1.64	-0.22	-0.34	0.07
30.30	4.22	1.22	-0.25	-0.32	0.08
35.30	4.65	1.65	-0.22	-0.33	0.09
37.80	4.94	1.94	-0.21	-0.27	0.05
KY09-3					
1.20	3.98	0.98	-0.26	-0.22	0.05
4.80	4.06	1.06	-0.26	-0.18	0.05
9.20	4.20	1.20	-0.25	-0.30	0.09
11.20	3.76	0.76	-0.28	-0.30	0.10
16.80	4.88	1.88	-0.21	-0.22	0.14
18.50	4.70	1.70	-0.22	-0.31	0.07
30.25	5.48	2.48	-0.19	-0.25	0.04
35.25	6.04	3.04	-0.17	-0.22	0.09
42.00	5.45	2.45	-0.19	-0.28	0.02

Table A 4.4 Results for the calculation of the authigenic U and Mo concentration ($w(U_{auth})$ and $w(Mo_{auth})$) and isotopic composition of the sediments for U and Mo ($\delta^{238}U_{sed}$ and $\delta^{98}Mo_{sed}$), after Eq. 4.6, Eq. 4.7 and Eq. 4.8.

Sediment depth cm	$w(U_{measured})$ µg/g	$w(U_{auth})$ (µg/g)	$\delta^{238}U_{sed}$ ‰	$\delta^{238}U_{measured}$ ‰	2 SD ‰	$w(Mo_{measured})$ µg/g	$w(Mo_{auth})$ µg/g	$\delta^{98}Mo_{sed}$ ‰	$\delta^{98}Mo_{measured}$ ‰	2 SD ‰
Landsort Deep										
0.5	6.02	3.52	0.05	-0.39	0.05	103.41	101.91	1.48	-0.08	0.10
1.5	5.02	2.52	0.00	-0.33	0.05	98.72	97.22	1.48	0.00	0.10
2.5	7.01	4.51	0.09	-0.18	0.05	152.20	150.70	1.49	-0.24	0.10
3.5	6.5	4.00	0.07	-0.38	0.05	163.82	162.32	1.49	0.25	0.10
4.5	8.07	5.57	0.11	-0.13	0.05	222.37	220.87	1.49	0.26	0.10
5.5	6.44	3.94	0.07	-0.23	0.05	81.08	79.58	1.47	0.13	0.10
6.5	5.38	2.88	0.02	-0.36	0.05	43.31	41.81	1.45	1.00	0.10
7.5	5.02	2.52	0.00	-0.36	0.05	25.57	24.07	1.41	1.12	0.10
8.5	5.18	2.68	0.01	-0.30	0.05	24.99	23.49	1.41	0.29	0.10
9.5	4.43	1.93	-0.04	-0.33	0.05	19.71	18.21	1.39	0.66	0.10
10.5	4.42	1.92	-0.04	-0.31	0.05	11.17	9.67	1.30	0.19	0.10
11.5	4.42	1.92	-0.04	-0.28	0.05	15.49	13.99	1.35	0.00	0.10
12.5	n.d.	n.d.	n.d.	n.d.	n.d.	11.16	9.66	1.30	0.27	0.10
13.5	4.56	2.06	-0.03	-0.26	0.05	7.18	5.68	1.19	0.29	0.10
14.5	n.d.	n.d.	n.d.	n.d.	n.d.	5.68	4.18	1.10	0.09	0.10

Supplementary text

For the mixing model, we used the end-member compositions as described in Table A 4.5 and applied the equations A1, A2 and A3.

Table A 4.5 Literature data used for the modeling of the Kyllaren fjord and Baltic Sea water columns, applying conservative mixing between seawater and fresh water (Ku et al., 1977; Collier, 1985; Palmer and Edmond, 1993; Siebert et al., 2003; Archer and Vance, 2008; Weyer et al., 2008; Noordmann et al., 2011).

Locality	Practical salinity	c(Mo) nmol/kg	δ^{98}Mo ‰	c(U) nmol/kg	δ^{238}U ‰
ocean water	35	105	2.3	14	-0.37
fresh water	0	5	0.7	1.3	-0.24

$$c(\mathrm{M})_{mix} = c(\mathrm{M})_{sw} \cdot \frac{S_m}{S_{sw}} + c(\mathrm{M})_{fw} \cdot \left(1 - \left(\frac{S_m}{S_{sw}}\right)\right) \quad \text{(A1)}$$

$$\delta^{98}Mo_{mix} = \frac{\delta^{98}Mo_{sw} \cdot c(\mathrm{Mo})_{sw} \cdot \frac{S_m}{S_{sw}} + \delta^{98}Mo_{fw} \cdot c(\mathrm{Mo})_{fw} \cdot \left(1 - \frac{S_m}{S_{sw}}\right)}{c(\mathrm{Mo})_{mix}} \quad \text{(A2)}$$

$$\delta^{238}U_{mix} = \frac{\delta^{238}U_{sw} \cdot c(\mathrm{U})_{sw} \cdot \frac{S_m}{S_{sw}} + \delta^{238}U_{fw} \cdot c(\mathrm{U})_{fw} \cdot \left(1 - \frac{S_m}{S_{sw}}\right)}{c(\mathrm{U})_{mix}} \quad \text{(A3)}$$

In the equations above, $c(\mathrm{M})_{mix}$ is the expected concentration of Mo and U from the mixing of seawater and fresh water; $c(\mathrm{M})_{sw}$ and $c(\mathrm{M})_{fw}$ are the Mo or U concentration of seawater or fresh water, respectively; S_m is the measured salinity of the water column and S_{sw} the salinity of seawater; $\delta^{98}Mo_{mix}$ and $\delta^{238}U_{mix}$ are the isotope compositions of Mo and U expected from mixing, respectively (see Table 4.1 and Table A 4.5). A comparison of the measured and modeled Mo and U concentrations and isotopic compositions can be found in Figs. 4.3a, 4.3b, 4.5a and 4.5b.

CHAPTER 5

Uranium isotope fractionation during hydrothermal alteration of the oceanic crust

Abstract

Previous studies and Chapter 4 of this thesis observed significant fractionation of the two primordial isotopes of uranium (^{238}U and ^{235}U) between seawater and diverse oceanic sinks, including suboxic sediments from marine margins (the largest U sink), organic-rich sediments from restricted basins and oxic sediments (both minor sinks). However, U isotope fractionation during the removal of U at mid-ocean ridges through alteration of the oceanic crust, the second most important sink for U, is essentially unknown. We addressed this question and analyzed hydrothermal water samples from the Juan de Fuca Ridge (low- and high-temperature fluids), altered basalts and their calcium carbonate veins from the Pigafetta Basin, Bermuda Rise and Reykjans Ridge (ODP samples). The hydrothermal water samples display low U concentrations (0.3 nmol/kg to 1 nmol/kg) and show variable U isotopic compositions ($\delta^{238}U$ = -0.59 ‰ to -0.28 ‰). However, due to their low U concentration and the small sample sizes available for this study, the uncertainty on $\delta^{238}U$ for the hydrothermal waters (2 SD = 0.15 ‰) is higher than for previously analyzed seawater samples. Altered basalts display moderately enriched U concentrations compared to those typically observed in fresh basalts from the oceanic crust. Additionally, altered basalts and carbonate veins show large U isotope fractionation towards both heavy and light U isotope compositions ($\delta^{238}U$ between -0.63 ‰ and 0.27 ‰).

In average, hydrothermal water displays a U isotope composition, which is slightly lighter than that of seawater ((-0.43 ± 0.25) ‰ vs. (-0.37 ± 0.03) ‰). Likewise, the strongest isotope fractionation observed for altered basalts relative to fresh basalt and for carbonate veins relative to seawater occurs towards heavier U isotope composition. These findings are in agreement with a model that assumes that the observed isotope fractionation is probably mostly a result of redox processes, i.e. 1) partial reduction of soluble U^{VI} from seawater during hydrothermal alteration, resulting in the enrichment of heavy U isotopes in the reduced U species and 2) the preferential removal of U^{IV} from hydrothermal fluids and incorporation into the altered oceanic crust. As hydrothermal water becomes depleted in heavy U isotopes by this process, altered basalts and carbonates may also display low $\delta^{238}U$, if they were affected by such light hydrothermal water. Our first findings are definitely not sufficient to understand the processes at MOR in detail, but they may indicate that net U isotope fractionation during U removal at MOR is only minor compared to that in anoxic water columns.

5.1 Introduction

Uranium is a redox-sensitive trace element, which commonly occurs in two redox-states (U^{IV} and U^{VI}). Under oxygenated conditions (e.g. in the modern ocean), it forms soluble and non-reactive complexes with carbonate (e.g. $[UO_2(CO_3)_3]^{4-}$) and under more reducing conditions, it forms insoluble U^{IV} complexes (e.g. $U(OH)_5^-$), which can further precipitate as uraninite (UO_2).

Due to the high incompatibility of U in mantle minerals, the continental crust is highly enriched in U to mass fractions in the lower µg/g range. Weathering and erosion results in the transport of material from the continental crust via rivers to the ocean. As a result of the long ocean residence time ($5 \cdot 10^5$ a, Colodner et al., 1995) compared to the ocean mixing time ($1.6 \cdot 10^3$ a), U is homogeneously distributed in the ocean. Also, the ocean contains a U concentration that is a factor of 14 higher than in rivers (3.3 ng/g vs. 0.24 ng/g). Uranium is removed from the ocean into four sinks: the two major sinks

are organic-rich suboxic sediments at continental margins (a large fraction of the U is likely buffered in carbonates) and altered oceanic crust through hydrothermal circulation at mid-ocean ridges. The two minor sinks are oxic sediments, e.g. ferromanganese crust, and euxinic sediments, e.g. organic-rich sediments that will become black shales during diagenesis.

Recently it was shown that the two primordial uranium isotopes, ^{238}U and ^{235}U, fractionate in near surface terrestrial environments (Stirling et al., 2007; Weyer et al., 2008), mainly under redox changing conditions. Therefore, U isotopes were used as a paleo-redox proxy to quantify the expansion of ocean anoxia during oceanic anoxic events (i.e. OAE-2; Montoya-Pino et al., 2010, Brennecka et al., 2011), similarly as previously modeled with Mo isotopes (e.g. Arnold et al., 2004; Kendall et al., 2009). Though, it is essential to quantify its modern oceanic cycle of U as precise as possible. In Chapter 3 we already determined the U sources to the ocean very precisely, which leaves only one unknown sink in the oceanic cycle: the hydrothermal alteration at mid-ocean ridges (the second most important sink of U in the oceanic cycle). As the other major sink, suboxic sediments, has a similar $\delta^{238}U$ as the continental crust, the hydrothermal sink is expected to display an isotopic composition not much different to the seawater value, for mass-balance reasons (Weyer et al., 2008).

However, hydrothermal processes can significantly affect the composition of seawater and the oceanic crust (as already shown for other elements, e.g. Li, Sr, Nd, Mills et al., 2001, Hongo et al., 2007, Krabbenhöft et al., 2010, Weyer and Seitz, 2012). Uranium is, along with e.g. Mg, one of the few elements that are depleted in hydrothermal fluids compared to seawater. If U is readily removed from seawater by hydrothermal activity (Michard et al., 1983; Chen et al., 1983, 1984; Michard and Albarede, 1985), bulk U isotope fractionation during hydrothermal alteration of the oceanic crust would be small. However, partial U removal may result in significant isotope fractionation, considering the large U isotope effects that occur during U reduction (e.g. in modern Black shales). Additionally, calcium carbonate minerals, which are well known to be associated with U, are deposited in veins from the hydrothermal fluids circulating within the oceanic crust (Bonatti et al., 1980).

Investigating those calcium carbonate veins may give additional information about element concentrations of the original seawater-derived solution. Therefore, we analyzed the U isotope compositions of hydrothermal fluids, hydrothermally altered oceanic crust, calcium carbonate veins and, for comparison, also fresh basalts (ocean island and intra-continental basalts) to constrain the process of U isotope fractionation on mid ocean ridges and to further complete the isotopic mass balance in the oceanic U cycle.

5.2 Sampling locations and description

5.2.1 Hydrothermal fluids

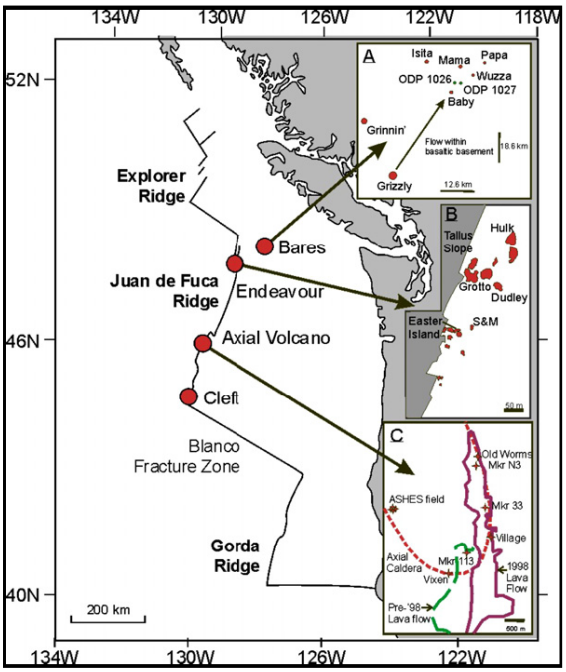

Fig. 5.1 Location of the hydrothermal fluids from the Juan de Fuca Ridge (Sharma et al., 2007).

Seven hydrothermal water fluids from the Juan de Fuca Ridge (Fig. 5.1, Sharma et al., 2007), a submarine volcanic ridge located off the coasts of the northwestern USA and southwestern Canada, have been provided by M. Sharma (Dartmouth College,

Hanover, USA). The samples include low temperature fluids (10-40 °C) from Baby Bare and high temperature fluids (265-353 °C) from Endeavour (Black Smokers: Hulk and Grotto) and a Monolith vent.

5.2.2 Hydrothermal altered oceanic crust

We analyzed hydrothermally altered oceanic crust from the Pigafetta Basin, Bermuda Rise and Reykjanes Ridge (Integrated Ocean Drilling Program – IODP, Leg and Site see). These samples were kindly provided by W. Bach (University of Bremen, Germany).

5.2.3 Non-altered fresh basalts

As a comparison for the isotopic composition of hydrothermally altered basalts, we analyzed non-altered recent ocean island and intra-continental basalts and one tephrite from the Canary Islands and one sample from Germany. Samples include olivine-bearing basalts from La Palma and Tenerife (LP8 and TF9), an ankaramite-basalt from Tenerife (TF12), a clinopyroxene-bearing tephrite from Tenerife (TF6) and one olivine-bearing nephelinite from the German Vogelsberg volcano (Vog13, Weyer and Seitz, 2012). Additionally, a basaltic standard, BCR-1, from the Columbia River was analyzed.

5.3 Analytical methods

The hydrothermal fluids were evaporated to dryness and then re-dissolved with 15 M HNO_3 and 30 % H_2O_2. After taking an aliquot for the trace element measurement

on the ICP-MS (Element 2 by Thermo Fisher Scientific), the samples were diluted to 3 M HNO_3 and a U double spike was added prior to the purification of U, according to the procedure described in detail in Weyer et al. (2008).

The ODP-samples were separated into two categories: the bulk sample and their calcium carbonate veins (CCVs). The bulk ODP-samples, further on described as altered basalts, and the fresh basalts were completely digested according to the procedure for basalts described in detail in Weyer et al. (2008). Briefly, about 300 mg of powdered basalts were digested with a mixture of conc. HF/HNO_3 (3:1) at 120 °C and, after evaporation to dryness, re-dissolved in 6 M HNO_3 and 6 M HCl to dissolve any remaining fluorites.

Veins of calcium carbonate that intruded the altered basalts (further on described as CCVs) were prepared by micro-drilling and handpicking to separate the CCVs from the bulk material. Afterwards, the CCVs were repeatedly leached with 6 M HCl to separate the carbonate phases from the bulk phase.

The further procedure, e.g. determining the concentrations for the trace elements on an ICP-MS (Element 2 by Thermo Fisher Scientific), addition of a U double spike, U isotope measurements on a MC-ICP-MS (Neptune by Thermo Fisher Scientific), was already described in detail in Chapter 2, 3 and 4. Uranium isotope compositions were measured and are reported relative to the U-standard NIST SRM 950-A, just like the measurements for the river samples. All measurements were performed at the Goethe University in Frankfurt.

5.4 Results

We analyzed hydrothermal fluids, altered basalts (ODP-samples), calcium carbonate veins and fresh basalts for selected major and trace element concentrations with ICP-MS (including Fe, Al, Mg, Ca, Sr, and U) and for their U-isotope composition

($\delta^{238}U$) with MC-ICP-MS. The results are presented in and Table 5.2 and Fig. 5.2 to Fig. 5.5.

The hydrothermally altered basalts display highly variable U concentrations from 0.20 µg/g to 1.28 µg/g and highly variable U isotope compositions ($\delta^{238}U$ from -0.46 ‰ to 0.27 ‰, Fig. 5.2,), with an average of $\delta^{238}U$ = -0.22 ‰ ± 0.55 ‰ (2 SD). The here analyzed fresh basalts show higher U concentrations, from 0.55 µg/g to 1.79 µg/g and a more homogeneous U isotope composition, with an average of $\delta^{238}U$ = -0.30 ‰ ± 0.07 ‰, (Fig. 5.2,). Also, the CCVs have highly variable U concentrations, ranging between 0.23 µg/g and 2.14 µg/g, and $\delta^{238}U$ ranging between -0.63 ‰ and 0.11 ‰ (Fig. 5.2,). No correlation between the U concentrations and $\delta^{238}U$ for neither basalts nor carbonate veins was observed.

Table 5.1 Results for the alteration products (calcium carbonate veins and altered basalts), compared to the fresh basalts.

Sample	Location	Leg	Site	Hole	Section	$w(Al_2O_3)$	$w(CaO)$	$w(FeO)$	$w(MgO)$	$w(Sr)$	$w(Zr)$	$w(U)$	$\delta^{238}U$	2 SD
						weight-%	weight-%	weight-%	weight-%	µg/g	µg/g	µg/g	‰	‰
calcium carbonate veins														
	Pigafetta Basin	185	801	C	37-2	0.35	26.89	2.00	0.83	40.52	0.83	0.40	0.04	0.00
	Bermuda Rise	51	417	D	39-5	0.12	28.72	1.63	0.58	64.46	0.67	0.58	0.11	0.04
	Pigafetta Basin	185	801	C	28-1	2.38	20.14	2.78	1.03	66.24	2.44	2.14	-0.22	0.05
	Pigafetta Basin	129	801	B	44-1	2.45	22.15	4.73	1.46	105.54	6.78	0.41	-0.58	0.06
	Bermuda Rise	52	417	D	48-6	0.32	26.81	2.06	0.67	48.41	2.30	0.23	-0.09	0.01
	Pigafetta Basin	129	801	B	40-1	2.14	18.31	2.88	2.90	120.68	0.60	0.43	-0.63	0.04
	Pigafetta Basin	185	801	C	6-4	0.09	23.50	1.95	0.91	48.17	0.60	0.55	-0.30	0.03
altered basalts														
	Bermuda Rise	52	417	D	80-6	0.38	n.d.	4.17	2.97	117.56	27.69	0.34	0.14	0.01
	Bermuda Rise	185	801	C	27-2	0.23	n.d.	3.16	1.18	544.58	73.63	1.16	-0.34	0.03
	Bermuda Rise	51	417	A	90-4	0.28	n.d.	6.39	2.70	90.06	61.45	0.20	-0.27	0.04
	Pigafetta Basin	183	801	C	67-1	0.26	n.d.	6.39	3.54	280.34	96.75	0.66	0.27	0.07
	Pigafetta Basin	129	801	B	105-2	0.29	n.d.	4.70	2.62	1459.11	167.15	0.80	-0.28	0.03
	Reykjans Ridge	49	407		34-4	0.26	n.d.	6.01	2.50	275.96	74.66	0.43	-0.42	0.02
	Bermuda Rise	52	418	A	137-2	0.33	n.d.	3.72	2.44	517.88	40.60	1.28	-0.44	0.04
	Pigafetta Basin	129	801	C	31-3	0.34	n.d.	2.66	1.31	181.91	25.41	0.32	-0.46	0.01
fresh basalts														
TF6	Tenerife					1.15	3.85	4.06	1.87	506.00	214.35	1.79	-0.29	0.04
TF9	Tenerife					2.49	4.42	6.05	12.19	252.07	92.9251	0.55	-0.27	0.01
TF12	Tenerife					3.33	3.67	4.79	2.42	371.64	159.247	1.12	-0.33	0.02
LP8	La Palma					1.66	5.23	4.54	4.22	467.66	158.679	1.75	-0.30	0.02
Vog13	Vogelsberg					0.42	6.76	4.96	11.74	737.20	155.066	1.72	-0.36	0.05
BCR-1	Columbia river					5.00	2.74	5.44	1.24	141.98	119.975	1.56	-0.27	0.04

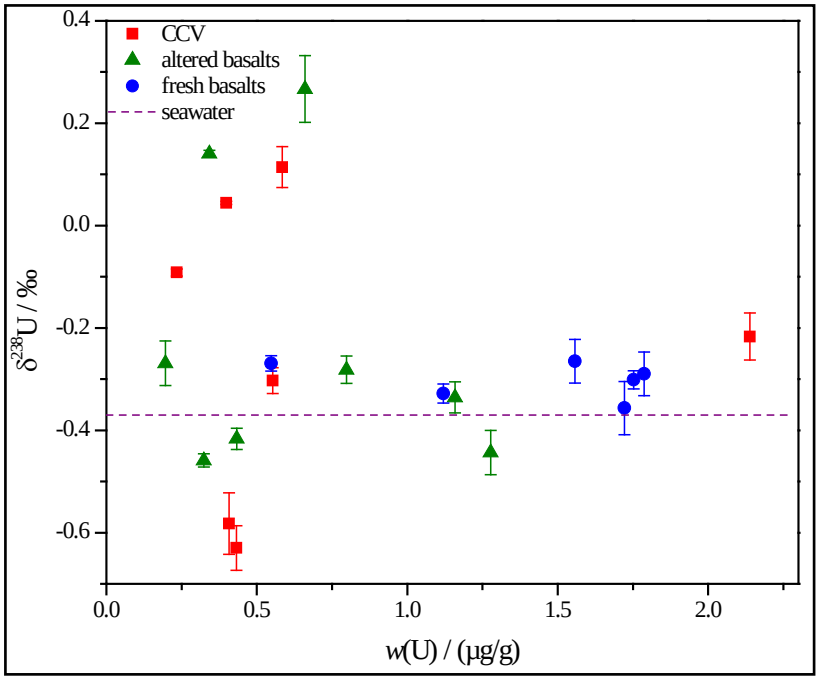

Fig. 5.2 Relationship between $\delta^{238}U$ and the U concentration in the calcium carbonate veins (CCV) and altered basalts from Pigafetta Basin, Bermuda Rise and Reykjans Ridge (MOR) and in the fresh basalts from La Palma, Tenerife, Vogelsberg and USA (BCR-2: Basaltic Columbia River): none of the sample groups shows a correlation between the U concentration and $\delta^{238}U$. However, both CCVs and altered basalts display a significantly larger spread in $\delta^{238}U$ than fresh basalts.

The hydrothermal fluids display variable U concentrations from 0.25 nmol/kg to 0.58 nmol/kg and are strongly depleted in their U concentration compared to seawater (14 nmol/kg, Weyer et al., 2008). Just one sample (J2010-M11) contains a higher U concentration with 6.4 nmol/kg. All samples show a U isotope composition very similar to the average value of seawater ($\delta^{238}U$ = -0.41 ‰), with isotopic compositions ranging from -0.28 ‰ to -0.59 ‰ (Fig. 5.3 and Table 5.2). However, the analyzed isotope compositions for some of the hydrothermal fluids have higher uncertainties than the reference value for seawater, due to the low U concentrations of the fluids.

Table 5.2 Results for the hydrothermal water samples.

Sample	Material	*c* (Ca)	*c* (Mg)	*c* (U)	$\delta^{238}U$	2 SD
		µmol/kg	mmol/kg	nmol/kg	‰	‰
J2005-B8	low-temperature	49.30	3.43	0.58	-0.55	0.05
J2007-B9	ODP Site 1026B	55.44	4.59	0.38	-0.42	0.08
2429-10		65.72	2.60	0.51	-0.59	0.04
J2010-M16		28.38	1.41	0.37	n.d.	n.d.
J2011_M16	high temperature: Endeavour (Grotto)	35.60	0.85	0.25	-0.28	0.10
J2010-M11		14.49	39.36	6.36	-0.28	0.11
J2010-M14	high temperature: Endeavour (Hulk)	36.53	2.26	0.31	-0.35	0.15

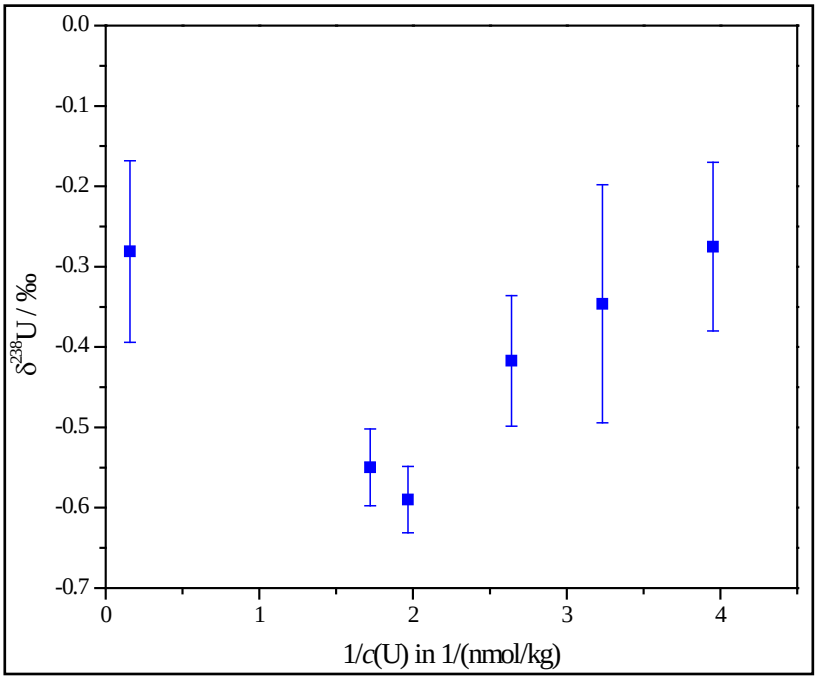

Fig. 5.3 Correlation between the U isotope composition and the inverse U concentration in the hydrothermal fluids, only the sample with the highest U concentration deviates from this trend.

With the exception of sample J2010-M11, which has a high U concentration, all other samples define a positive correlation of $\delta^{238}U$ and 1/*c*(U), (Fig. 5.3). However, due to the low U concentration, the analytical uncertainty is relatively high for most of the

analyzed water samples (2 SD can be up to 0.15 ‰). Additionally, we observed a positive correlation between the Mg and the U concentration and an inverse correlation between $\delta^{238}U$ and the Ca concentration (Fig. 5.4 and Fig. 5.5).

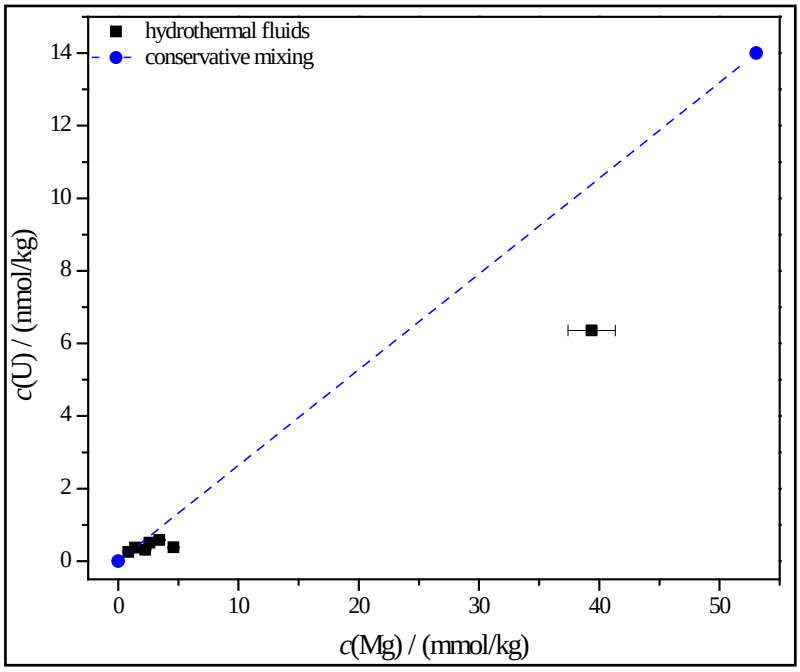

Fig. 5.4 Correlation between the U- and the Mg-concentration in the hydrothermal fluids, compared to a conservative mixing between seawater (c(Mg) = 53 mmol/kg, c(U) = 14 nmol/kg) and a hydrothermal component (assumed to have c(Mg) = 0 mmol/kg, c(U) = 0 nmol/kg) (blue dashed line).

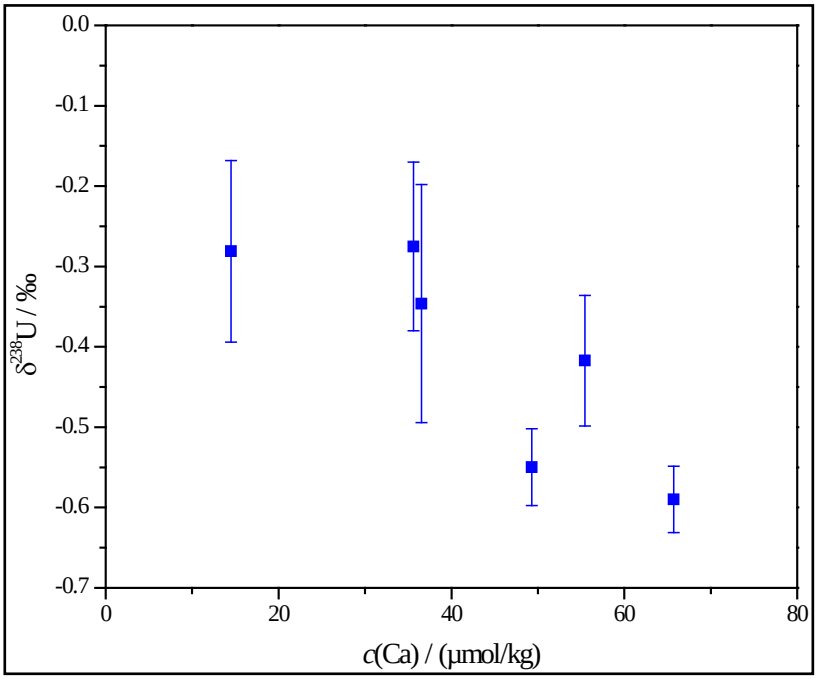

Fig. 5.5 Negative correlation between the U isotope composition and the Ca concentration in the hydrothermal fluids.

5.5 Discussion

In light of the current lack of knowledge in the U ocean cycle, here we want to prove whether hydrothermal reactions between seawater and oceanic crust (represented here by the altered basalts) are recorded in systematic variations of their U concentrations and U isotope compositions and if the calcium carbonate veins record the uranium isotope composition from their source, the circulating hydrothermal fluids.

5.5.1 Uranium isotope fractionation in hydrothermally altered samples

Penetration of seawater into the oceanic crust is associated with 1) a large temperature increase (e.g. from about 3 °C to 60 °C or even > 300 °C) and 2) a

transition from oxic to anoxic conditions. The latter results in the reduction of soluble U^{VI} from the fluids to insoluble U^{IV}. Additionally, hydrothermal fluids convert the primary mineral composition of fresh basalts, including olivine, plagioclase and clinopyroxene, to secondary minerals, such as iron-oxyhydroxides, smectite and celadonite (Honnorez, 1981; Alt, 1995; Bach et al., 2003).

The reaction between hydrothermal fluids and oceanic crust is known to result in a U enrichment in the oceanic crust (Mills et al., 1993). This is assumed to be generated by an almost quantitative transfer of U from seawater by the hydrothermal fluids into the secondary minerals (Chen et al., 1986; Morford and Emerson, 1999). The eight investigated altered basalts have U concentrations between 0.20 µg/g and 1.28 µg/g, which is a factor of 3 to 18 higher than that of average normal mid-ocean ridge basalt (71 ng/g U, Hofmann, 1988). In addition to those variable U concentrations, we also observed a large range in the U isotope composition ($\delta^{238}U$ from 0.27 ‰ to -0.46 ‰). However, there is no correlation between the U concentration and the U isotope composition. As a reference for the U isotope composition of fresh MORB, we used the U isotope composition from the here investigated fresh ocean island- and intra-continental basalts, assuming that MORB and OIBs have within uncertainties identical U isotope compositions. In theory, OIBs may contain a higher portion of recycled MORB and crustal material than MORB, which may affect their U isotope compositions. However, this should result in variable U isotope compositions of OIBs, which is not observed. Rather, all fresh basalts analyzed here show a homogenous U isotope composition with $\delta^{238}U$ ranging between -0.27 ‰ and -0.36 ‰. Of the altered basalts, only two samples deviate significantly in their $\delta^{238}U$ from the average of non-altered basalts (i.e. $\delta^{238}U$ = 0.14 ‰ for one sample from the Bermuda Rise and $\delta^{238}U$ = 0.27 ‰ for a sample from the Pigafetta Basin). The other samples display a more uniform $\delta^{238}U$, with an average of -0.37 ‰ ± 0.17 ‰ (double standard deviation). These latter samples are only slightly enriched in light U isotopes compared to the here investigated fresh ocean island basalts. We speculate that redox reactions, which generate the largest known U isotope fractionation in nature (e.g. Weyer et al., 2008), are responsible for the variable, and in particular, for the heavy U isotope composition observed for two altered basalts, i.e. by selective reduction of U^{VI} from the fluid and

incorporation into secondary minerals. The remaining U in the fluid should therefore contain a predominantly light U isotope signature, which may have been further transported by the hydrothermal fluids to be reduced in other basalts. This process will generate altered basalts that are both enriched in heavy and light U isotopes, which may explain the heterogeneous U isotope composition observed for the altered basalts. However, further investigations are required to prove this assumption.

5.5.2 Uranium isotope fractionation within the hydrothermal fluids

Magnesium and U are known as some of the few elements that get removed from seawater during the hydrothermal interaction with fresh basalt and thus enriched in hydrothermally altered crust (Chen et al., 1983, 1984; Michard et al., 1983; Michard and Albarede, 1985). According to the study of Pogge et al. (2008), the removal of Mg occurs through exchange with Ca during low-temperature basalt-seawater interaction, e.g. formation of dolomite and ion exchange reactions with clays (Mottl and Wheat, 1994; Sharma et al, 2007). The here-investigated hydrothermal fluids are indeed highly depleted in their U and Mg concentrations (c(U) = 0.25 nmol/kg to 6.36 nmol/kg and c(Mg) = 0.85 mmol/kg to 39.36 mmol/kg) compared to seawater (c(U) = 14 nmol/kg and c(Mg) = 53 mmol/kg, respectively, Fig. 5.4), implying almost quantitative removal of these elements during hydrothermal alteration at MOR (Michard and Albarede, 1985). The correlation between Mg and U may indicate mixing of the hydrothermal fluids with seawater during sampling. Most of the samples follow crudely a conservative mixing line from seawater and a hydrothermal component (c(Mg) = 0 mmol/kg and c(U) = 0 nmol/kg, as indicated by the blue dashed line in Fig. 5.4). However, at least the sample with the highest Mg and U concentration shows a significant deviation from this mixing line towards a lower U concentration, indicating a more complex story, at least for this sample. Potentially, the mixing of the fluids with seawater has resulted in the precipitation of secondary minerals containing U but no Mg (Michard and Albarede, 1985; Chen and Wasserburg, 1986).

The hydrothermal fluids display a heterogeneous U isotope composition from $\delta^{238}U$ = -0.28 ‰ to -0.59 ‰, with uncertainties as high as 0.15 ‰ (2 SD). Different kinds of processes can cause this isotope fractionation compared to seawater and isotope variation within the hydrothermal fluids: one reason is in agreement with our previous assumption that the U isotopic variation in the altered basalts are caused by selective reduction of U^{VI}, which resulted in two isotopically heavy samples. The remaining fluid should therefore contain a predominantly light U isotope signature. Actually, this is what we observed for two samples of the hydrothermal fluids, sample J2005-B8 ($\delta^{238}U$ = -0.55 ‰) and sample 2429-10 ($\delta^{238}U$ = -0.59 ‰). Another reason for the isotopic variation within the hydrothermal fluids may be their large double standard deviation, implying that due to the large analytical uncertainty the measured $\delta^{238}U$ values cannot be resolved from one another. This large analytical uncertainty is usually caused by low amounts of concentration and sample, which results in low intensities during the mass spectrometric measurements.

Two samples, J2011_M16 and J2010-M11, contain a $\delta^{238}U$ that is significantly heavier than seawater, both -0.28 ‰ vs. -0.41 ‰. One reason for this difference may just be their large double standard deviation of 0.11 ‰, implying that within the large analytical uncertainty the samples are identical with the value for seawater. Another reason may be that the light U isotope, ^{235}U, prefers to adsorb onto minerals from the oceanic crust, which leaves a slightly heavier hydrothermal solution behind (as observed for adsorption to Mn oxides by Brennecka et al., 2011a).

The positive correlation of $\delta^{238}U$ and the inverse U concentration (Fig. 5.3) suggests that the light $\delta^{238}U$ is not a primary signature, but instead resulting from coupled U reduction and U removal into the alteration products. Another reason for this correlation may be mixing of an isotopically light U and U depleted fluid with seawater.

The formation of calcium carbonate in the veins (CCV) within the basalts contains an even more complex history than the hydrothermal fluids. As the hydrothermal fluids alter the oceanic crust, the fluids get depleted in U and enriched in calcium. As the conditions (e.g. pressure and temperature) change, the hydrothermal

fluids get supersaturated with calcium and carbon dioxide, which has been released from the basalts, and calcium carbonate is precipitated. The here-analyzed calcium carbonates contain in general low U concentrations, between 0.23 µg/g and 0.58 µg/g, compared to the other U sinks from the ocean, e.g. suboxic, euxinic and oxic sediments. However, as the concentration of U in calcium carbonates covers a large range from 0.025 µg/g in foraminifera (Dunk et al., 2002) to 2.3 µg/g in coral reef complexes (Dunk et al., 2002), even the one sample with the comparatively high U concentration with 2.14 µg/g is not uncommon.

5.6 Conclusion

Our investigation of U concentrations and isotope compositions of hydrothermal fluids, altered basalts and carbonate veins improved our understanding for the behavior of U under hydrothermally altering conditions. We observed significant U isotope fractionation ($\delta^{238}U$ between -0.63 ‰ to -0.27 ‰) associated with the circulation of the hydrothermal fluids through the oceanic crust. Hydrothermal fluids display $\delta^{238}U$ between -0.28 ‰ and -0.59 ‰, i.e. in average slightly lighter than seawater coupled with a strong depletion in the U concentration of the fluids compared to that of seawater (0.4 nmol/kg vs. 14 nmol/kg). These findings show that significant amounts of U are removed during the interaction of hydrothermal fluids with oceanic crust, leaving behind hydrothermal waters being in general enriched in a lighter U isotope composition.

The investigated altered basalts are fractionated towards both heavy and light U isotope compositions ($\delta^{238}U$ between 0.27 ‰ to -0.46 ‰), coupled with U enrichment by a factor of 3 to 18, compared to average MORB. The most prominent U isotope fractionation these basalts towards high $\delta^{238}U$ combined with the slightly lower $\delta^{238}U$ observed for hydrothermal fluids indicates that partial U reduction and incorporation into the secondary minerals of the altered crust may be an important process at MORB. Open system behavior is likely responsible for the variable U isotope compositions

observed in this study. However, the mechanisms involved in the removal process are still not completely understood.

The investigated carbonate veins show also U isotope fractionation towards both heavy and light U isotope compositions ($\delta^{238}U$ between -0.63 ‰ to 0.11 ‰), exceeding the range observed for hydrothermal fluids. Accordingly, these veins do likely not simply resample the U isotope composition of the fluids and U isotope fractionation occurs during the precipitation of the CCVs.

CHAPTER 6

Uranium isotope fractionation in a mine tailing

Abstract

As a case study, we tested if U isotope compositions are potentially suitable to constrain U mobilization in tailings from mining activity. We investigated a highly U-enriched sediment depth profile from a mine tailing in Schneckenstein (Germany). The profile shows well correlated U mass fractions and isotope signatures in the sediments with depth. The strongest U enrichment, along with the heaviest $\delta^{238}U$ are observed at a depth of about 25 cm. Potentially, U was mobilized in the upper part of the profile, but precipitated at a certain depth, when conditions become more anoxic. Potentially, U reduction occurred in a zone of Fe-reduction (and mobilization) or of sulfate reduction, driven by microorganisms. Further investigations are necessary to address these hypotheses.

6.1 Introduction

Uranium is a very important element for the nuclear industry, due to the fissile properties of ^{235}U. Mining of U has been conducted at a couple of places in East Germany, e.g. Schneckenstein, after World War II. Uranium was mined and processed in Schneckenstein between 1946 and 1957. The residua of the ore processing were

deposited in tailing ponds close to the processing site and tailings management areas (TMAS), respectively. The typical degree of efficiency for processing of U ores was around 90 %, resulting in significant accumulation of radioactive material (e.g. U and their daughter nuclides: thorium and radium) in tailings. Release of such material to the environment may generate critical environmental problems, as many of the metals, including U, are not only radioactive, but also highly poisonous. During the environmental remediation a protective coating and a couple of drainage pipes have been installed. Nevertheless, the protective coating of the tailing might have been damaged by erosion throughout the past years and as U is very mobile and soluble under oxidizing conditions, U contamination may be at hand. Another environmental problem can be caused by contaminated seepage water, which is being discharged into the river Bodabach through the drainage pipes of the tailing. Previous studies revealed already that the drainage pipes contain a lot of ballast, which implies discharge of U (Diploma thesis by Gottschalk, 1997 and Kutschke, 1998 and a more comprehensive study by Merkel et al., 1998). Therefore, the contamination of soil and groundwater is still a major problem in those sites. In this study, we investigated those contaminated sites regarding their variations in the ratio of the long-lived U isotopes ^{238}U and ^{235}U. The goal of this study is to investigate if direction and extend of $^{238}U/^{235}U$ isotope fractionation can provide information about the mobilization and fixation processes during U remobilization from a mine tailing. Therefore, we analyzed soil samples from different depths and localities from a former tailing as well as the water from the drainage pipes for their U mass fraction and U isotope composition.

6.2 Location and description of the samples

Soil and water samples were taken from a small wetland that developed at the foot of the main tailings dam in Schneckenstein, Germany (Landgraf et al., 2002; Mbudi and Merkel, 2005). It is located in the Vogtland region of Saxony, Germany (Fig. 6.1). Probably, before the wetland was formed, the tailing was covered with multiple layers of waste rock. The water samples correspond to the tailing water from the former U mine. The soil samples are taken directly from the wetland, which differs in its consistency and therefore in its available depth. Wondem Gezahegne (a Ph.D. student in Freiberg at Prof. Broder Merkel) took all samples on the 23rd of September 2008.

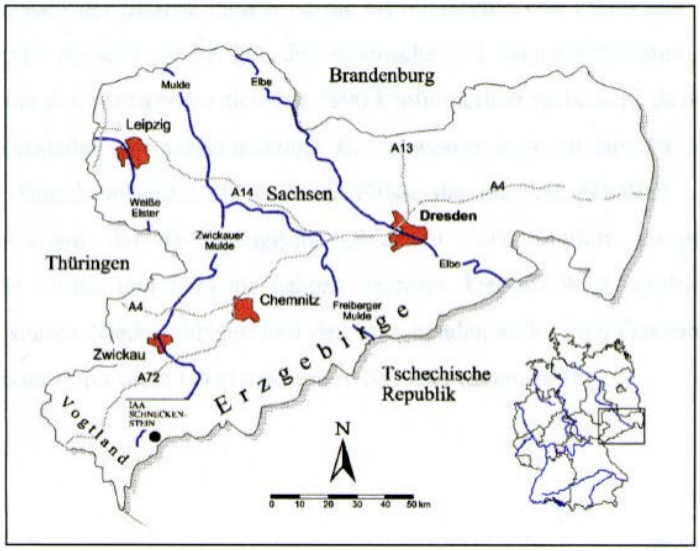

Fig. 6.1 Location of the tailings management area (TMAS) in Schneckenstein, Germany.

6.3 Analytical methods

Around 300 mg of each soil sample were ashed at 550 °C and digested in aqua regia, followed by taking an aliquot and measuring it at a ICP-MS (Thermo Fisher Scientific Element 2, Goethe University Frankfurt) to determine the concentrations of trace elements and especially the U concentration for further spiking with IRMM 3636-A (containing only ^{236}U and ^{233}U) of the samples. The spiked sample was purified through an anionic exchange resin (UTEVA) according to the procedure described in detail by Weyer et al. (2008). The procedure for measuring the U isotope composition ($n(^{238}U)$ / $n(^{235}U)$) of each sample on a MC-ICP-MS (Neptune by Thermo Fisher Scientific, Goethe University Frankfurt) has already been described in detail in Chapters 2, 3 and 4. Uranium isotope compositions were measured and are reported here relative to the U-standard NBL CRM 112-A, just like the measurements for the samples in Chapter 4. Around 80 mL of each water sample was evaporated to dryness and then re-dissolved in 6 M HCl. Additionally, an aliquot was taken and measured at the ICP-MS (Thermo Fisher Scientific Element 2) to determine the concentrations of Mg, Ca and U. The samples were also spiked with IRMM 3636-A (containing only ^{236}U and ^{233}U), according to their U mass fraction. After the purification of the sample by an anionic exchange resin (UTEVA), the U isotope composition ($n(^{238}U)$ / $n(^{235}U)$) was determined by measurements on a MC-ICP-MS (Neptune by Thermo Fisher Scientific, Goethe University Frankfurt).

6.4 Results

We analyzed water and soil samples from the wetland in Schneckenstein for selected major and trace element concentrations (including Mg, Al, Ca, Fe, Ni, Cu, Zn, Mo, Cd, Pb and U for the soil and Mg, Ca and U for the water samples) and their U isotope composition ($\delta^{238}U$ relative to NBL CRM 112-A). The results are presented in Table 6.1 and Table 6.2 and Fig. 6.2. The soil samples represent depth sections of 10 cm and 15 cm from two different localities (Table 6.2). From locality 3, we analyzed a

depth profile from 0 cm to 60 cm (6 samples). Accuracy and precision is better than 1 % for the determination of the U concentrations (with ID) and about 5 % for the other element concentrations, which were determined by ICP-MS. The reproducibility for $\delta^{238}U$ is about 0.05 ‰.

All of the drain tubes display high U enrichment compared to common natural waters (e.g. rivers: $2.4 \cdot 10^{-4}$ mg/L and seawater: $3.3 \cdot 10^{-3}$ mg/ L), with values from 0.06 mg/L to 0.59 mg/L. The major elements magnesium and calcium are also slightly enriched compared to typical river values (Mg: 4.1 mg/L, Ca: 15 mg/L). Three of the four water samples contain an uranium isotopic composition ($n(^{238}U) / n(^{235}U)$ = 138.113 mol/mol to 141.916 mol/mol), which deviates largely from the so far observed range for the uranium isotopic composition. However, the sample with the highest U concentration (0.59 mg/L) displays a more natural $\delta^{238}U$ of -0.03 ‰.

Table 6.1 Results for the water samples.

Location	Pipe	γ(Mg) mg/L	γ(Ca) mg/L	γ(U) mg/L	$n(^{238}U) / n(^{235}U)$ mol/mol	2 SD mol/mol	$\delta^{238}U$ ‰	2 SD ‰
1	9	8.36	23.18	0.06	141.916	0.030	29.31	0.17
2	7	3.29	16.89	0.13	138.757	0.008	6.41	0.05
3	6	9.09	33.25	0.39	138.113	0.002	1.73	0.05
4	4	7.13	25.94	0.59	137.871	0.011	-0.03	0.03

Table 6.2 Results for the soil samples.

Average depth cm	Sediment section cm	*w* (Mg) mg/g	*w* (Al) mg/g	*w* (Ca) mg/g	*w* (Fe) mg/g	*w* (Ni) µg/g	*w* (Cu) mg/g	*w* (Zn) µg/g	*w* (Mo) µg/g	*w* (Cd) µg/g	*w* (Pb) µg/g	*w* (U) mg/g	δ^{238}U ‰	2 SD ‰
Location 1														
5	0-10	6.62	78.72	3.97	29.76	25.15	0.12	155.5	3.35	1.51	63.68	0.04	-0.18	0.06
15	10-20	5.68	65.43	3.25	25.19	25.16	0.14	158.1	4.40	2.11	51.74	0.04	-	-
Location 2														
5	0-10	5.33	74.74	10.78	51.03	156.34	2.50	783.4	36.03	17.66	140.27	2.38	-0.37	0.05
20	10-30	2.00	44.34	11.12	14.62	257.14	4.17	976.9	25.63	18.53	136.61	2.84	-0.27	0.05
Location 3														
5	0-10	2.97	48.01	10.91	49.17	93.03	2.46	472.6	16.27	12.43	90.84	1.99	-0.31	0.06
15	10-20	1.80	47.47	13.83	25.50	135.96	3.79	615.4	12.52	17.05	98.52	3.44	-0.27	0.06
25	20-30	5.49	34.61	8.63	29.04	277.32	1.61	818.1	99.83	17.29	66.24	4.73	-0.16	0.06
35	30-40	6.47	37.20	6.92	24.23	62.77	0.89	379.3	13.92	8.74	62.53	1.67	-0.30	0.06
45	40-50	3.20	43.76	14.47	21.48	49.51	2.59	257.2	7.67	7.78	56.54	2.04	-0.35	0.06
55	50-60	4.56	51.95	16.83	25.59	40.93	2.73	166.2	10.06	4.67	63.98	3.15	-0.34	0.06

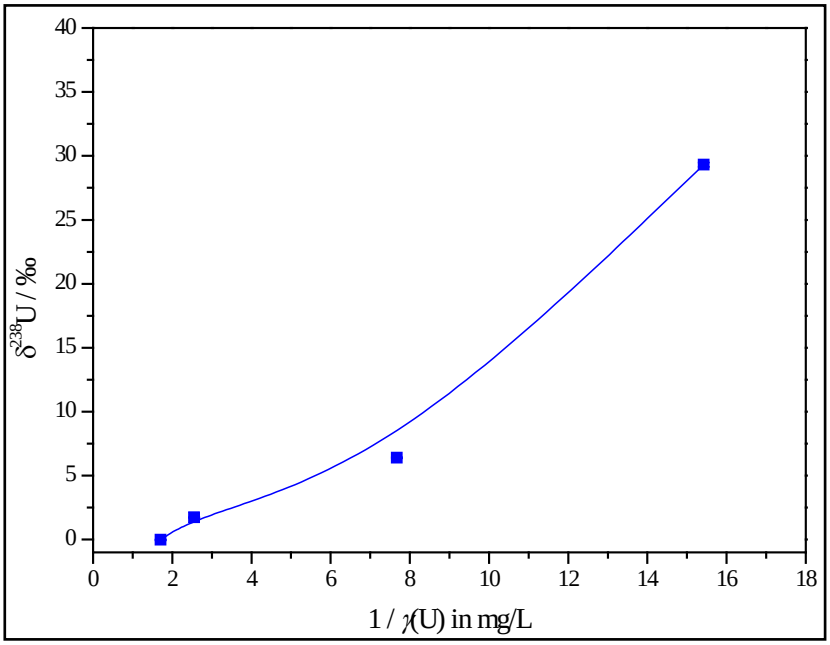

Fig. 6.2 Correlation between δ^{238}U and the inverse U concentration in the water samples from the tailing indicates a mixing between depleted and natural uranium.

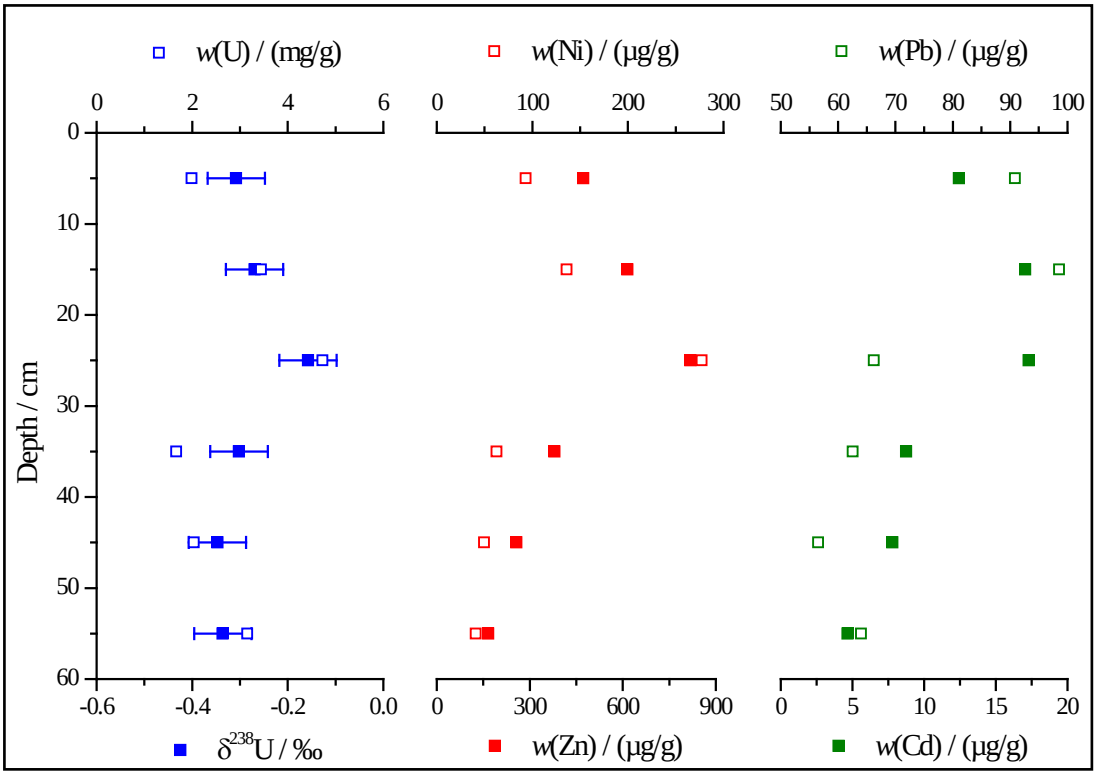

Fig. 6.3 Correlated U mass fractions and $\delta^{238}U$ in a depth profile of a highly U-enriched soil from a mine tailing in Schneckenstein (Germany). The highest U mass fractions and heaviest $\delta^{238}U$ occur at 25 cm depth, potentially where conditions get suboxic.

Due to the consistency of the wetland, only from locality 3 a full depth profile with samples from six different depths could be taken. The analyzed metal concentrations from the soil samples were plotted against depth to identify possible redox changes in the depositional environment (Fig. 6.3). The depth profile can be divided in two segments, according to a sharp change in the content of redox sensitive metals: the profile is separated at a depth of 30 cm. The upper segment displays increasing concentrations of Ni, Pb, Zn, Cd and U and increasingly heavier U isotope compositions (with $\delta^{238}U$ up to -0.16 ‰). Within the lower segment the concentrations of Ni, Pb, Zn and Cd drop to values that are even lower than those at the surface. The U concentration sharply drops from the highest concentration at 25 cm to the lowest concentration at 35 cm, and henceforward increases again with depth to a value slightly higher than the initial value (3.15 mg/g vs. 1.99 mg/g). The depth distribution of U

isotopes is crudely correlated with that of the concentrations of U and other redox-sensitive elements. All $\delta^{238}U$ values are within the typical range that is observed for granites and shales and agree within uncertainties with the average value of the continental crust (see Chapter 3). The only exceptions are sample three from locality 3, at 25 cm that shows the highest concentration of all redox-sensitive elements, and the surface sample of locality 1.

6.5 Discussion

The soil samples from the wetland of Schneckenstein display high trace metal concentrations (e.g. lead, zinc and nickel are enriched compared to regular non-contaminated soil), particular for U. The observed correlation between the U concentration and the U isotope composition along a depth profile reveals different redox conditions within the core (Fig. 6.3). Remarkable is the coupled concentration and isotope peak at a depth of 25 cm. According to previous findings (Bigeleisen, 1996; Schauble, 2007; Weyer et al., 2008), the heavy U isotope composition strongly indicates reduction of soluble U^{VI} to U^{IV}. Likely, oxidizing conditions at the surface have resulted in the mobilization and lateral and vertical transport of U from the tailing water in the upper soil sections. At a depth of ca. 25 cm, U becomes reduced, resulting in a peak of high U (and other redox-sensitive element) concentrations and high $\delta^{238}U$ values. Below a depth of 25 cm, $\delta^{238}U$ and the U concentration decrease again to a similar level that was measured at the surface. This level may represent a local “steady state” enrichment level for these metals, which are immobile under reducing conditions. Limited remobilization of e.g. U may also be initiated by bacteria transporting/reacting with U^{IV} (Beazley et al., 2011; Ray et al., 2011).

All analyzed water samples contain an U concentration, which is substantially higher than that of common natural water (i.e. also higher than the critical value of the

World Health Organization, WHO, which is 0.0015 mg/L). This strongly indicates that the concentration in all drainage pipes is not just a result of a natural geological enrichment, but instead seepage water contamination from the tailing. A likely explanation for the really high U concentrations may be a longer residence time in the tailing body. Another problematic factor regarding the contamination of water is rainwater. As rainwater seeps through the deposited materials it likely promotes the oxidation of former precipitated U and then discharging it via the drainage pipes to the Bodabach river. Fortunately, the Bodabach is not being used as a source for drinking water; further remediation appears to be necessary.

One water sample contains a $\delta^{238}U$ of -0.03 ‰, together with the highest U concentration (0.59 mg/L), compared to the other water samples from this tailing. This U isotopic composition is heavier in ^{238}U than the average value for rivers or other oxidized water. However, it is still a natural U isotopic composition and can therefore be the result of redox related reactions within the tailing. Though, it is heavier than all the here analyzed soil samples, indicating a more complicated history of this water sample. The other three water samples contain an uranium isotopic composition ($\delta^{238}U$ from 1.73 ‰ to 29.31 ‰ or $n(^{238}U) / n(^{235}U)$ = 138.113 mol/mol to 141.916 mol/mol), which is not explainable with a natural redox-related uranium isotopic fractionation. The origin of this deviation is probably a contamination with depleted uranium (DU). Depleted uranium can contain a $n(^{238}U) / n(^{235}U)$ of up to 500 mol/mol, compared to the natural occurring ratio of 137.84 mol/mol (or the formerly accepted ratio of 137.88 mol/mol). Notably, only a small amount of depleted uranium would be needed to explain the anomalous uranium isotopic composition, i.e. 0.06 %, 0.23 % and 1.14 % of DU in the respective samples. These calculations are based on the individual U concentration in the water samples and assuming a natural ratio of $n(^{238}U) / n(^{235}U)$ = 137.84 mol/mol for the samples and a $n(^{238}U) / n(^{235}U)$ of ca. 500 mol/mol for a DU contaminant. DU accumulates as a waste product after the enrichment of ^{235}U from natural uranium ores for the use in nuclear plants. As DU is also commonly used for the preparation of commercially available, isotopically uncertified U standards, it is also possible, in theory, that the water samples have been contaminated during the handling of the samples in the laboratory.

6.6 Conclusion

In this study we tested the use of U isotopes for investigation of U mobilization in the environment, particularly in a region with previous mining activity. The soil profile shows well-correlated U mass fractions and isotope signatures with depth, indicating a strong interaction of the seepage water with the soil within the uppermost 25 cm. Redox processes likely result in U enrichment in the soil to values of 4.73 mg/g with $\delta^{238}U$ of up to -0.16 ‰.

Due to the redox sensitive behavior of U, associated with U isotope fractionation, U isotopes are suitable tools to determine if the conditions (oxic to reducing conditions) change within a tailing. Future U isotope investigations of soil and water from U tailings combined with experimental studies on U reduction and remobilization may provide more detailed information on the mobilization process of U. This should result in additional constraints on the original source and the contribution of the tailings for the observed U contamination in the environment.

CHAPTER 7

Uranium isotopic composition of terrestrial uranium minerals

7.1 Introduction

The Pb-Pb dating method is widely used to date accessory minerals, especially zircon, that are between 1 million and 4.5 billion years old. As this dating method is based on two different decay chains, i.e. of ^{238}U to ^{206}Pb (with 8 α and 6 β particles) and ^{235}U to ^{207}Pb (with 7 α and 4 β particles), a prerequisite for its successful application is the precise knowledge of the $n(^{238}U) / n(^{235}U)$ ratio. For over 30 years scientist used a canonical $n(^{238}U) / n(^{235}U)$ ratio of 137.88, assuming that due to the heavy mass of U, no isotope fractionation would occur. However, recent studies observed significant variations of $n(^{238}U) / n(^{235}U)$ in terrestrial material (on the order of 1.3 ‰; Stirling et al., 2007; Weyer et al., 2008) and in meteorites (Brennecka et al., 2010a; Brennecka and Wadhwa, 2012). Significant U isotope fractionation is assumed to be caused by the reduction of U^{VI} to U^{IV} (Bigeleisen, 1996; Schauble, 2007; Weyer et al., 2008) or by adsorption on the surface of minerals, e.g. Mn-oxyhydroxides (Brennecka et al., 2011a). Recently, Hiess et al. (2012) determined the U isotope composition in U-bearing accessory minerals, which are used for U-Pb dating (zircon, monazite, apatite, titanite, uraninite, xenotime and baddeleyite). They observed variations in the $n(^{238}U) / n(^{235}U)$ ratio of even 5 ‰ (Hiess et al., 2012). However, they were not able to assign those variations to petrogenic, age or regional origin (Hiess et

al., 2012). For future Pb-Pb dating, they suggested to use their mean value of 137.818 ± 0.045 (2σ), which is based on their zircon measurements.

In this study, we focused on minerals that contain U as a major constituent, to give an overview on the natural range of isotope variations within and between U^{VI}–, U^{IV}– minerals and U mineralized bedrocks.

7.2 Materials and methods

Around 1 mg of each sample was consecutively digested at 150 °C for 20 h and re-dissolved with concentrated nitric acid (15 M), aqua regia (30 %), a mix of conc. HNO_3 (15 M) and HF (24 M), HCl (10 M) and finally in HNO_3 (6 M). After taking an aliquot for the measurement of U concentration with ICP-MS (Thermo Scientific Element 2), the samples were dissolved in 6 M HNO_3 and a U double spike (containing a $n(^{236}U) / n(^{233}U)$ ratio of 0.65917) was added prior to the purification of U, according to the procedure described in detail in Weyer et al. (2008).

Uranium isotope compositions were measured on a MC-ICP-MS (Thermo Scientific Neptune) and are reported relative to the U-standard NIST SRM 950-A (assuming a $n(^{238}U) / n(^{235}U) = 137.88$, Weyer et al., 2008). The measurement conditions have already been described in detail in Chapter 2, 3 and 4 of this thesis. All measurements were performed at the Goethe University in Frankfurt.

7.3 Results

We analyzed the minerals and the mineralized bedrocks for their U content and U-isotope composition. The results are presented in Table 7.1 and Fig. 7.1. $\delta^{238}U$ is calculated relative to the U-standard NIST SRM 950-A. Accuracy and precision is better than 1 % for the determination of the U concentrations (with ID) and the reproducibility for $\delta^{238}U$ is about 0.05 ‰, respectively.

Uranium minerals contain high and variable U content: U^{IV} minerals are between 17 mg/g and 810 mg/g and U^{VI} minerals are between 234 mg/g and 705 mg/g. Uranium mineralized bedrocks display only a minor enrichment of U compared to the U^{IV} and U^{VI} minerals with a concentration between 0.2 mg/g and 0.9 mg/g. However, they are still enriched in U compared to the average continental crust, which contains between 1 µg/g and 10 µg/g.

U^{IV} minerals display U isotope compositions ranging between 0.01 ‰ and -0.29 ‰, while U^{VI} minerals display $\delta^{238}U$ ranging between -0.02 ‰ and -0.50 ‰, thus are in average isotopically lighter than U^{IV} minerals. Uranium mineralized bedrocks display the largest variation in $\delta^{238}U$, ranging between -0.46 ‰ and 0.43 ‰

Table 7.1 Results for the investigated minerals.

Mineral	Chemical formula	Valence state	w(U) mg/g	$n(^{238}U) / n(^{235}U)$ mol/mol	2 SD mol/mol	$\delta^{238}U$ ‰	2 SD ‰
pitchblende (botryoidal)	UO_2	IV	809.54	137.8295	0.0020	-0.29	0.02
uraninite	UO_2	IV	775.14	137.8404	0.0017	-0.22	0.03
coffinite	$USiO_4$	IV	387.44	137.8497	0.0094	-0.18	0.03
pitchblende, boron	UO_2	IV	760.45	137.8455	0.0045	-0.16	0.02
pitchblende	UO_2	IV	708.47	137.8498	0.0095	-0.14	0.04
pitchblende in sandstone	UO_2	IV	16.97	137.8717	0.0113	0.01	0.02
curite of soddyite	$Pb_3[(UO_2)_4\|O_4\|(OH)_3]_2 \cdot 2\ H_2O$	VI	611.39	137.8005	0.0071	-0.50	0.01
schröckingerite (copper schist)	$NaCa_3(UO_2)(CO_3)_3(SO_4)F \cdot 10\ H_2O$	VI	234.14	137.8087	0.0077	-0.45	0.01
uranocircite	$Ba(UO_2)_2(PO_4)_2 \cdot 12\ H_2O$	VI	482.95	137.8201	0.0006	-0.39	0.03
liebigite	$Ca_2(UO_2)(CO_3)_3 \cdot 11\ H_2O$	VI	705.10	137.8209	0.0048	-0.36	0.02
autunite on quarz	$Ca(UO_2)_2(PO_4)_2 \cdot 10 - 12\ H_2O$	VI	538.00	137.8249	0.0053	-0.35	0.01
phosphuranylite	$KCa(H_3O)_3(UO_2)_7(PO_4)_4O_4 \cdot 8\ H_2O$	VI	487.32	137.8309	0.0052	-0.29	0.02
zeunerite	$Cu(UO_2)_2(AsO_4)_2 \cdot 10 - 16\ H_2O$	VI	288.90	137.8657	0.0119	-0.03	0.06
schoepite	$[(UO_2)_8O_2(OH)_{12}](H_2O)_{12}$	VI	255.19	137.8698	0.0129	-0.02	0.04
coal			0.42	137.8040	0.0097	-0.46	0.04
syenite			0.91	137.8078	0.0026	-0.44	0.00
sandstone, coal schist			0.39	137.8501	0.0091	-0.13	0.05
uranium mineralized wood			0.16	137.9290	0.0042	0.43	0.04

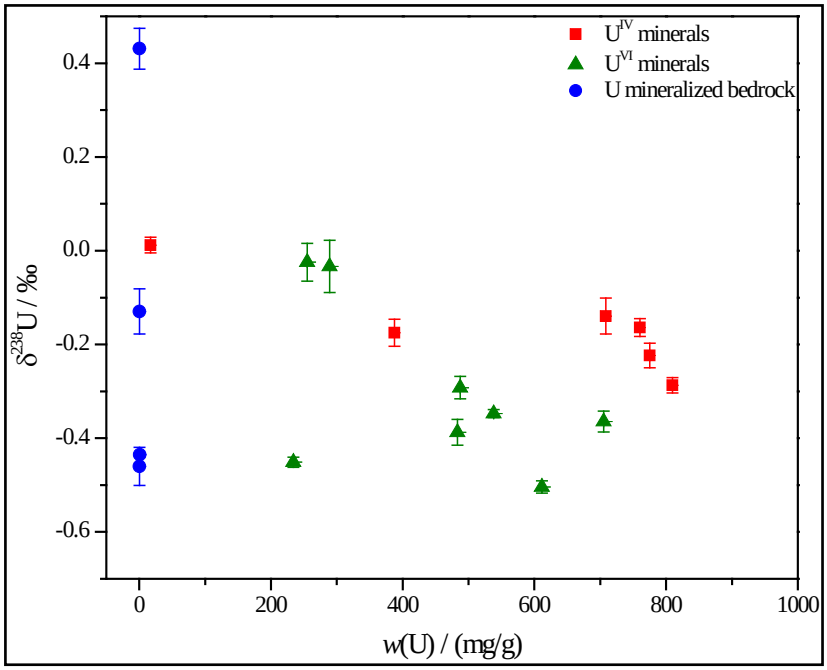

Fig. 7.1 Investigation of a possible relation between the U isotope composition and the U concentration in the investigated minerals: Apparently, $\delta^{238}U$ is not affected by the U concentration.

7.4 Discussion

In agreement with recent results from sediments containing U^{IV} and U^{VI} (Stirling et al., 2007; Weyer et al., 2008; Montoya-Pino et al., 2010), the here investigated U^{IV} minerals display a tendency towards enrichment of the heavier U isotope (^{238}U) compared to the continental crust (Chapter 3 of this thesis). U^{VI} minerals show a larger range of U isotope compositions, which is in average more similar to that of the continental crust. The U isotope fractionation observed between U^{IV} and U^{VI} minerals is similar to that previously observed for sedimentary environments (e.g. Weyer et al., 2008). In more comprehensive studies by Bopp et al. (2009) and Brennecka et al. (2010b), U ore deposits from low-temperature (sandstone samples), high-temperature (magmatic-type samples) and non-redox sensitive (quartz-pebble conglomerate) environments have been investigated. These studies revealed that in general the low-

temperature samples contain the largest spread in $n(^{238}U) / n(^{235}U)$, which was assigned to the nuclear-volume effect causing the fractionation of U isotopes. The nuclear-volume effect correlates with the temperature, with $1/T$ (Schauble, 2007), which explains the observed minor isotopic fractionation of high-temperature samples. The results of the study by Hiess et al. (2012) suggested also that magmatic samples are usually well-mixed with the continental or the oceanic crust, which was indicated by the magmatic samples overlapping isotopically with crustal samples. Our results show that the U isotope compositions of U^{IV} and U^{VI} minerals largely overlap, indicating that other factors but their valence state control their ratio of $n(^{238}U) / n(^{235}U)$. Therefore, the deposition temperature of our samples may play a larger role affecting $\delta^{238}U$. Only four of the here analyzed 18 samples deviate significantly from a narrow range in $\delta^{238}U$ (ranging here from -0.50 ‰ to -0.14 ‰) that overlaps with the observed range for crustal samples (Chapter 3). Three of the four samples are around 0 ‰ (pitchblende in sandstone, zeunerite and schoepite) and one is at 0.43 ‰ (uranium mineralized wood): however, two of those samples originate from a low-temperature depositions (wood and schoepite) and two from a high-temperature deposition (pitchblende and zeunerite), indicating that those samples were deposited under variable temperatures during the deposition and / or an incomplete reduction to U^{IV} during the process. Changing the coordination of U during formation of the minerals may result in a different enrichment of U isotopes: a recent study observed that the adsorption of U onto Mn-oxyhydroxides results in significant U isotope fractionation of 0.2 ‰ in $\delta^{238}U$ (Brennecka et al., 2011a). This process was discussed as a result of changing the coordination of U (Brennecka et al., 2011a). Additionally, the U source of these minerals (e.g. a hydrothermal fluid), may have had highly variable $\delta^{238}U$, as a result of a complex history of oxidation and reduction processes that resulted in the mobilization and enrichment of U.

The latter may be supported by the highly variable U isotope compositions, observed for U mineralized bedrocks that show a large range of $\delta^{238}U$ between -0.46 ‰ and 0.43 ‰. These variations are in the already observed range for different kind of samples formed under variable redox conditions at low-temperature (e.g. reducing sediments from euxinic basins or oxic sediments from the continental crust, Stirling et

al., 2007; Weyer et al., 2008). Additionally, U adsorption may have further enhanced the observed range of $\delta^{238}U$ values.

7.5 Conclusion

Our results suggest that minerals containing the oxidized U species (U^{VI}) usually display a lighter $\delta^{238}U$ compared to samples containing the reduced U species (U^{IV}). However, our results are only based on a very limited amount of samples and the results of the U isotope composition for the U^{IV} and U^{VI} minerals overlap with each other. This suggests that the U isotope composition of U^{IV} and U^{VI} minerals does not only depend on the valence state of U. Other processes, e.g. the coordination of U in the minerals or a variable $\delta^{238}U$ in their sources, may also explain the overlapping range in $\delta^{238}U$ observed for U^{IV} and U^{VI} minerals. The U-mineralized bedrocks show the largest variations in $\delta^{238}U$. Accordingly, combined with other information, their U isotope composition may provide a useful tool to constrain the processes that caused U enrichment.

CHAPTER 8

Conclusion

The topic of this thesis was the investigation of U ($n(^{238}U)$ / $n(^{235}U)$) isotope variations in nature with a focus on samples (1) that represent the continental crust and its weathering products (i.e. granites, shales and river water) (2) that represent products of hydrothermal alteration on mid-ocean ridges (i.e. altered basalts, carbonate veins and hydrothermal water) and (3) from restricted euxinic basins (i.e. from the water column and respective sediments). The overall goal was to explore the environmental conditions and unravel the mechanisms that fractionate the two most abundant U isotopes, $n(^{238}U)$ and $n(^{235}U)$, on Earth.

In Chapter 3 we investigated U isotope fractionation during weathering of the continental crust and subsequent transportation through rivers to the ocean. As representative for the continental crust, a variety of granites from different localities (Greenland, Japan, Germany and Swaziland) and of different ages, as well as post-Archean shales from Australia have been selected. Additionally, the U isotope composition in the dissolved load of major- and tributary rivers, i.e. from Venezuela (Rio Portuguesa), India (Alaknanda, Bhagirathi, Ganges, Brahmaputra), Pakistan (Indus), Germany (Main and Nidda) and Switzerland (Ticino, Birs, Saane), was determined. Our results revealed that the U isotope variation within the continental crust, $\delta^{238}U$, from -0.21 ‰ to -0.45 ‰ is independent of the U concentration (11.8 µg/g to 1.3 µg/g), age (3.80 Ga to 328 Ma), sample locality or degree of differentiation as

indicated by the La/Yb ratio. The analyzed rivers display U isotope variations ranging between $\delta^{238}U$ = -0.32 ‰ to 0.01 ‰. However, despite differences in the catchment lithologies, all major rivers define a narrow range between -0.31 ‰ and -0.13 ‰ and can barely be resolved from the new estimate for the upper continental crust (-0.30 ‰). In comparison to the major rivers, tributary rivers from the Swiss Alps display a larger range in $\delta^{238}U$ (-0.29 ‰ to 0.01 ‰) and they also have lower U concentrations (0.87 to 3.08 nmol/kg) compared to the investigated major rivers (5.19 - 11.69 nmol/kg).

As large rivers are the major U source to the oceans, we infer from our findings that the U input to the ocean is barely (if at all) fractionated relative to the U isotope composition of the continental crust. For mass balance consideration, we propose to use the average $\delta^{238}U$ of major rivers from this study (-0.23 ‰) as best estimate for the oceans U source.

In Chapter 4 we investigated modern anoxic basins, e.g. Baltic Sea and the Kyllaren fjord (Norway), for their uranium and molybdenum isotopic composition. Within this case study, we wanted to explore the parameters that control U isotope fractionation in anoxic environments and compare U-isotope fractionation with that of Mo, a similar redox-sensitive trace metal with well-investigated isotope systematics. We therefore analyzed the concentrations and isotope compositions of dissolved U and Mo from the water column and organic-rich sediments from three currently anoxic basins (Baltic Sea: Landsort and Gotland Deeps and the Kyllaren fjord in Norway). Though, the Kyllaren fjord is of much smaller size compared to the Black Sea (depth: 29 m vs. 2500 m), our results display a very similar behavior for Mo and U concentrations and isotope compositions in the deep euxinic water column: Molybdenum is strongly and U only moderately removed from the water column. Both Mo and U isotopes of the deep water column are fractionated towards a heavier ($\delta^{98}Mo$) and a lighter ($\delta^{238}U$) composition, respectively. These findings are in accordance with the observation that the sediments of such restricted euxinic basins (i.e. Black Sea, Kyllaren fjord), are commonly enriched in heavy U isotopes, compared to the initial value of the water column (i.e. seawater). Similar to previous findings from the Black

Sea, no Mo isotope fractionation between the original water mass and the sediment of the Kyllaren fjord was observed, due to the almost quantitative Mo removal from the water column. However, the deep water column display slightly heavier Mo isotope compositions, indicating the preferential reduction and deposition of light Mo isotopes into the sediments. On the other hand, the Baltic Sea water column displays only weak depletion of Mo and U and negligible Mo and U isotope fractionation. Variations of the Mo and U concentrations in the water column can be explained by conservative mixing of seawater with freshwater. However, the constant depletion of Mo (20 % to 40 %) and U (0 % to 20 %) in the deep water column indicates that reduction and scavenging of Mo and U from the water column into authigenic sediments occurred and resulted in an overall depletion of these elements in Baltic Sea water. The constant Mo- and U depletion in surface and deep water indicates that water mass exchange between Baltic Sea and open ocean water is longer than the (current) deep water renewal time in the Landsort and Gotland Deep. Additionally, a strong Mo- and weak U-isotope fractionation between water and sediments from the Landsort Deep (δ^{98}Mo: 2.4 ‰ vs. -0.1 ‰ and δ^{238}U -0.4 ‰ vs. -0.4 ‰) has been observed. However, the shift towards lower δ^{98}Mo and variable low δ^{238}U in sediments is not in accord with the predominantly anoxic to euxinic conditions during the deposition of these sediments (for further discussion see Chapter 4). We infer from these findings that during frequently occurring flushing events with oxygenated water, the originally anoxic Mo and U isotope signatures of the sediments were modified, possibly due to multiple remobilizations of Mo and U by oxic pore waters and subsequent partial re-precipitation under anoxic conditions. Our findings demonstrate that only sediments that formed under strong and persistently euxinic conditions display heavy δ^{238}U and seawater-like δ^{98}Mo and thus record the redox conditions during the time of their deposition.

In Chapter 5 U isotope fractionation during hydrothermal alteration on mid-ocean ridges (second most important sink for U from the ocean) is discussed based on the investigation of hydrothermal fluids, hydrothermally altered oceanic crust (ODP samples) and calcium carbonate veins that formed in altered basalts. In order to extend

the data base on fresh basalts, we also determined the U isotope composition of ocean island basalts (OIB) from the Canary Islands (Tenerife and La Palma) and a volcanic region in Germany (Vogelsberg). Hydrothermal fluids displayed $\delta^{238}U$ between -0.28 ‰ to -0.59 ‰, i.e. in average slightly lighter than seawater coupled with a strong depletion in the U content of the fluids compared to that of seawater (0.4 nmol/kg vs. 14 nmol/kg). These findings show that significant amounts of U are removed during the interaction of hydrothermal fluids with oceanic crust, leaving behind hydrothermal waters that tend to be enriched in lighter U isotope compositions. Hydrothermally altered oceanic crust (ODP samples) and their leached calcium carbonate veins showed significant U isotope variations (ranging between -0.63 ‰ and 0.27 ‰), which is a result of the circulation of the hydrothermal fluids through the oceanic crust. The altered basalts show also an U enrichment by a factor of 3 to 18 compared to fresh MORB, in average. These findings support that partial U reduction and incorporation into the secondary minerals of the altered crust is an important process at MOR. There is only a weak tendency in the removal of heavy U isotopes during hydrothermal alteration, which may be expected if U reduction is a dominant process. The variety of U isotope fractionation in the carbonate veins indicates that they unlikely resemble the U isotope composition of the fluids and U isotope fractionation occurs during the precipitation of the calcium carbonate veins. However, the mechanisms involved in the removal process of U, resulting in the observed U isotope variations, are still not completely understood.

In addition to the investigation of U isotope fractionation in the major U reservoirs on the Earth's surface, some preliminary investigations have been performed, regarding the suitability of U isotope signatures as a fingerprint for the mechanisms of U mobilization in contaminated soils and for the formation of U minerals and/or U deposits. The results are presented in Chapter 6 and Chapter 7.

In Chapter 6 we presented the results of soil samples from different depths and water samples from a former U mine tailing in Schneckenstein (Germany). We tested

the use of U isotopes for investigation of U mobilization in the environment, particularly in a region with previous mining activity. The soil profile shows well-correlated U concentrations and isotope signatures with depth, indicating a strong interaction of the seepage water with the soil within the uppermost 25 cm. These findings indicate that redox processes likely control U enrichment and depletion in the soil, resulting in reduction-related U enrichment to values of 4.73 mg/g U at a depth of ca. 25 cm, with high $\delta^{238}U$ of up to -0.16 ‰. Due to the redox sensitive behavior of U, associated with U isotope fractionation, U isotopes are suitable tools to determine if the conditions (oxic to reducing conditions) change within a tailing. Future U isotope investigations of soil and water from U tailings combined with experimental studies on U reduction and remobilization may provide more detailed information on the mobilization process of U. This should result in additional constraints on the original source and the contribution of the tailings for the observed U contamination in the environment.

In Chapter 7 the U isotope composition of U minerals (U^{IV}, U^{VI} and mineralized bedrock) has been investigated, in order to explore the relationship between their isotope composition and their genetic conditions as expressed in their valence state. Our results suggest that minerals containing the oxidized U species (U^{VI}) usually display a lighter $\delta^{238}U$ compared to samples containing the reduced U species (U^{IV}). However, our results are only based on a very limited amount of samples and the results of the U isotope composition for the U^{IV} and U^{VI} minerals overlap with each other. This suggests that the U isotope composition of U^{IV} and U^{VI} minerals does not only depend on the valence state of U. Other processes, e.g. adsorption processes during mineral formation, the coordination of U in the minerals or a variable $\delta^{238}U$ in their sources, may also explain the overlapping range in $\delta^{238}U$ observed for U^{IV} and U^{VI} minerals. The U-mineralized bedrocks show the largest variations in $\delta^{238}U$. Accordingly, combined with other information, the U isotope composition of U^{IV} and U^{VI} minerals may provide a useful tool to constrain the processes that caused U enrichment, e.g. in U deposits.

Future perspectives

This work profoundly improved our understanding of the parameters that control the natural fractionation of uranium isotopes under different anoxic and oxic conditions. Especially in Chapter 4, a comparison of the isotopic behavior of U with the already better understood Mo isotopic system revealed a partially oppositional behavior of Mo and U isotopes in strong euxinic water columns ($c(H_2S)$ > 11 µmol/L). Accordingly, both isotope systems may be used in a complementary way to investigate the depositional conditions of restricted basins in the past and the redox evolution of paleo-oceans.

Further studies may focus on the determination of the U isotopic composition and U speciation (U^{IV} or U^{VI}) in pore water and their associated sediments. Furthermore, U reduction and mobilization may be investigated by applying experimental approaches. Such investigations may give more insight into the mechanisms of U scavenging and/or remobilization, e.g. whether U removal/remobilization is triggered by a distinct pore water chemistry, the presence of distinct particles or organic complexes or stimulated by microorganisms.

Additionally, it would be interesting to trace the U isotope composition in rivers in more detail (Chapter 3). Therefore, it would be useful to combine investigations of the U isotopic composition of river water with that of respective bedrock lithologies in their catchment. In addition, it might be useful to compare the filtrate river water with the remaining particles in the filters, which could contain organic complexed U.

The here presented results on U isotopes in a former mining area showed that U isotopes have a potential to trace mechanisms of U mobilization, which may support the development of remediation strategies.

ABBREVIATIONS

BIFs	Banded Iron Formations
CI	Chondrites that are a group of stony meteorites
DU	Depleted uranium
Grav Roch Mo2	A gravimetrically prepared molybdenum standard, Grav Rochester Mo2
ICP-MS	Inductively coupled plasma mass spectrometer
IRMM	Institute for Reference Materials and Measurement, Belgium
IUPAC	International Union of Pure and Applied Chemistry
Mbsl	Meters below sea level
MC-ICP-MS	Multi collector inductively coupled plasma mass spectrometer
MORB	Mid-ocean ridge basalt
NBL CRM	New Brunswick Laboratory Certified Reference Materials
NBS SRM	National Bureau of Standards Standard Reference Material
NIST SRM	National Institute of Standards and Technology Standard Reference Materials, USA

OAE-2	Oceanic anoxic events that occurred ~ 93.5 Ma
ODP	Ocean Drilling Program
OIB	Ocean island basalts
PFA	Perfluoroalkoxy
REE	Rare earth elements
REIMEP	Regular European Interlaboratory Measurement Evaluation Programme from the IRMM
Roch Mo2	A Johnson Matthey SPECPURE® Mo plasma standard, Lot #802309E
SDO-1	A certified USGS Ohio Devonian Shale
TTG	Tonalite-Trondjemite-Granodiorite

REFERENCES

Abe M., Suzuki T., Fujii Y., Hada M. and Hirao K. (2008) An ab initio molecular orbital study of the nuclear volume effects in uranium isotope fractionations. *J. Chem. Phys.*, **129**, 164309.

Algeo T. J. and Maynard J. B. (2004) Trace-element behavior and redox facies in core shales of Upper Pennsylvanian Kansas-type cyclothems. *Chem. Geol*., **206**, 289-318.

Alt J.C. (1995) Sulfur isotope profile through the oceanic crust: Sulfur mobility and seawater-crustal sulfur exchange during hydrothermal alteration. *Geology*, **23**, 585-588.

Anbar A.D., Knab K.A. and Barling, J. (2001) Precise determination of mass-dependent variations in the isotopic composition of molybdenum using MC-ICPMS. *Anal. Chem*, **73**, 1425-1431.

Anbar A.D. (2004) Molybdenum stable isotopes: Observations, interpretations and directions. *Reviews in Mineralogy and Geochemistry*, **55**, 429-454.

Andersen M.B., Romaniello S., Vance D., Little S.H., Herdman R. and Lyons T.W. (2014) A modern framework for the interpretation of 238U/235U in studies of ancient ocean redox. *Earth Planet. Sci. Lett.*, **400**, 184-194.

Ando A., Mita N. and Terashima S. (1987) 1986 Values for 15 GSJ Rock Reference Samples, Igneous Rock Series. *Geostandards Newsletters*, **11**, 159-166.

Anderson R.F., Fleisher M.Q., and Lehuray A.P. (1989) Concentration, oxidation state, and particulate flux of uranium in the Black Sea. *Geochim. Cosmochim. Acta*, **53**, 2215–2224.

Archer C. and Vance D. (2008) The isotopic signature of the global riverine molybdenum flux and anoxia in the ancient oceans. *Nature Geoscience*, **1**, 597-600.

Arnold G.L., Anbar A.D., Barling J. and Lyons T.W. (2004) Molybdenum isotope evidence for widespread anoxia in mid-proterozoic oceans. *Science*, **304**, 87-90.

Arnold G.L., Lyons T.W., Gordon G.W. and Anbar A.D. (2012) Extreme change in sulfide concentrations in the Black Sea during the Little Ice Age reconstructed using molybdenum isotopes. *Geology*, **40**, 595–598.

Asael D., Tissot F.L.H., Reinhard C.T., Rouxel O., Dauphas N., Lyons T.W., Ponzevera E., Liorzou C. and Chéron S. (2013) Coupled molybdenum, iron and uranium stable isotopes as oceanic paleoredox proxies during the Paleoproterozoic Shunga Event. *Chem. Geol.*, **362**, 193-210.

Baadsgard H., Nutman A. and Bridgewater D. (1986) Geochronology and Isotopic Variation of the Early Archean Amitsoq Gneisses of the Isukasia Area, Southern West-Greenland. *Geochim. Cosmochim. Acta*, **50**, 2173-2183.

Bach W., Peucker-Ehrenbrink B., Hart S.R. and Blusztajn J.S. (2003) Geochemistry of hydrothermally altered oceanic crust : DSDP/ODP Hole 504B – Implications for seawater-crust exchange budgets and Sr- and Pb-isotopic evolution of the mantle. *Geochem. Geophys. Geosyst.*, **4**, 8904, doi:10.1029/2002GC000419, 3.

Bajo C., Rybach L. and Weibel M. (1983) Extraction of uranium and thorium from Swiss granites and their microdistribution: I. Extraction of uranium and thorium. *Chem. Geol.*, **39**, 281-297.

Barling J., Arnold G.L. and Anbar A.D. (2001) Natural mass-dependent variations in the isotopic composition of molybdenum. *Earth Planet. Sci. Lett.*, **193**, 447-457.

Barling J. and Anbar A.D. (2004) Molybdenum isotope fractionation during adsorption by manganese oxides. *Earth Planet. Sci. Lett.*, **217**, 315-329.

Barnes C.E. and Cochran J.K. (1990) Uranium removal in oceanic sediments and the oceanic U balance. *Earth Planet. Sci. Lett.*, **97**, 94-101.

Barnes C.E. and Cochran J.K. (1991) Geochemistry of uranium in Black Sea sediments. *Deep-Sea Res.*, **38**, S1237–S1254.

Basu A., Sanford R.A., Johnson T.M., Lundstrom C.C. and Löffler F.E. (2014) Uranium Isotopic Fractionation Factors during U(VI) Reduction by Bacterial Isolates. *Geochim. Cosmochim. Acta*, **136**, 100-113.

Beazley M.J., Martinez R.J., Webb S.M., Sobecky P.A. and Taillefert M. (2011) The effect of pH and natural microbial phosphatase activity on the speciation of uranium in subsurface soils. *Geochim. Cosmochim. Acta*., **75**, 5648-5663.

Bertine K.K. and Turekian K.K. (1973) Molybdenum in marine deposits. *Geochim. Cosmochim. Acta.*, **37**, 1415-1434.

Bertine K.K. and Goldberg E.D. (1977) History of heavy metal pollution in Southern California coastal zone - Reprise. *Environ. Sci. Technol.*, **11**, 297-299.

Bigeleisena J. and Mayer M.G. (1947) Calculation of equilibrium constants for isotopic exchange reactions. *Journal of Chemical Physics*., **15** (5), 261-267.

Bigeleisen J. (1965) Chemistry of isotopes. *Science*, **147**, 463-471.

Bigeleisen J. (1996) Nuclear size and shape effects in chemical reactions. Isotope chemistry of the heavy elements. *J. Am. Chem. Soc.*, **118**, 3676-3680.

Bonatti E., Lawrence J.R., Hamlyn P.R. and Breger D. (1980) Aragonite from deep sea ultramafic rocks. *Geochim. Cosmochim. Acta*., **44**, 1207-1214.

Bopp C.J., Lundstrom C.C, Johnson T.M. and Glessner J.J.G. (2009) Variations in (238)U/(235)U in uranium ore deposits: Isotopic signatures of the U reduction process?. *Geology*, **37**, 611-614.

Bopp C.J., Lundstrom C.C., Johnson T.M., Sanford R.A., Long P.E. and Williams K.H. (2010) Uranium U-238/U-235 isotope ratios as indicators of reduction: Results from an in situ biostimulation experiment at Rifle, Colorado, USA. *Environ. Sci. Technol.*, **44**, 5927-5933.

Bowen H:J:M. (1979) Environmental chemistry of the elements. Academic Press, London.

Böttcher M.E. (1998) Manganese(II) partitioning during experimental precipitation of rhodochrosite-calcite solid solutions from aqueous solutions. *Marine Chemistry*, **62**, 287-297.

Borole D., Krishnaswami S. and Somayajulu B. (1982) Uranium isotopes in rivers, estuaries and adjacent coastal sediments of Western India - Their weathering, transport and oceanic budget. *Geochim. Cosmochim. Acta.*, **46**, 125-137.

Brennecka G.A., Weyer S., Wadhwa M., Janney P.E, Zipfel J. and Anbar A.D. (2010a) (238)U/(235)U variations in meteorites: Extant (247)Cm and implications for Pb-Pb dating. *Science*, **327**, 449-451.

Brennecka G.A., Borg L.E., Hutcheon I.D., Sharp M.A. and Anbar A.D. (2010b) Natural variations in uranium isotope ratios of uranium ore concentrates: Understanding the (238)U/(235)U fractionation mechanism. *Earth Planet. Sci. Lett.*, **291**, 228-233.

Brennecka G.A., Wasylenki L.E., Bargar J.R., Weyer S. and Anbar A.D. (2011a) Uranium isotope fractionation during adsorption to Mn-oxyhydroxides. *Environ. Sci. Technol.*, **45**, 1370-1375.

Brennecka G.A., Herrmann A.D., Algeo T.J. and Anbar A.D. (2011b) Rapid expansion of oceanic anoxia immediately before the end-Permian mass extinction. *Proc. Natl. Acad. Sci. U.S.A.*, **108**, 17631-17634.

Brennecka G.A. and Wadhwa M. (2012) Uranium isotope compositions of the basaltic angrite meteorites and the chronological implications for the early Solar System, *Proc. Natl. Acad. Sci. U.S.A.*, **109**, 9299-9303.

Bruland K. W. (1983) Trace elements in seawater. In Chemical Oceanography, vol. 8 (eds. J. P. Riley and R. Chester) Academic Press, London UK. pp. 157-220.

Brumsack H.J. (2006) The trace metal content of recent organic carbon-rich sediments: Implications for Cretaceous black shale formation. *Palaeography Palaeoclimatology Palaeoecology*, **232**, 344-361.

Chen C., Sharma M. and Bostick B.C. (2006) Lithologic controls on osmium isotopes in the Rio Orinoco. *Earth Planet. Sci. Lett.*, **252**, 138-151.

Chen J.H., Wasserburg G.J., Von Damm K.L., and Edmond J.M. (1983) Pb, U and Th in hot springs on the East Pacific Rise at 21 °N and Guaymas Basin, Gulf of California, *EOS*, **64**, 724.

Chen J.H., Wasserburg G.J., Von Damm K.L., and Edmond J.M. (1984) 234U/238U and lead isotopic compositions in hot springs on the East Pacific Rise at 21°N, *Geol. Soc. Amer., Abstr. Prog.*, **16**, 469.

Chen J., Edwards R. and Wasserburg G. (1986) U-238, U-234 and TH-232 in seawater. *Earth Planet. Sci. Lett.*, **80**, 241-251.

Clark S.K., Johnson T.M. (2008) Effective isotopic fractionation factors for solute removal by reactive sediments: A laboratory microcosm and slurry study. *Environ. Sci. Technol.* 42(21): 7850-7855.

Collier R. W. (1985) Molybdenum in the northeast Pacific Ocean. *Limnol. Oceanogr.*, **30**, 1351-1354.

Colodner D., Edmond J. and Boyle E. (1995) Rhenium in the Black-Sea – Comparison with molybdenum and uranium. *Earth Planet. Sci. Lett.*, **131**, 1-15.

Crusius J., Calvert S., Pedersen T. and Sage D. (1996) Rhenium and molybdenum enrichments in sediments as indicators of oxic, suboxic and sulfidic conditions of deposition. *Earth Planet. Sci. Lett.*, **145**, 65-78.

Dahl T.W., Anbar A.D, Gordon G.W., Rosing M.T., Frei R. and Canfield, D.E. (2010) The behavior of molybdenum and its isotopes across the chemocline and in the sediments of sulfidic Lake Cadagno, Switzerland. *Geochim. Cosmochim. Acta.*, **74**, 144-163.

Dahl T.W., Boyle R.A., Canfield D.E., Connelly J.N., Gill B.C., Lenton T.M. and Bizarro M. (2014) Uranium isotopes distinguish two geochemically distinct stages during the later Cambrian SPICE event. *Earth Planet. Sci. Lett.*, **401**, 313-326.

De Laeter J., Bohlke J., De Bievre P., Hidaka H., Peiser H., Rosman K. and Taylor P. (2003) Atomic Weights of the Elements: Review 2000 - (IUPAC Technical Report). *Pure Appl. Chem.*, **75**, 683-800.

Dellwig O., Beck M., Lemke A., Lunau M., Kolditz K., Schnetger B. and Brumsack H. (2007) Non-conservative behaviour of molybdenum in coastal waters: Coupling geochemical, biological, and sedimentological processes. *Geochim. Cosmochim. Acta.*, **71**, 2745-2761.

Dellwig, O., Leipe, T., März, C., Glockzin, M., Pollehne, F., Schnetger, B., Yakushev, E.V., Böttcher, M.E., Brumsack, H.-J. (2010) A new particulate Mn-Fe-P-shuttle at the redoxcline of anoxic basins. *Geochim. Cosmochim. Acta*, **74**, 7100-7115.

Dellwig O., Schnetger B., Brumsack H., Grossart H. and Umlauf L. (2012) Dissolved reactive manganese at pelagic redoxclines (part II): Hydrodynamic conditions for accumulation. *Journal of marine systems*, **90**, 31-41.

Dunk R.M., Mills R.A. and Jenkins W.J. (2002) A reevaluation of the oceanic uranium budget for the Holocene. *Chem. Geol.*, **190**, 45-67.

Enkelmann E., Ehlers T.A., Zeitler P.K. and Hallet B. (2011) Denudation of the Namche Barwa Antiform, Eastern Himalaya. *Earth Planet. Sci. Lett.*, **307**, 323-333.

Erickson B.E. and Helz, G.R. (2000) Molybdenum(VI) speciation in sulfidic waters: Stability and lability of thiomolybdates. *Geochim. Cosmochim. Acta.*, **64**, 1149-1158.

Esser B.E. (1991) Osmium isotope geochemistry of terrigenous and marine sediments. *Yale University, New Haven*, Connecticut. 300.

Feistel R., Nausch G. and Hagen E. (2006) Unusual Baltic inflow activity in 2002-2003 and varying deep-water properties. *Oceanologia*, **48**, 21-35.

Feistel R., Nausch G., Matthäus W. and Hagen E. (2003) Temporal and spatial evolution of the Baltic deep water renewal in spring 2003. *Oceanologia*, **45**, 623-642.

Fonselius S. and Valderrama J. (2003) One hundred years of hydrographic measurements in the Baltic Sea. *J. Sea Res.*, **49**, 229-241.

Garzanti E., Vezzoli G., Ando S., Paparella P. and Clift P. (2005) Petrology of Indus River Sands: a key to interpret erosion history of the Western Himalayan Syntaxis. *Earth Planet. Sci. Lett.*, **229**, 287-302.

Georg R.B., Reynolds B.C., Frank M. and Halliday A.N. (2006) Mechanisms controlling the silicon isotopic compositions of river waters. *Earth Planet. Sci. Lett.*, **249**, 290-306.

Gerdes A. (2001) Magma Homogenization During Anatexis, Ascent and/or Emplacement? Constraints From the Variscan Weinsberg Granites. *Terra Nova*, **13**, 305-312.

Goldberg T., Archer C., Vance D. and Poulton S.W. (2009) Mo isotope fractionation during adsorption to Fe (oxyhydr)oxides. *Geochim. Cosmochim. Acta*, **73**, 6502-6516.

Goldberg T., Archer C., Vance D., Thamdrup B., McAnena A. and Poulton S.W. (2012) Controls on Mo isotope fractionations in a Mn-rich anoxic marine sediment, Gullmar Fjord, Sweden. *Chem. Geol.*, **296**, 73-82.

Gordon G.W., Lyons T.W., Arnold G.L., Roe J., Sageman B.B. and Anbar A.D. (2009) When do black shales tell molybdenum isotope tales?. *Geology*, **37**, 535-538.

Guilmette C., Indares A. and Hebert R. (2011) High-Pressure Anatectic Paragneisses From the Namche Barwa, Eastern Himalayan Syntaxis: Textural Evidence for Partial Melting, Phase Equilibria Modeling and Tectonic Implications. *Lithos*, **124**, 66-81.

Helz G.R., Miller C.V., Charnock J.M., Mosselmans J. F.W., Pattrick R.A.D., Garner C.D. and Vaughan D. J. (1996) Mechanism of molybdenum removal from the sea and its concentration in black shales: EXAFS evidence. *Geochim. Cosmochim. Acta*., **60**, 3631–3642.

Herrmann A.D., Wasylenki, L.E. and Anbar, A.D. (2010) Uranium isotopic compositions of carbonate sediments as a potential redox proxy. *Geological Society of America Abstracts with Programs*, **42**, 514.

Hiess J., Condon D.J., McLean N., Noble S.R. (2012) 238U/235U systematics in terrestrial uranium-bearing minerals. *Science*, **335**, 1610-1614.

Hoefs J. (2004) Stable Isotope Geochemistry. *Springer*, 244 p.

Hoffmann J.E., Muenker C., Naeraa T., Rosing M.T., Herwartz D., Garbe-Schoenberg D. and Svahnberg H. (2011) Mechanisms of Archean crust formation inferred from High-Precision HFSE systematics in TTGs. *Geochim. Cosmochim. Acta.*, **75**, 4157-4178.

Hofmann A.W. (1988) Chemical differentiation of the Earth : the relationship between mantle, continental crust, and oceanic crust. *Earth Planet. Sci. Lett.*, **90**, 297-314.

Hongo Y., Obata H., Gamo T., Nakaseama M., Ishibashi J., Konno U., Saegusa S., Ohkubo S., Tsunogai U. (2007) Rare Earth Elements in the hydrothermal system at Okinawa Trough back-arc basin. *Geochem. J.*, **41**, 1-15.

Honnorez J., Herzen von R.P., Barrett T.J., Becker K., Bender M.L., Borella P.E., Hubberten H.-W., Jones S.C., Karato S., Laverne C., Levi S., Migdisov A.A., Moorby S.A., Schrader E.L. (1981) Hydrothermal mounds and young ocean crust of the Galapagos : Preliminary Deep Sea Drilling results, Leg 70. *Geol. Soc. Am. Bull.*, **92**, 457-472.

Huckriede H. and Meischner D. (1996) Origin and environment of manganese-rich sediments within black-shale basins. *Geochim. Cosmochim. Acta.*, **60**, 1399-1413.

Jilbert T. and Slomp C.P. (2013) Iron and manganese shuttles control the formation of authigenic phosphorous minerals in the euxinic basins of the Baltic Sea. *Geochim. Cosmochim. Acta*, **107**, 155-169.

Jost G., Zubkov M.V., Yakushev E., Labrenz M. and Jürgens K. (2008) High abundance and dark CO2 fixation of chemolithoautotrophic prokaryotes in anoxic waters of the Baltic Sea. *Limnol. Oceanogr.*, **53**, 14-22.

Kendall B., Creaser R.A., Gordon G.W. and Anbar A.D. (2009) Re-Os and Mo isotope systematics of black shales from the Middle Proterozoic Velkerri and Wollogorang Formations, McArthur Basin, northern Australia. *Geochim. Cosmochim. Acta.*, **73**, 2534-2558.

Klinkhammer G. and Palmer M. (1991) Uranium in the oceans - Where it goes and why. *Geochim. Cosmochim. Acta.*, **55**, 1799-1806.

Kowalski N., Dellwig O., Beck M., Grunwald M., Fischer S., Piepho M., Riedel T., Freund H., Brumsack H. and Böttcher M.E. (2009) Trace metal dynamics in the water column and pore waters in a temperate tidal system: response to the fate of algae-derived organic matter. *Ocean dynamics*, **59**, 333-350.

Krabbenhöft A., Eisenhauer A., Böhm F., Vollstaedt H., Fietzke J., Liebetrau V., Augustin N., Peucker-Ehrenbrink B., Müller M.N., Horn C., Hansen B.T., Nolte N., Wallmann K. (2010) Constraining the marine strontium budget with natural strontium isotope fractionations (87Sr/86Sr*, δ88/86Sr) of carbonates, hydrothermal solutions and river waters. *Geochim. Cosmochim. Acta*., **74**, 4097-4109.

Ku T.-L., Knauss K.G. and Mathieu G.G. (1977) Uranium in open ocean: concentration and isotopic composition. *Deep-Sea Res*, **24**, 1005-1017.

Landgraf A., Planer-Friedrich B. and Merkel B. (2002) Natural attenuation in a wetland under unfavorable conditions - Uranium tailing Schneckenstein/Germany, in: Uranium in the Aquatic Environment (B.J. Merkel, B. Planer-Friedrich, C. Wolkersdorfer, Eds.), Berlin, p. 852-860.

Langmuir D. (1978) Uranium solution-mineral equilibria at low temperatures with applications to sedimentary ore deposits. *Geochim. Cosmochim. Acta*., **42**, 547-569.

Lepland A. and Stevens R. (1998) Manganese authigenesis in the Landsort Deep, Baltic Sea. *Mar. Geol.*, **151**, 1-25.

Lenz C., Behrends T., Jilbert T., Silveira M. and Slomp C.P. (2014) Redox-dependent changes in manganese speciation in Baltic Sea sediments from the Holocene Thermal Maximum: An EXAFS, XANES and LA-ICP-MS study. *Chem. Geol.*, **370**, 49-57.

Matthäus W. and Franck H. (1992) Characteristics of major Baltic inflows - a statistical analysis. *Cont Shelf Res*, **12**, 1375-1400.

Mbudi C., Merkel B. (2005) A laboratory assessment of uranium and arsenic removal efficiency from Schneckenstein uranium tailing leachates using scrap iron. Wiss. Mitt. Inst. Geol. TU BAF, Vol 28, 43-48 (ISSN 1433-1284).

McDonough W. and Sun S. (1995) The composition of the Earth. *Chem. Geol.*, **120**, 223-253.

McLennan S. and Taylor S. (1981) Role of subducted sediments in Island-Arc magmatism: Constraints from REE patterns. *Earth Planet. Sci. Lett.*, **54**, 423-430.

McManus J., Berelson W.M., Severmann S., Poulson R.L., Hammond D.E., Klinkhammer G.P. and Holm C. (2006) Molybdenum and uranium geochemistry in continental margin sediments: Paleoproxy potential. *Geochim. Cosmochim. Acta*, **70**, 4643-4662.

Merkel B.J. (1998) Untersuchungen zur radiologischen Emission des Uran-Tailings Schneckenstein, im Auftrag des Sächsisches Staatsministerium für Umwelt und Landesentwicklung, Dresden.

Michard A., Albaréde F., Michard G., Minster J.F., Charlou J.L. (1983) Rare-earth elements and uranium in high-temperature solutions from East Pacific Rise hydrothermal vent field (13 °N), *Nature*, **303**, 795-797.

Michard A. and Albarede F. (1985) Hydrothermal uranium uptake at ridge crests, *Nature*, **317**, 244-246.

Mills R.A., Elderfield H., Thomson J. (1993) A dual origin for the hydrothermal component in a metalliferous sediment core from the Mid-Atlantic Ridge, *J. Geophys. Res.*, **98**, 9671-9681.

Mills R.A., Wells D.M. and Roberts S. (2001) Genesis of ferromanganese crusts from the TAG hydrothermal field, *Chem. Geol*., **176**, 283-293.

Montoya-Pino C., Weyer S, Anbar A.D, Pross J, Oschmann W, van de Schootbrugge B and Arz H.W. (2010) Global enhancement of ocean anoxia during Oceanic Anoxic Event 2: A quantitative approach using U isotopes. *Geology*, **38**, 315-318.

Morford J. and Emerson S. (1999) The geochemistry of redox sensitive trace metals in sediments. *Geochim. Cosmochim. Acta.*, **63**, 1735-1750.

Morris A. W. (1975) Dissolved molybdenum and vanadium in the northeast Atlantic Ocean. *Deep Sea Res*., **22**, 49-54.

Mottl M. J. and Wheat C. G. (1994) Hydrothermal circulation through mid-ocean ridge flanks: Fluxes of heat and magnesium. *Geochim. Cosmochim. Acta.*, **58**, 2225-2237.

Nameroff T.J., Balistrieri L.S. and Murray J.W. (2002) Suboxic trace metal geochemistry in the eastern tropical North Pacific. *Geochim. Cosmochim. Acta*, **66**, 1139-1158.

Nance, W. and Taylor, S (1976) Rare Earth Element patterns and crustal evolution – 1. Australian Post-Archean sedimentary rocks. *Geochim. Cosmochim. Acta.*, **40**, 1539-1551.

Nägler T.F., Siebert C., Luschen H and Böttcher M.E. (2005) Sedimentary Mo isotope record across the Holocene fresh-brackish water transition of the Black Sea. *Chem. Geol.*, **219**, 283-295.

Nägler T.F., Neubert N, Böttcher M.E., Dellwig O and Schnetger, B. (2011) Molybdenum isotope fractionation in pelagic euxinia: Evidence from the modern Black and Baltic Seas. *Chem. Geol.*, **289**, 1-11.

Neretin, L.N., Volkov, I.I., Böttcher, M.E., and Grinenko, V.A. (2001) A sulfur budget for the Black Sea anoxic zone: Deep-Sea Research. Part I, *Oceanographic Research Papers*, v. 48, p. 2569–2593, doi: 10.1016/S0967-0637(01)00030-9.

Neretin L., Pohl C., Jost G., Leipe T. and Pollehne F., (2003) Manganese cycling in the Gotland Deep, Baltic Sea. *Marine Chemistry*, **82**, 125-143.

Neubert N., Nägler T.F. and Böttcher M.E. (2008) Sulfidity controls molybdenum isotope fractionation into euxinic sediments: Evidence from the modern Black Sea. *Geology*, **36**, 775-778.

Neubert N., Heri A.R., Voegelin A.R., Naegler T.F., Schlunegger F. and Villa, I.M. (2011) The molybdenum isotopic composition in river water: Constraints from small catchments. *Earth Planet. Sci. Lett.*, **304**, 180-190.

Noordmann J., Weyer S., Sharma M., Georg R.B., Rausch S. and Bach W. (2011) Fractionation of 238U/235U during weathering and hydrothermal alteration. *Geochim. Cosmochim. Acta.*, **76**, A1548.

Nutman A., Bennett V., Friend C. and Norman M. (1999) Meta-Igneous (Non-Gneissic) Tonalites and Quartz-Diorites from an extensive ca. 3800 Ma terrain South of the Isua Supracrustal Belt, Southern West Greenland: Constraints on early crust formation. *Contributions to Mineralogy and Petrology*, **137**, 364-388.

Palmer M. and Edmond J. (1992) Controls over the strontium isotope composition of river water. *Geochim. Cosmochim. Acta.*, **56**, 2099-2111.

Palmer M. and Edmond J. (1993) Uranium in river water. *Geochim. Cosmochim. Acta.*, **57**, 4947-4955.

Pearce C.R., Cohen A.S., Coe A.L. and Burton, K.W. (2008) Molybdenum isotope evidence for global ocean anoxia coupled with perturbations to the carbon cycle during the early Jurassic. *Geology*, **36**, 231-234.

Pogge von Strandmann P.A.E., James R.H., Calsteren van P., Gíslason S.R., Burton K.W. (2008) Lithium, magnesium and uranium isotope behaviour in the estuarine environment of basaltic islands. *Earth Planet. Sci. Lett.*, **274**, 462-471.

Poulson R., Siebert C, McManus J. and Berelson W. (2006) Authigenic molybdenum isotope signatures in marine sediments. *Geology*, **34**, 617-620.

Poulson R.L., McManus J., Severmann S. and Berelson W.M. (2009) Molybdenum behavior during early diagenesis: Insights from Mo isotopes. *Geochem. Geophys. Geosyst.* 10, 6, doi:10.1029/2008GC002180.

Pradeepkumar T.B., Fahmi S. and Sharma S.K. (2008) Uranium in ancient slag from Rajasthan. *Curr. Sci.*, **94**, 1031-1034.

Rahaman W., Singh S.K. and Raghav S. (2010) Dissolved Mo and U in Rivers and estuaries of India: Implication to geochemistry of redox sensitive elements and their marine budgets. *Chem. Geol.*, **278**, 160-172.

Ray A.E., Bargar J.R., Sivaswamy V., Dohnalkova A.C., Fujita Y., Peyton B.M., Magnuson T.S. (2011) Evidence for multiple modes of uranium immobilization by an anaerobic baterium. *Geochim. Cosmochim. Acta*., **75**, 2684-2695.

Reissmann J.H., Burchard H., Feistel R., Hagen E., Lass H.U., Mohrholz V., Nausch G., Umlauf L. and Wieczorek G. (2009) Vertical mixing in the Baltic Sea and consequences for eutrophication - A review. *Prog. Oceanogr.*, **82**, 47-80.

Richter S., Alonso-Munoz A., Eykens R., Jacobsson U., Kuehn H., Verbruggen A., Aregbe Y., Wellum R. and Keegan E. (2008) The isotopic composition of natural uranium samples - Measurements using the new n(U-233)/n(U-236) double spike IRMM-3636. *Int. J. Mass spectrom.*, **269**, 145-148.

Richter S., Eykens R., Kuhn H., Aregbe Y., Verbruggen A. and Weyer S. (2010) New average values for the n((238)U)/n((235)U) isotope ratios of natural uranium standards. *Int. J. Mass spectrom.*, **295**, 94-97.

Romaniello S.J., Brennecka G., Anbar A.D. and Colman A.S. (2009) Natural isotopic fractionation of 238U/235U in the water column of the Black Sea. *Eos Trans. AGU*, **90**(52), V54C-06.

Romaniello S.J., Herrmann A.D. and Anbar A.D (2013) Uranium concentrations and 238U/235U isotope ratios in modern carbonates from the Bahamas: Assessing a novel paleoredox proxy. *Chem. Geol.* **362**, 305-316.

Rosman K. and Taylor P. (1998) Isotopic compositions of the elements 1997. *Journal of Physical and Chemical Reference Data*, **27**, 1275-1287.

Sarin M., Krishnaswami S., Dilli K., Somayajulu B. and Moore W. (1989) Major ion chemistry of the Ganga-Brahmaputra River system - Weathering processes and fluxes to the Bay of Bengal. *Geochim. Cosmochim. Acta.*, **53**, 997-1009.

Sarin M., Krishnaswami S., Somayajulu B. and Moore W. (1990) Chemistry of uranium, thorium, and radium isotopes in the Ganga-Brahmaputra River system - Weathering processes and fluxes to the Bay of Bengal. *Geochim. Cosmochim. Acta.*, **54**, 1387-1396.

Sarin M., Krishnaswami S., Trivedi J. and Sharma K. (1992) Major ion chemistry of the Ganga source waters - Weathering in the high-altitude Himalaya. *Proceedings of the Indian Academy of Sciences-Earth and Planetary Sciences*, **101**, 89-98.

Schauble E.A. (2007) Role of nuclear volume in driving equilibrium stable isotope fractionation of mercury, thallium, and other very heavy elements. *Geochim. Cosmochim. Acta.*, **71**, 2170-2189.

Scheiderich K., Helz G.R. and Walker R.J. (2010) Century-long record of Mo isotopic composition in sediments of a seasonally anoxic estuary (Chesapeake Bay). *Earth Planet. Sci. Lett.*, **289**, 189-197.

Schinke H. and Matthäus W. (1998) On the causes of major Baltic inflows - an analysis of long time series. *Cont Shelf Res*, **18**, 67-97.

Schulz M. and Bischoff M. (2008) Variation in Riverine phosphorus between 1994 and 2003 as affected by land-use and loading reductions in six medium-sized to large German Rivers. *Limnologica*, **38**, 126-138.

Scholz F., McManus J. and Sommer S. (2013) The manganese and iron shuttle in a modern euxinic basin and implications for molybdenum cycling at euxinic ocean margins. *Chem. Geol.* **355**, 56-68.

Sharma M., Wasserburg G., Hoffmann A. and Chakrapani G. (1999) Himalayan uplift and osmium isotopes in oceans and rivers. *Geochim. Cosmochim. Acta.*, **63**, 4005-4012.

Sharma M., Rosenberg E.J. and Butterfield D.A. (2007) Search for the proverbial mantle osmium sources to the oceans: Hydrothermal alteration of mid-ocean ridge basalt. *Geochim. Cosmochim. Acta*., **71**, 4655-4667.

Siebert S., Nägler T.F., and Kramers J.D. (2001) Determination of molybdenum isotope fractionation by double-spike multicollector inductively coupled plasma mass spectrometry. *Geochem. Geophys. Geosyst*. 2 paper number 2000GC000124.

Siebert C., Nägler T.F., von Blanckenburg F. and Kramers J.D. (2003) Molybdenum isotope records as a potential new proxy for paleoceanography. *Earth Planet. Sci. Lett.*, **211**, 159-171.

Siebert C., McManus J., Bice A., Poulson R. and Berelson W. (2006) Molybdenum isotope signatures in continental margin marine sediments. *Earth Planet. Sci. Lett.*, **241**, 723-733.

Singh S., Dalai T. and Krishnaswami S. (2003) U-238 series isotopes and Th-232 in carbonates and Black Shales from the lesser Himalaya: Implications to dissolved uranium abundances in Ganga-Indus source waters. *Journal of Environmental Radioactivity*, **67**, 69-90.

Smittenberg R., Pancost R., Hopmans E., Paetzel M. and Damste J. (2004) A 400-year record of environmental change in an euxinic fjord as revealed by the sedimentary biomarker record. *Palaeography Palaeoclimatology Palaeoecology*, **202**, 331-351.

Sternbeck J. and Sohlenius G. (1997) Authigenic sulfide and carbonate mineral formation in Holocene sediments of the Baltic Sea. *Chem. Geol.*, **135**, 55-73.

Sternbeck J., Sohlenius G. and Hallberg R. (2000) Sedimentary trace elements as proxies to depositional changes induced by a Holocene fresh-brackish water transition. *Aquatic geochemistry*, **6**, 325-345.

Stewart R.J., Hallet B., Zeitler P.K., Malloy M.A., Allen C.M. and Trippett D. (2008) Brahmaputra sediment flux dominated by highly localized rapid erosion from the easternmost Himalaya. *Geology*, **36**, 711-714.

Stirling C.H., Andersen M.B., Potter E. and Halliday A.N. (2007) Low-temperature isotopic fractionation of uranium. *Earth Planet. Sci. Lett.*, **264**, 208-225.

Stirling C.H. (2012) Keeping time with Earth´s heaviest element. *Science*, **335**, 1585-1586.

Suess E. (1979) Mineral phases formed in anoxic sediments by microbial decomposition of organic matter. *Geochim. Cosmochim. Acta.*, **43**, 339-352.

Taylor R.N. and McLennan S. (1985) The continental crust: Its composition and evolution. *Blackwell Scientific Publications, Boston.*

Telus M., Dauphas N., Moynier F., Tissot F.L.H., Teng F.-Z., Nabelek P.I., Craddock P.R. and Groat L.A. (2012) Iron, zinc, magnesium and uranium isotopic fractionation during continental crust differentiation: The tale from migmatites, granitoids, and pegmatites. *Geochim. Cosmochim. Acta*, **97**, 247-265.

Turekian K.K. and Wedepohl K.H. (1961) Distribution of the Elements in some major units of the Earth's crust. *Geol. Soc Am Bull.*, **72**: 175-192.

Urey H.C. (1947) The thermodynamic properties of isotopic substances. *Journal of the Chemical Society*, 562-281.

van Breugel Y., Schouten S., Paetzel M., Nordeide R. and Damste J. (2005a) The impact of recycling of organic carbon on the stable carbon isotopic composition

of dissolved inorganic carbon in a stratified marine system (Kyllaren fjord, Norway). *Org. Geochem.*, **36**, 1163-1173.

van Breugel Y., Schouten S., Paetzel M., Ossebaar J. and Damste J. (2005b) Reconstruction of delta(13)C of chemocline CO(2) (aq) in past oceans and lakes using the delta(13)C of fossil isorenieratene. *Earth Planet. Sci. Lett.*, **235**, 421-434.

Voegelin A.R., Nägler T.F., Samankassou E. and Villa I.M. (2009) Molybdenum isotopic composition of modern and Carboniferous carbonates. *Chem. Geol.*, **265**, 488-498.

Voegelin A.R., Pettke T., Greber N.D., von Niederhäusern B. and Nägler T.F. (2014) Magma differentiation fractionates Mo isotope ratios: Evidence from the Kos Plateau Tuff (Aegean Arc). *Lithos.*, **190-191**, 440-448.

Wasylenki L.E., Rolfe B.A., Weeks C.L., Spiro T.G. and Anbar A.D. (2008) Experimental investigation of the effects of temperature and ionic strength on Mo isotope fractionation during adsorption to manganese oxides. *Geochim. Cosmochim. Acta.*, **72**, 5997-6005.

Wedepohl K. H. (1971) *Environmental influences on the chemical composition of shales and clays*. Pergamon, Oxford.

Wedepohl K. H. (2004) The composition of earth´s crust, natural cycles of elements, natural resources. *2nd ed. Wiley-VCH*.

Weyer S. and Schwieters J. (2003) High precision Fe isotope measurements with high mass resolution MC-ICPMS. *Int. J. Mass spectrom.*, **226**, 355-368.

Weyer S., Anbar A.D., Gerdes A, Gordon G.W., Algeo T.J. and Boyle E.A. (2008) Natural fractionation of 238U/235U. *Geochim. Cosmochim. Acta.*, **72**, 345-359.

Weyer S. and Seitz H.-M. (2012) Coupled lithium- and iron isotope fractionation during magmatic differentiation, *Chem. Geol.*, **294-295**, 42-50.

Wille M., Kramers J.D., Nägler T.F., Beukes N.J., Schroder S, Meisel T., Lacassie J.P. and Voegelin A.R. (2007) Evidence for a gradual rise of oxygen between 2.6 and 2.5 Ga from Mo isotopes and Re-PGE signatures in shales. *Geochim. Cosmochim. Acta.*, **71**, 2417-2435.

Wille M., Nägler T.F., Lehmann B., Schroeder S. and Kramers J.D. (2008) Hydrogen sulphide release to surface waters at the Precambrian/Cambrian boundary. *Nature*, **453**, 767-769.

Windom H.L., Silpipat S., Chanpongsang A., Smith R.G. and Hungspreugs M. (1984) Trace metal composition of and accumulation rates of sediments in the Upper Gulf of Thailand. *Estuarine, coastal and Shelf Science*, **19**, 133-142.

Yadav S.K. and Chakrapani G.J. (2011) Geochemistry, dissolved elemental flux rates, and dissolution kinetics of lithologies of Alaknanda and Bhagirathi Rivers in Himalayas, India. *Environmental Earth Sciences*, **62**, 593-610.

Zeh A., Gerdes A. and Millonig L. (2011) Hafnium isotope record of the Ancient Gneiss Complex, Swaziland, Southern Africa: Evidence for Archaean crust-mantle formation and crust reworking between 3.66 and 2.73 Ga. *Journal of the Geological Society*, **168**, 953-963.

Zillen L., Conley D.J., Andren T., Andren E. and Bjorck S. (2008) Past occurrences of hypoxia in the Baltic Sea and the role of climate variability, environmental change and human impact. *Earth-Science Reviews*, **91**, 77-92.